Statistical learning and inverse uncertainty quantification in nuclear thermal-hydraulic simulation : application to the condensation modelling at the safety injection

Riccardo Cocci

université PARIS-SACLAY

Statistical learning and inverse uncertainty quantification in nuclear thermal-hydraulic simulation: application to the condensation modelling at the safety injection

Apprentissage statistique et quantification inverse des incertitudes en simulation thermohydraulique nucléaire : application à la modélisation de la condensation à l'injection de sécurité

Thèse de doctorat de l'université Paris-Saclay

École doctorale n° 579, Sciences mécaniques et énergétiques, matériaux et géosciences (SMEMAG)
Spécialité de doctorat: Mécanique des fluides
Graduate School : Sciences de l'ingénierie et des systèmes
Référent : CentraleSupélec

Thèse préparée dans l'unité de recherche Service de Thermo-hydraulique et de Mécanique des Fluides (Université Paris-Saclay, CEA), sous la direction de **Didier LUCOR**, Directeur de recherche et le co-encadrement de **Guillaume DAMBLIN**, Docteur, **Alberto GHIONE**, Docteur et **Lucia SARGENTINI**, Docteure

Thèse soutenue à Paris-Saclay, le 03 Novembre 2022, par

Riccardo COCCI

Composition du jury

Enrico ZIO Full Professor, Mines ParisTech and Polytechnic of Milan	Président
Tomasz KOZLOWSKI Associate Professor, University of Illinois	Rapporteur & Examinateur
Nicola PEDRONI Associate Professor, Polytechnic of Turin	Rapporteur & Examinateur
Pierre BARBILLON Professeur à AgroParisTech	Examinateur
Jordi FREIXA Fellow Professor, Technical University of Catalonia	Examinateur
Jean-Luc VACHER Ingénieur en thermohydraulique à Electricité De France	Examinateur
Didier LUCOR Directeur de thèse au CNRS - LISN	Directeur de thèse

THESE DE DOCTORAT
NNT : 2022UPAST122

Abstract

Title: Statistical learning and inverse uncertainty quantification in nuclear thermal-hydraulic simulation: application to the condensation modelling at the safety injection

The methodology called BEPU (which stands for *Best Estimate Plus Uncertainty*) is increasingly attracting interest in the nuclear thermal-hydraulic field. It is composed of two steps: the simulation of physical phenomena through the best available knowledge (e.g. using physical models, also called correlations) and the estimation of the uncertainties affecting the predictions. Before the application of the BEPU methodology to safety studies, the thermal-hydraulic models used in the nuclear codes should be appropriately developed, validated and the associated uncertainties quantified. These correlations are assessed tuning their parameters using the available experimental databases. Ideally, the database is composed by Separate Effect Tests (SETs) (i.e. tests where the phenomenon to be modelled has an effect on the measurable Quantity of Interest (QoI) that can be separated and quantified). Nevertheless, SETs are not often available, but Combined Effect Tests (CETs) are. If the database is composed by CETs, the correlation modelling the physical phenomenon of interest interacts with, at least, another one (which is uncertain as well).

This doctoral research aims at developing advanced statistical methodologies for the Inverse Uncertainty Quantification (IUQ) (i.e. the estimation of the input uncertainties from the discrepancy between the predicted QoI and its experimental value) of thermal-hydraulic models and apply them to the practical case of the condensation model at the Emergency Core Cooling (ECC) system of a nuclear reactor. It consists, more in detail, on the development, validation and uncertainty quantification of a new physical correlation in presence of SETs and the IUQ of an existing model against a CETs database. The PhD thesis is arranged in three main parts. In the first part, the development, validation and quantification of the uncertainty of thermal-hydraulic models is approached by Bayesian inference using SETs. In this approach, a multiplicative random variable (representing the model uncertainty) links the experimental value to the model prediction. This multiplicative variable suits models that scale many orders of magnitude, as in the case of thermal-hydraulic tests. A set of statistical indicators is identified to assess the predictive performance of the best-estimate model. Moreover, since the available thermal-hydraulic databases are often composed by a limited number of tests, the physical model is validated using a cross-validation technique called Leave One Out (LOO), which allows using the same database for both the assessment and validation phases.

The second part is focused on one of the most widely applied IUQ methods in nuclear thermal-hydraulic: the CIRCE methodology (French acronym for *Calculation of the Uncertainties Related to the Elementary Correlations*) and its extension to CETs applications. CIRCE estimates the (log-)normal probability distribution representing the reference model uncertainty in the computer code. However, when applied to several models using CETs, this methodology may suffer of unidentifiability (i.e. different combination of uncertainties explain the missmatch between the code output and the experimental data) resulting in less accurate and precise estimated uncertainties. The unidentifiability may result in an estimation of the least influential model uncertainty (least influential on the code output) characterised by low accuracy and precision (in the estimation of the (log-)normal law parameters). Furthermore, even the estimation

of the most influential model uncertainty may be affected by low precision. Thus, an extension of the method (named CIRCE 2-Steps) is proposed for the improved estimation of the most influential model uncertainty. The methodology is composed of two successive steps. In the first step, the uncertainties for which SETs are available are evaluated. These uncertainties are then properly taken into account when quantifying the remaining uncertainties against CETs. Such an approach is proven to provide more accurate and precise results.

In the third part, the two methodologies are applied to a practical case: the physical models used for the prediction of the condensation in the cold leg of a nuclear Pressurised Water Reactor (PWR) during a Loss of Coolant Accident (LOCA). In such a scenario, two condensation phenomena are influent on the QoI, i.e. the temperature of the liquid at the entrance of the downcomer. The former is the condensation of the steam on the cold jet of the ECC system and then its impact in the liquid flow. The latter is the condensation of the steam at the liquid interface of the stratified flow between the jet region and the downcomer. The experimental facilities COSI, TOPFLOW-PTS and UPTF compose the experimental database. The configuration and scale is different for all of them, resulting in a broad range of injection temperature, mass flowrate and pressure. These experiments are classified as CETs. Nevertheless, since the condensation at the safety injection can be isolated, they can also be rearranged as SETs. This database is thus appropriate to test both methodologies. After testing correlations from the literature on the new experimental database with poor results, a new approach is presented. The condensation is quantified by a potential, which describes the heat exchanger that models the cold jet. In this way, the condensation is a function of the shape of the jet and a variable η depending on the ECC fluid velocity, the ECC geometry, the steam mass flowrate, the fluid temperature and the pressure. The Bayesian framework presented in the first part is applied to the COSI and TOPFLOW-PTS SETs to calibrate a correlation for the variable η. The new model reduces significantly the standard deviation between the predictions and the corresponding experimental values. The new correlation is then statistically validated and applied to the UPTF database for physical validation. The correlation shows a good capability of accurately predict the condensation at the injection in all the studied configurations. The newly developed CIRCE 2-Steps methodology is then applied, showing significant improvements on the estimation of the uncertainty of the jet condensation model (i.e. the most influential one). The resulting model uncertainty is compared with the one computed by the Bayesian framework, showing good agreement between the two results.

Keywords: Bayesian calibration, Inverse Uncertainty Quantification, CIRCE, Combined Effect Tests, Condensation, ECC

Questa tesi è dedicata ai miei genitori e a mia sorella
Per il loro supporto, incoraggiamento e amore senza fine

This thesis is dedicated to my parents and my sister
For their support, encouragement and endless love

Cette thèse est dédiée à mes parents et ma soeur
Pour leur soutien, encouragement et amour sans fin

Gëram naa la fi ngëram yam, Awa!
Maa ngi la'y jaa jëfal ci sa taxawaay. Sama mbëgeel ci yaw fi ak allaxira du dakk.

Acknowledgements

The acknowledgements for this manuscript are of great importance to me. They are the least I can do to thank all the people who supported me during this three years long journey. I will name you in alphabetical order.

First and foremost, I would like to express my special thanks of gratitude to my thesis director Dr. Didier Lucor and my supervisors Dr. Guillaume Damblin, Dr. Alberto Ghione and Dr. Lucia Sargentini. Without their advices, support, help and patience this thesis would have less than half of the contents. I owe you more than you think.

I thank Prof. Tomasz Kozlowski and Prof. Nicola Pedroni for accepting to review my manuscript. I am thankful to Prof. Pierre Barbillon, Prof. Jordi Freixa, Mr. Jean-Luc Vacher and Prof. Enrico Zio for accepting to be part of the committee as examiners of my PhD dissertation.

I am also grateful to the people in the laboratories that welcomed me at the French Alternative Energies and Atomic Energy Commission (CEA): the Laboratory of Applications of Thermal-hydraulic and Fluid-mechanics (LATF) and the Laboratory of Instrumentation and Experimentation in Fluid-mechanics and Thermal-hydraulic (LIEFT). A special mention goes to the ones who became good friends as well as collegues: Alain, Antoine, Arnaud, Aurélien, Benjamin, Cassiano, Clément, Constantin, Diana Milena, Etienne, Fred, Hervé, Loïc, Pierre-Luis, Sergey, Sonia and Vincent Pascal Philippe (my "*reuf*"). Moreover, I would also thank the interns that I was lucky enough to meet: Alessandro, Francesco, Guillaume, Ignazio, Luca, Medhi, Natacha, Rosanna, Teiva and Zuzanna.

A big special *Thank you!* goes to (future Dr.) Arthur Iziquel, who became firstly a collegue, then a friend and in the end a flatmate.

Thanks to the Italian friends I met during my Master's thesis at Framatome and throughout the PhD: Andrea S., Angelo, Annibale, Gervasio, Giulio, Luca, Massimo, Matteo, Paolo, Roberta, Vincenzo and Wanda. A special word of thanks to Francesco and Michele who pushed and encouraged me to begin this doctorate, I did not regret it. My thanks also to: Andrea B., Boris, Farès, Khady, Leonardo, Leslie, Ornella, Rofeida, Sandra, Stéphanie Simone Angeline and Valentina.

I owe a very important debt to the friends who supported me from Italy and welcomed me back each time I flew back to Rome: Andrea C., Claudia, Claudio, Daniele, Marko, Mattia, Riccardo, Sara, Silvia, Simone, Stefano A., Stefano F. and Valentino.

Last but not least, I would like to thank my whole family for his support during this journey.

List of Publications

This thesis is an introduction to and a summary of the work published in the following papers:

PAPER I

R. Cocci, G. Damblin, A. Ghione, L. Sargentini and D. Lucor. "A comprehensive Bayesian framework for the development, validation and uncertainty quantification of thermal-hydraulic models" *Annals of Nuclear Energy* 172, 109029, 2022. Available at: `https://www.sciencedirect.com/science/article/pii/S0306454922000640`

PAPER II

R. Cocci, A. Ghione, L. Sargentini, G. Damblin and D. Lucor. "Model Assessment for Direct Contact Condensation Induced by a Sub-cooled Water Jet in a Circular Pipe" *International Journal of Heat and Mass Transfer* 195, 123162, 2022. Available at: `https://www.sciencedirect.com/science/article/pii/S0017931022006329`

PAPER III

R. Cocci, G. Damblin, A. Ghione, L. Sargentini and D. Lucor. "Extension of the CIRCE methododology to improve the inverse uncertainty quantification of several combined thermal-hydraulic models" *Nuclear Engineering and Design* 398, 111974, 2022. Available at: `https://www.sciencedirect.com/science/article/pii/S0029549322003259`

Contents

Nomenclature

Acronym	Description
ASN	French Nuclear Safety Authority
BE	Best-Estimate
BEPU	Best-Estimate Plus Uncertainty
BIC	Bayesian Information Criterion
CEA	Commisariat à l'Energie Atomique et aux énergies alternatives
CET	Combined Effect Test
CFD	Computational Fluid Dynamics
CIRCE	Calculs des Incertitudes Relatives aux Corrélations Elémentaires
COSI	COndensation at Safety Injection
DC	Downcomer
DNS	Direct Numerical Simulation
ECC	Emergency Core Cooling
ECCS	Emergency Core Cooling System
ECME	Expectation-Conditional Maximisation Either
F&B	Feed & Bleed
IET	Integral Effect Test
IF	Interval of Fluctuation
IUQ	Inverse Uncertainty Quantification
KS	Kolmogorov-Smirnov
LOCA	Loss Of Coolant Accident
LOO	Leave One Out
LWR	Light Water Reactor
MAP	Maximum A Posteriori
MLE	Maximum Likelihood Estimation
NEC	Normalised Error Coefficient
NPP	Nuclear Power Plant
pdf	probability density function
PTS	Pressurised Thermal Shock
PWR	Pressurised Water Reactor
QoI	Quantity of Interest
QQ	Quantile-Quantile
SET	Separate Effect Test
sssw	steady state steam water
TC	Thermocouple
tsw	transient steam water
UPTF	Upper Plenum Test Facility
UQ	Uncertainty Quantification
V&V&UQ	Verification, Validation and Uncertainty Quantification

Symbol	Dimensions	Description
	General symbols	
A	m^2	Area
b	-	Bias distribution
c_p	$J/kg/K$	Specific heat capacity at constant pressure
d	m	Diameter
D	m	Diameter of the cold leg
$\mathbb{E}$	-	Expected value
f	-	Function
Fr	-	Froude number $\sqrt{u^2/g/l_{Fr}}$
G	$kg/s/m^2$	Specific mass flowrate
g	m/s^2	Gravitational acceleration (9.807)
h	$W/m^2/K$	Heat transfer coefficient
H	m	Liquid height
I	J/kg	Specific enthalpy
i	-	Index
I_{ls}	J/kg	Latent heat of condensation
$\mathscr{IG}$	-	Inverse-gamma distribution
J	-	Jacobian matrix
Ja	-	Jakob number $\rho_l \cdot c_p \cdot (T_g - T_l)/\rho_g/I_{lg}$
K	-	State variable associated matrix
k	-	Scale parameter
k_{th}	$W/m/K$	Thermal conductivity
l	m	Characteristic length
Δl	m	Free surface length
L	m	Jet length
$\mathcal{L}$	-	Likelihood
$\mathscr{LN}$	-	Log-normal distribution
m	-	Mean of a probability distribution
$\dot{m}$	kg/s	Mass flowrate
$\mathscr{N}$	-	Normal distribution
n	-	Number of tests
$\mathscr{NIG}$	-	Normal-inverse-gamma distribution
Nu	-	Nusselt number $h \cdot l_{Nu}/k_{th}$
o	-	Number of parameters
P	MPa	Pressure
Pr	-	Prandtl number $\mu_{dyn} \cdot c_p/k_{th}$
p	-	Number of models
$\dot{Q}$	m^3/s	Volumetric flowrate
$\dot{q}$	W	Heat flux
$\dot{q}''$	W/m^2	Specific heat flux
$\dot{q}'''$	W/m^3	Volumetric heat flux
R	-	Condensation potential
R^2	-	Coefficient of determination
r	-	Relative residual

Re	-	Reynolds number $\rho \cdot u \cdot l_{Re}/\mu_{dyn}$
S	m^2	Surface
St	-	Stanton number $Nu/Re/Pr$
T	K	Temperature
t	s	Time
u	m/s	Velocity
$\mathbb{V}$	-	Variance
x	-	State variable
z	-	Generic variable

Greek symbols

α	-	Void fraction
Δ	-	Difference
ϵ	-	Experimental error
η	-	Condensation variable
θ	-	Model parameter
Λ	-	Model uncertainty distribution
λ	-	Model uncertainty realisation
μ		Arithmetic mean
μ_{dyn}	$Pa \cdot s$	Dynamic viscosity
π	-	Mathematical constant (3.142)
ρ	kg/m^3	Density
Σ	-	Variance-covariance matrix
σ	-	Standard deviation
σ^2	-	Variance
τ	-	Probability distribution
ϕ	-	Dissipation function
φ	-	Angle in the horizontal plane
ψ	-	Angle in the vertical plane
ω	-	Angle at the center

Subscripts

abs	absolute
adj	adjusted
calc	calculated
code	code output
cond	condensation
ecc	emergency core cooling
ex	exchange
exp	experimental
l	liquid
ln	logarithmic
pot	potential
pred	predicted
ps	pump simulator
ref	reference
rel	relative
rk	rake

s	steam
sat	saturation

1 - Introduction

With 56 nuclear reactors in operation, 1 under construction and 6 more planned, France is a pioneer in the production of electricity from nuclear energy [1]. The French fleet is composed by Pressurised Water Reactors (PWRs), where the nuclear core is cooled down by light water at high pressure. The performances of these reactors must be assessed during the design phase, for safety analyses of accidental scenarios and for licensing purposes. In particular, the cooling of the reactor core should be ensured at any time to avoid fuel damage and potential release of radiation. For those reasons, simulation tools have been developed in the past 70 years to simulate the transient behaviour of the reactors.

1.1 . Simulation tools for nuclear systems and calibration of empirical correlations

Since the 70s, simulations of a complex and large system, such as a PWR composed by several compontents (e.g. pipes, pumps and steam generators), have been a challenge. The behaviour of all the components in the reactor must be simulated in a wide range of physical situations (e.g. all two-phase flow regimes, heat transfer regimes, flow conditions and geometries) to prove to the regulatory authority the safety of the nuclear power plant during normal and accidental conditions [2].

Different levels of detail can be reached on the description of the thermal-hydraulic phenomena in the cooling loops. For example, the understanding of local aspects can be handled with a CFD (Computational Fluid Dynamics) code (e.g. one-phase flow inlet pressure drop in the nuclear core [3]), but a significant computational cost is required. The whole cooling loop is instead modelled via thermal-hydraulic system codes which capture its macroscopic behavior and represent a good compromise between simulation accuracy and computational cost.

Thermal-hydraulic system codes (such as RELAP [4], TRACE [5] and CATHARE [6]) are usually based on the so-called 2-fluid 6-equations model [7]. In order to reduce the complexity of the simulation, the balance equations of mass, momentum and energy (3 for liquid and 3 for gas) are time- and space-averaged on appropriate time steps and control volumes. Hence, the spatial distribution and the temporal variations of the phases in the control volumes are not taken into account.

Due to the time- and space-averaging procedure, several closure laws (also called physical models or correlations) need to be defined in the equations. The energy equation [8] to be averaged is reported as example here below:

$$\rho \cdot \frac{DI}{Dt} = -grad(\dot{\mathbf{q}}'') + \dot{q}''' + \frac{DP}{Dt} + \phi \tag{1.1}$$

where the product of the density ρ and the Lagrangian derivative of the entalphy I in the control volume is equal to the sum of the negative gradient of the specific heat flux vector $\dot{\mathbf{q}}''$, the volumetric heat flux $\dot{q}'''$, the Lagrangian derivative of the pressure P and a dissipation function ϕ (i.e. the dissipation to heat due to viscous stresses). In this equation, the specific heat flux vector $\dot{\mathbf{q}}''$ can represent the heat transfer with the walls and the volumetric heat flux $\dot{q}'''$ the heat transfer at the liquid interface. These heat fluxes are part of the Quantities of Interest (QoIs) for thermalhydraulic codes. Unfortunately, they are unknown and they should be modelled through empirical correlations. Let us call $z_{calc}(\mathbf{x}, \boldsymbol{\theta})$ a generic QoI (e.g. $\dot{\mathbf{q}}''$, $\dot{q}'''$) as a function of state variables $\mathbf{x}$ (e.g. the experimental conditions, such as temperature, pressure or dimensionless numbers) and a set of parameters $\boldsymbol{\theta}$. An example of physical model is the following one:

$$z_{calc}(\mathbf{x}, \boldsymbol{\theta}) = \theta_0 \cdot x_1^{\theta_1} \cdot x_2^{\theta_2} \tag{1.2}$$

where (x_1, x_2) are 2 state variables and (θ_0, θ_1, θ_2) are 3 parameters (e.g. the Dittus and Boelter correlation [9] for the turbulent wall-liquid heat transfer in a circular smooth pipe $Nu = 0.023 \cdot Re^{0.8} \cdot Pr^{0.4}$).

The estimation of $z_{calc}(\mathbf{x}, \boldsymbol{\theta})$ requires to calibrate the model parameters $\boldsymbol{\theta}$ through comparison between experiments and the calculated QoI [10]. The discrepancy between real world experiments and their mathematical representation shoud be reduced as low as possible in order to have an accurate representation of the reality. Moreover, the experimental QoI used in the calibration phase should be dependent as much as possible on the phenomenon to be mathematically modelled. Thus, the employed experimental database is of great importance.

In thermal-hydraulic, the experiments (often carried out at a smaller scale than a real PWR) can be divided in:

- Separate Effect Tests (SETs), where only one physical phenomenon has a measurable effect on the experimental QoI (e.g. in single-phase flow experiments, the measured wall temperature is mostly impacted by the wall-liquid heat transfer coefficient);
- Combined Effect Tests (CETs), where multiple phenomena interact with each other and affect simultaneously the experimental QoI;
- Integral Effect Tests (IETs), where all the main components of a PWR are simulated and the integral effect on the thermal-hydraulic system is observed.

When SETs are available, the calibration of the mathematical model can be easily performed (e.g. [9]). However, sometimes only CETs are available. This complicates the calibration with a risk to introduce compensating errors. In some cases, an experimental analysis of the tests may allow the thermal-hydraulic experts to decouple the effects and reduce the CETs in SETs. Hence, the experimental analysis is fundamental for the robustness of the calibration.

Finally, the whole process described above allows computing the macroscopic behaviour of the cooling system in a fast and reliable way.

1.2 . Best Estimate Plus Uncertainty (BEPU)

The aim of the licensing and safety studies is to prove to the regulatory authority that the reactor can operate safely in nominal conditions and that certain safety limits (e.g. the fuel cladding should not melt) are respected during postulated accidental scenarios. As schematised in Fig. 1.1, the real safety margin can be ideally evaluated comparing the real value of the QoI (e.g. the peak cladding temperature in the core) to its associated safety limit (e.g. the fusion temperature of the cladding).

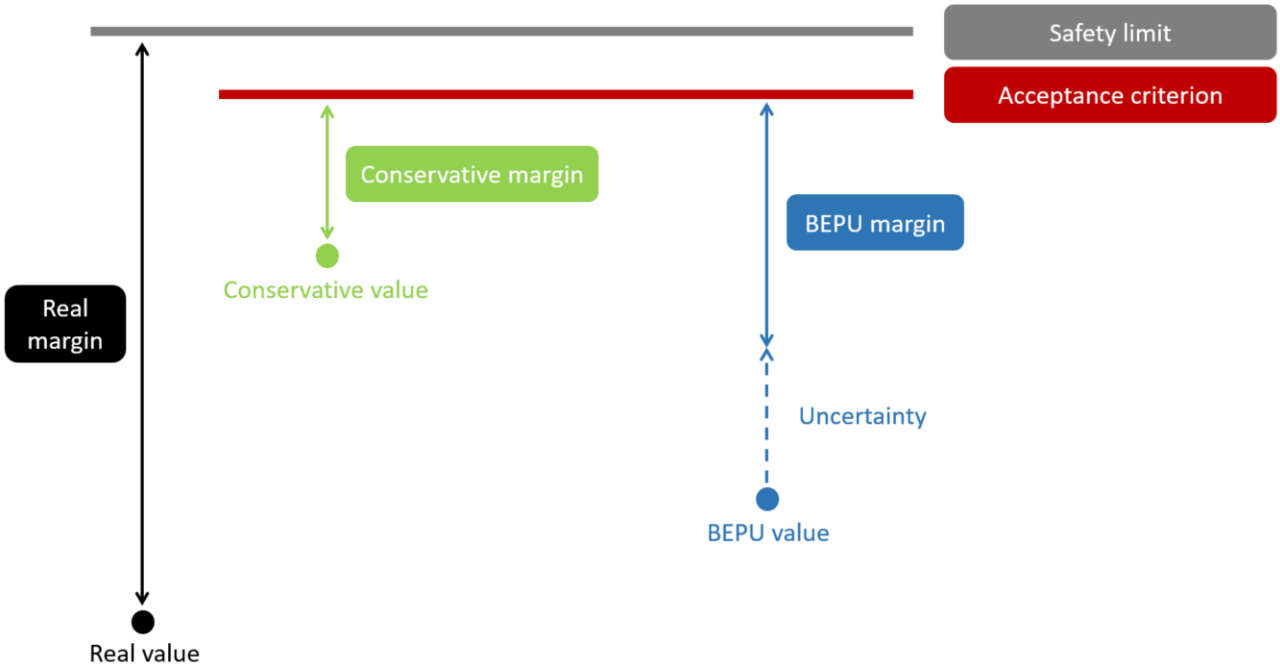

Figure 1.1: Safety margin calculations with different approaches.

Unfortunately, the real value is unknown in practical applications. The safety limit is defined by the regulatory body as an acceptance criterion, lower than the actual safety limit. For example, the acceptance criterion for the peak cladding temperature is 1204.4 °C, according to the US federal regulation 10 CFR50.46 [11].

The real value of the QoI can be estimated only via simulations with thermal-hydraulic system codes. Two main kinds of approaches are possible [12]: the conservative (green in Fig. 1.1) and the Best Estimate Plus Uncertainty (BEPU) one (blue in Fig. 1.1). The conservative simulations are performed with penalising (and sometimes unphysical) assumptions both for the input parameters and the physical models in the code. The goal is to obtain the worst possible value of the QoI, in order to quantify a conservative safety margin. This approach started to be questioned at the end of the 80s, since it may lead to results which are unrealistic and possibly non-conservative. In fact, the use of individually penalising assumptions does not guarantee that their combination results in the worst possible set of conditions. These considerations led to the development of BEPU. In this approach, the simulations are performed via Best-Estimate (BE) system codes, where the physical phenomena are modelled as realistically as possible (the blue point in Fig. 1.1, i.e. nearer to the real value than the green one). The uncertainties associated to the BE value of the QoI are then quantified and the upper (or lower) limit of the uncertainty band is employed to evaluate the safety margin.

In order to demonstrate the capability of the system codes to be best-estimate, a process of Verification and Validation (V&V) is necessary [13, 14]. The verification phase aims at verifying that the equations are correctly implemented and solved and the code behaves numerically as intended. The validation consists in comparing the code calculation results with the measurements obtained in thermal-hydraulic experiments, in order to demonstrate the capability of the code to predict the reactor behaviour in the range of conditions of interest. In the validation phase, all the experiments (i.e. SETs, CETs and IETs) can be simulated through the BE code to validate its predictions. The Uncertainty Quantification (UQ) aims at evaluating the uncertainty on the QoI.

Several methods (e.g. CSAU [15], GRS [16], CIAU [17]) have been developed for the UQ required by BEPU. Among these methods, the most commonly used are based on the propagation of input uncertainties. Thus, one of the crucial issue in the BEPU methodology is the identification and quantification of the input uncertainties to be propagated. The latter are part of the following sources of input uncertainty [13]:

- Experimental uncertainty, e.g. due to the measurement noise;
- Model (or epistemic) and parameter uncertainties, caused by the incomplete mathematical modelling of the phenomena and the inaccurate calibration of the correlation parameters $\boldsymbol{\theta}$;
- Code uncertainty, due to the mathematical approximations and numerical schemes of the code when computing the output value;
- Plant uncertainty, related to the geometry of the system and its initial and boundary conditions;
- Scaling uncertainty, due to the use of models developed on scaled experiments to a full scale reactor;
- Representation uncertainty, caused by the nodalisation of the systems [18], i.e. the uncertainty in the physical discretisation;
- User's uncertainty, related to the modelling choices of the code user.

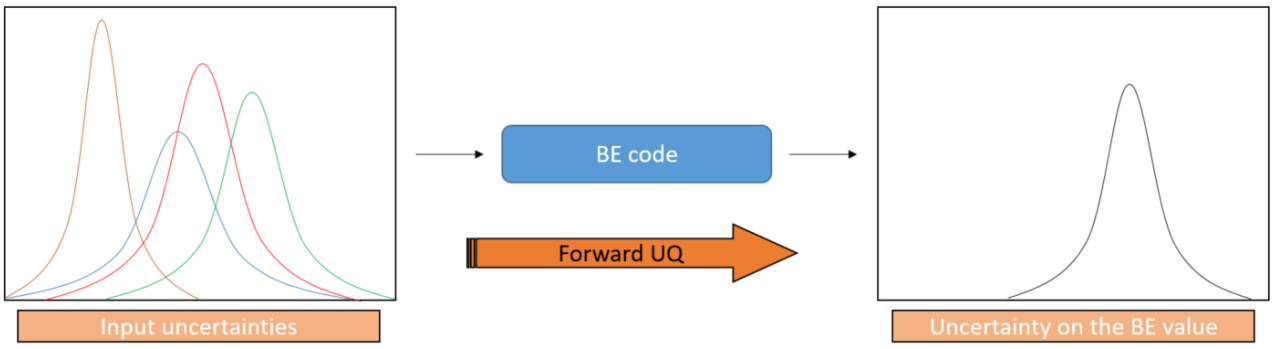

Figure 1.2: Forward UQ for BEPU applications.

The thermal-hydraulic expert, depending on the chosen UQ method, select several uncertainties from the list above as input uncertainties (expressed via a probability distribution function -

pdf). Then, the pdfs are propagated throughout the BE code and a pdf of the output QoI is obtained (as shown in Figure 1.2). This process is called Forward UQ.

1.3 . Inverse Uncertainty Quantification (IUQ)

One of the major issues for the Forward UQ is to define the input uncertainties. Historically, the estimation of these uncertainties relied heavily on expert judgment [19]. However, nowadays, more rigorous and robust methodologies (e.g. CIRCE [20] and many more [21]) are usually applied. These methodologies quantify the uncertainties associated to the physical models in the code through an Inverse Uncertainty Quantification (IUQ). As shown in Figure 1.3, the input uncertainties are estimated by comparing the BE simulation results to the measurements from experiments representative of the phenomenon, component or cooling system under study.

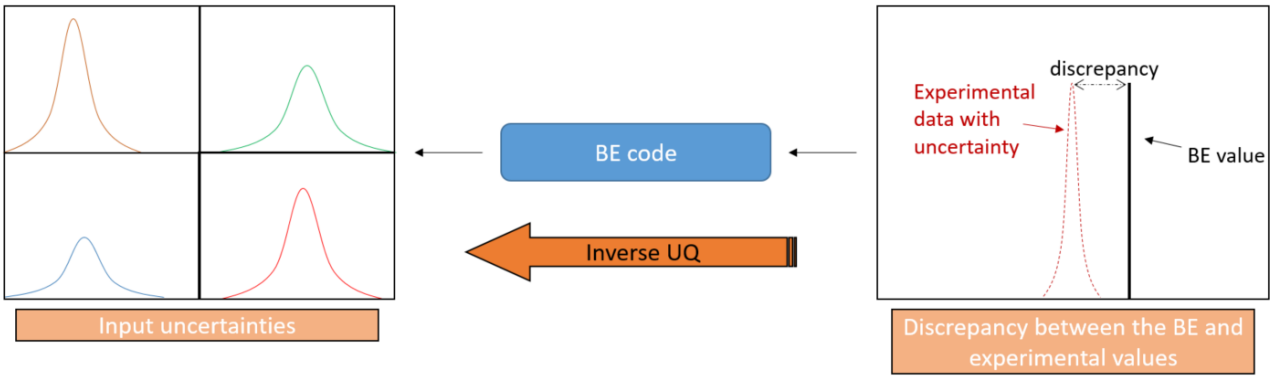

Figure 1.3: IUQ for the estimation of the input uncertainties.

Ideally, the IUQ should be applied to SETs in order to quantify the uncertainty of the model influencing the QoI. However, SETs are not always available and sometimes CETs should be used. In this case, the IUQ methodology is applied to jointly assess the uncertainty of two or more models. The model uncertainty of a closure law can be modelled as follows:

$$\mathbf{z}_{pred}(\mathbf{x}, \boldsymbol{\theta}) = \Lambda \cdot \mathbf{z}_{calc}(\mathbf{x}, \boldsymbol{\theta}) \tag{1.3}$$

where $\mathbf{z}_{calc}(\mathbf{x}, \boldsymbol{\theta})$ is the punctual value computed by the physical model, $\Lambda = (\mathscr{L})\mathscr{N}(m_\lambda, \sigma_\lambda^2)$ is the (log-)normal distribution that represents the model uncertainty and links the *calculated* value to the *predicted* one $\mathbf{z}_{pred}(\mathbf{x}, \boldsymbol{\theta})$.

The goal of the IUQ is to estimate the mean m_λ and variance σ_λ^2 of the distribution. However, in the case where CETs are used to jointly quantify the uncertainties of several models, if one model is not highly influential on the code output, the IUQ methodology (namely CIRCE) might estimate its uncertainty with low accuracy and precision due to the identifiability issue [22].

1.4 . Condensation phenomena in the cold leg of a PWR in case of LOCA

In this doctoral work, we focus on the calibration and IUQ of the steam-liquid heat transfer closure law in the energy equation (i.e. $\dot{q}'''$ in Eq. 1.1). In particular, we focus on the Emergency Core Cooling (ECC) condensation model, for which only CETs are available. Indeed, during a

postulated Loss of Coolant Accident (LOCA), a break occurs in the primary loop that causes a sudden depressurisation, a loss of liquid inventory and a significant steam production. In order to cool down the reactor core, cold water is injected in the cold legs of the PWR via the ECC system, as shown in Fig. 1.4.

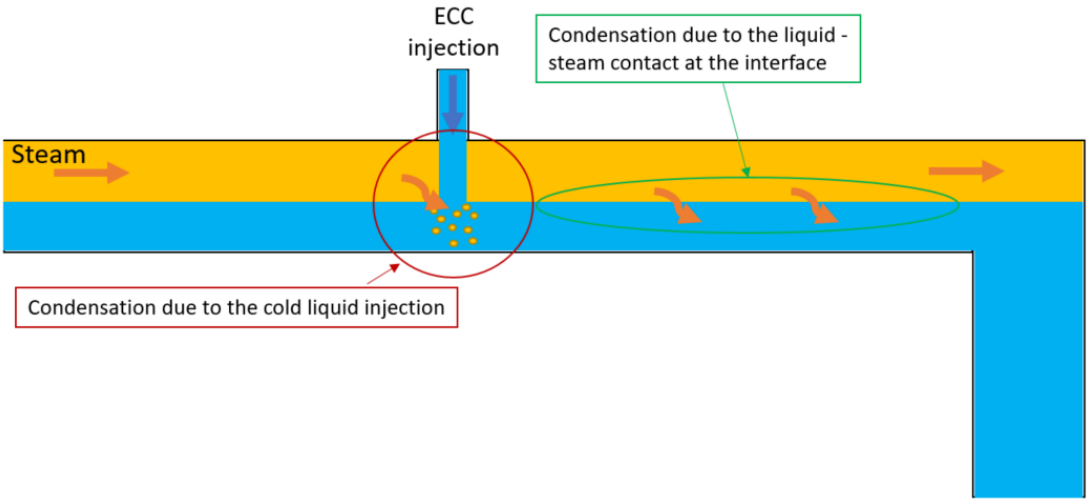

Figure 1.4: Main phenomena occurring in the cold leg of a PWR during the ECC injection.

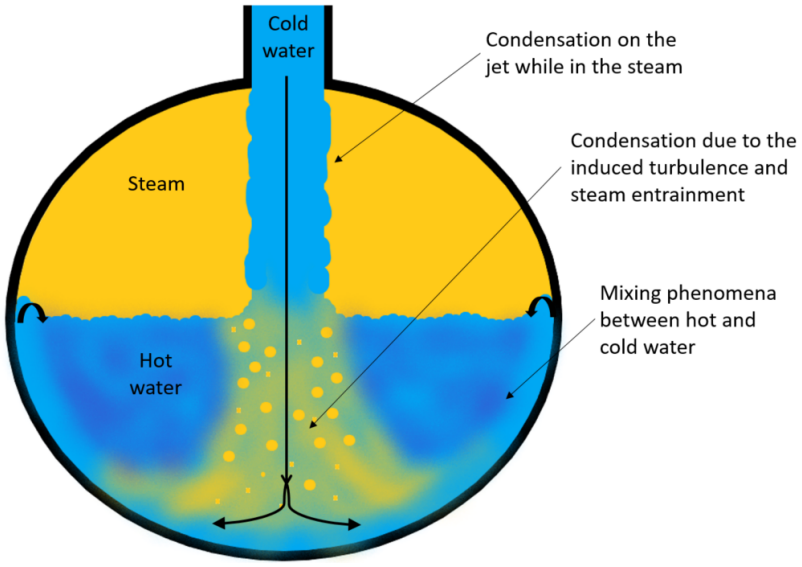

Figure 1.5: Local condensation phenomena occurring in the ECC region.

The contact between the cold water (in blue) and the steam (in yellow) causes the condensation of the latter which heats up the injected water. An accurate modelling of the condensation in the cold leg is crucial to correctly predict the pressure evolution in the primary loop and to evaluate the potential risk of Pressurized Thermal Shock (PTS) on the vessel walls. The PTS phenomenon can occur when the cold liquid flow coming from the cold leg enters in contact with the vessel generating high temperature gradients, which could damage its structural integrity [23].

In Fig. 1.4, two main condensation phenomena can be identified at the safety injection: the condensation induced by the cold liquid injection on the liquid jet, turbulence and steam entrainment in the ECC region (red circle) and the condensation at the liquid interface of the stratified flow (green ellipse). The former is the main driver mechanism of the global condensation inside the cold leg [24] and we are interested in modelling it.

In Fig. 1.5, the local phenomena occurring during the cold injection are illustrated [25]. From the ECC pipe exit until the impact with the liquid flow, the steam condenses over the cold jet. Then, the impact generates steam entrainment in the liquid that strengthens the condensation. At the same time, mixing phenomena occur in the liquid flow between the cold and hot water. At the flow surface, the lateral rebounds caused by the injection create waves that increase the condensation. These phenomena have been studied in the past [25] as presented in Chapter 5. However, the condensation mechanisms at the ECC are not clear nowadays and further investigations are needed to model them.

1.5 . Objective of the research work

The current doctoral research aims at developing, validating and quantifying the uncertainties of a new ECC condensation model. Advanced statistical methodologies for the calibration and IUQ of thermal-hydraulic models are presented.

The first objective is the development of a Bayesian framework for the calibration, validation and uncertainty quantification of thermal-hydraulic models, where the predictions and the model outputs are linked by a multiplicative model uncertainty (Eq. 1.3). Usually, the parameters of the correlations are calibrated against SETs (e.g. through a multivariate linear regression) and only the model uncertainty is quantified. However, if the experimental database is small (as it is the case in nuclear thermal-hydraulic), the uncertainty on the parameter values may not be negligible. Thus, in this new framework the Bayesian inference is employed to estimate also the uncertainty of the model parameters.

The second objective of the work is the extension of the CIRCE methodology (i.e. one of the most widely applied IUQ methods in nuclear thermal-hydraulic [26]) to improve the IUQ in the presence of CETs. The goal is to find an appropriate solution to this issue extending the applicability of the CIRCE methodology.

The third objective is the detailed experimental analysis of three CET experiments (COSI, TOPFLOW-PTS and UPTF) with the goal to decouple the condensation phenomena into SETs. Then, a condensation model at the ECC injection is assessed, developed and validated using the reduced experimental database.

1.6 . Outline of the thesis

This doctoral thesis is composed by 7 chapters. In Chapter 2, the Bayesian framework for the assessment, validation and UQ of a thermal-hydraulic model is presented. In particular, the model updating equation and its main assumptions are introduced. Then, the Bayesian calibration is proposed to estimate the parameter and the model uncertainties. In Chapter 3, the CIRCE methodology is briefly summarised and improved for CETs under the name of CIRCE 2-Steps. Chapter 4 presents the ECC injection phenomenology and the thermal-hydraulic analysis of the experimental database. In Chapter 5, the correlations found in the literature are assessed and a new ECC condensation model is developed and validated using

the Bayesian framework described in Chapter 2 and the experimental database established in Chapter 4. In Chapter 6, the CIRCE methodology and the newly developed CIRCE 2-Steps are applied to the IUQ of the condensation models in the cold leg. The results are summarised in Chapter 7 and recommendations for future works are given.

1.7 . Outline of the published work

Paper I is related to the Bayesian methodology proposed in Chapter 2. Moreover, the framework is applied to a reduced experimental database (with respect to the one used in this doctoral work) to calibrate a condensation model. In Paper II, the thermal-hydraulic analysis of Chapter 4 and the calibration of the new condensation model (Chapter 5) through a multivariate linear regression are presented. Paper III briefly summarises the CIRCE methodology and improves it for CETs under the name of CIRCE 2-Steps. After the application of both methods to some analytical exercises, they are applied to the correlations simulating the condensation in the cold leg.

2 - The Bayesian framework for the development, validation and uncertainty quantification of a physical model

This chapter is related to Paper I, where the Bayesian methodology is proposed and the framework is applied to the COSI database to calibrate a condensation model.

The calibration of physical correlations is generally performed by minimising a cost function, which quantifies the discrepancy between the model outputs and the experimental values [10]. The correlation best-fitting parameters $\boldsymbol{\theta}$ (see Eq. 1.2) are often calibrated through a multivariate log-linear regression [27]. A disadvantage of this calibration is that it does not allow jointly estimating the parameter and model uncertainties. On the contrary, modelling $\boldsymbol{\theta}$ as a random variable, the Bayesian probabilistic framework [28, 29] is more and more employed in nuclear thermal-hydraulics [30, 31, 32] and permits the calibration of the best-fitting parameters and the estimation of the associated uncertainties [33]: the one called parameter uncertainty and associated to the parameters $\boldsymbol{\theta}$ and the one called model uncertainty and associated to the lack of knowledge of the phenomenon and its imperfect modelling [34].

In Section 2.1, the model updating equation and the modelling of the associated uncertainties are defined. The Bayes theorem and its resolution when a noninformative prior probability is selected is presented in Section 2.2. In Section 2.3, the statistical indicators used to assess the best-estimate model performances are introduced. Finally, the model is statistically validated in Section 2.4 and the associated uncertainties are quantified in Section 2.5.

2.1 . Model updating equation

The predicted QoI $z_{pred}(\mathbf{x}, \boldsymbol{\theta})$ of a physical model is composed by two terms, the punctual value calculated by the mathematical function $z_{calc}(\mathbf{x}, \boldsymbol{\theta})$, which includes the parameters uncertainty, and the probability density representing the model uncertainty $\Lambda(\mathbf{x})$ [30]:

$$\mathbf{z}_{pred}(\mathbf{x}, \boldsymbol{\theta}) = \mathbf{z}_{calc}(\mathbf{x}, \boldsymbol{\theta}) + \Lambda(\mathbf{x}) \tag{2.1}$$

where $\mathbf{x}$ is the vector of the state features (e.g. dimensionless numbers) and $\boldsymbol{\theta}$ are the model parameters to be calibrated against the experimental database.

The following model updating equation [35] represents the statistical problem, which assumes that the experimental QoI $\mathbf{z}_{exp}(\mathbf{x})$ is equal to the predicted value in Eq. 2.1 up to an experimental error or uncertainty ϵ:

$$\mathbf{z}_{exp}(\mathbf{x}) = \mathbf{z}_{pred}(\mathbf{x}, \boldsymbol{\theta}) + \epsilon = \mathbf{z}_{calc}(\mathbf{x}, \boldsymbol{\theta}) + \Lambda(\mathbf{x}) + \epsilon \tag{2.2}$$

where the experimental uncertainty is modelled as a normal distribution $\epsilon \sim \mathcal{N}(0, \sigma_\epsilon^2)$. Being often difficult or impossible to quantify, the variance σ_ϵ^2 can be neglected. This strong assumption is motivated by the request of nuclear safety authorities to conservatively quantify the uncertainties of physical models used in thermal-hydraulic system codes. Thus, the experimental uncertainty is neglected and the model one is overestimated [26, 36].

Following this assumption, the probabilistic relationship between $\mathbf{z}_{exp}(\mathbf{x})$ and $\mathbf{z}_{calc}(\mathbf{x}, \boldsymbol{\theta})$ from Eq. 2.2 can be rewritten as:

$$\mathbf{z}_{exp}(\mathbf{x}) = \mathbf{z}_{calc}(\mathbf{x}, \boldsymbol{\theta}) + \Lambda(\mathbf{x}) \tag{2.3}$$

where the variance of the model uncertainty is dependent on the experimental conditions: $\Lambda(\mathbf{x}) \sim \mathcal{N}(0,\, \sigma^2(\mathbf{x}))$.

The Bayesian framework calibrates the set of parameters $\boldsymbol{\theta}$ so that the physical model $\mathbf{z}_{calc}(\mathbf{x}, \boldsymbol{\theta})$ can reproduce as correctly as possible the experimental data $\mathbf{z}_{exp}(\mathbf{x})$.

The additive model uncertainty in Eq. 2.3 is function of the experimental setups and thus difficult to estimate (e.g. in [37] it is modelled as a Gaussian Process). In [30, 31], the authors proposed to drop the hypothesis of dependance between the uncertainty variance and the experimental conditions: $\Lambda \sim \mathcal{N}(0,\, \sigma^2)$. However, this approach leads to homoscedastic realisations of Λ which are not appropriate for the calibration of thermal-hydraulic models (where the absolute error is proportional to the experimental value). In this doctoral work, the model uncertainty is thus scaled with the calculated QoI [38], taking indirectly into account the different thermal-hydraulic scales of the experiments composing the database:

$$\mathbf{z}_{exp}(\mathbf{x}) = \mathbf{z}_{pred}(\mathbf{x}, \boldsymbol{\theta}) = \Lambda \cdot \mathbf{z}_{calc}(\mathbf{x}, \boldsymbol{\theta}) \tag{2.4}$$

where the uncertainty Λ is equal to $\Lambda \sim \mathscr{LN}(0,\, \sigma^2)$. After the application of the logarithm function, Eq. 2.4 gives homoscedastic discrepancies $\ln(\mathbf{z}_{exp}(\mathbf{x})) - \ln(\mathbf{z}_{calc}(\mathbf{x}, \boldsymbol{\theta}))$. Thus, the variance is constant and independent to the experimental conditions (resulting in an easier estimation of σ^2).

The Bayesian methodology can be applied to Eq. 2.4, where the unknown parameters $\boldsymbol{\theta}$ are estimated as probability densities.

2.2 . Bayesian calibration of the model parameters

In the proposed Bayesian inference [39] approach, the model parameters $\boldsymbol{\theta}$ are modelled as random variables and the joint *posterior* distribution $\tau(\boldsymbol{\theta}, \sigma^2 | \mathbf{z}_{exp}(\mathbf{x}))$ is estimated. The Bayes formula relies the *posterior* distributions to its *prior* $\tau(\boldsymbol{\theta}, \sigma^2)$ through the likelihood-function $\mathcal{L}(\mathbf{z}_{exp}(\mathbf{x}) | \boldsymbol{\theta}, \sigma^2)$:

$$\tau(\boldsymbol{\theta}, \sigma^2 | \mathbf{z}_{exp}(\mathbf{x})) \propto \mathcal{L}(\mathbf{z}_{exp}(\mathbf{x}) | \boldsymbol{\theta}, \sigma^2) \cdot \tau(\boldsymbol{\theta}, \sigma^2) \tag{2.5}$$

The estimator denoted by $\boldsymbol{\theta}^{MAP}$ (Maximum A Posteriori) refers to the parameter value that maximises this *posterior* distribution.

Assuming that the experimental database is composed by n experimental realisations $z_{exp}(\mathbf{x}_i)$, the logarithm of Eq. 2.4 reads for $1 \leq i \leq n$:

$$\ln(z_{exp}(\mathbf{x}_i)) = \ln(z_{calc}(\mathbf{x}_i, \boldsymbol{\theta})) + \ln(\lambda_i) \quad \text{with} \quad \ln(\lambda_i) \sim \mathcal{N}(0, \sigma^2) \tag{2.6}$$

If $\ln(z_{calc}(\mathbf{x}_i, \boldsymbol{\theta}))$ is linear in the parameters $\boldsymbol{\theta}$, we can write $\ln(\mathbf{z}_{calc}(\mathbf{x}, \boldsymbol{\theta})) = K(\mathbf{x}) \cdot \boldsymbol{\theta}$ (with $K(\mathbf{x}) = [k(\mathbf{x}_1), ..., k(\mathbf{x}_n)]^T$ matrix of the model features). Eq. 2.6 is a log-log linear regression characterised by a dimensionless and symmetrical uncertainty distribution. The analytical solution reads:

$$\boldsymbol{\theta}^{MAP} = \Big(K(\mathbf{x})^T \cdot K(\mathbf{x})\Big)^{-1} \cdot K(\mathbf{x})^T \cdot \ln(z_{exp}(\mathbf{x})) \tag{2.7}$$

In order to estimate the parameter uncertainty, the distribution of $\boldsymbol{\theta}$ must be computed. Since we have no information on the parameters, their joint *prior* distribution $\tau(\boldsymbol{\theta}, \sigma^2)$ is assumed to be uninformative. Thus, a common choice is to select the independent Jeffreys prior [40], resulting in $\boldsymbol{\theta}$ and σ^2 to be independent:

$$\tau(\boldsymbol{\theta}, \sigma^2) \propto \tau(\boldsymbol{\theta}) \cdot \tau(\sigma^2) \propto 1 \cdot \frac{1}{\sigma^2} \tag{2.8}$$

where the marginal *prior* distribution of $\boldsymbol{\theta}$ is set to 1 since all the values have the same probability. The Bayes formula gives a well-defined *posterior* distribution, which is normalised and explicited as a normal-inverse-gamma distribution:

$$\tau(\boldsymbol{\theta}, \sigma^2 | \ln(z_{exp}(\mathbf{x}))) = \overbrace{\tau(\boldsymbol{\theta} | \ln(z_{exp}(\mathbf{x})), \sigma^2)}^{\mathcal{N}} \overbrace{\tau(\sigma^2 | \ln(z_{exp}(\mathbf{x})))}^{\mathcal{IG}} \tag{2.9}$$

The marginal posterior distribution of $\boldsymbol{\theta}$ is a Student law. This distribution can be traced by firstly sampling $\sigma^2 | \ln(z_{exp}(\mathbf{x}))$ and then sampling $\boldsymbol{\theta}$ conditional on σ^2 and $\ln(z_{exp}(\mathbf{x}))$. When n is high enough, the marginal *posterior* distribution $\tau(\boldsymbol{\theta} | \ln(z_{exp}(\mathbf{x})), \sigma^2)$ can be approximated by a normal distribution [41].

Finally, the model calculates the best estimate value of the QoI $z_{calc}(\mathbf{x}, \boldsymbol{\theta}^{MAP})$ with a model uncertainty equal to $\Lambda = \mathscr{LN}(0,\ {\sigma^2}^{MAP})$ (where ${\sigma^2}^{MAP}$ is the MAP value of $\tau(\sigma^2 | \ln(z_{exp}(\mathbf{x})))$) and a parameter uncertainty given by $\tau(\boldsymbol{\theta} | \ln(z_{exp}(\mathbf{x})), \sigma^2)$. The final expressions for the model and parameters uncertainty are described in Section 2.5.

2.3 . Model performance assessment

The performance of the correlation at predicting the QoI can be evaluated over two statistical indicators: the R-squared and relative and absolute residuals.

2.3.1 . The R-squared

The measure of goodness of the fit can be measured by the coefficient of determination R^2. It reads [42]:

$$R^2 = 1 - \frac{\sum_{i=1}^{n} (\ln(z_{exp,i}(\mathbf{x}_i)) - \ln(z_{calc,i}(\mathbf{x}_i, \boldsymbol{\theta}^{MAP})))^2}{\sum_{i=1}^{n} (\ln(z_{exp,i}(\mathbf{x}_i)) - \overline{\ln(z_{exp}(\mathbf{x}))})^2} \tag{2.10}$$

The statistical indicator R^2 can be seen as the ratio of the predictions variance to the experimental variance. Hence, it varies between 0 and 1. A $R^2 = 1$ corresponds to the higher prediction quality.

2.3.2 . Relative and absolute residuals

The residuals can be calculated using the experimental and calculated data. From Eq. 2.6, the residual is the difference between two logarithms. However, this difference is hardly interpretable from a physical point of view. Thus, the residuals r_{QoI} are written as a relative or absolute difference between the calculated and experimental QoI.

Without loss of generality, let us take a calculated z_{calc} and experimental z_{exp} value. The relative difference (in percentage) is expressed in Eq. 2.11, while the absolute difference in Eq. 2.12. Both the residuals are given with and without modulus.

$$\begin{aligned} r_{rel,z} &= \frac{z_{calc,i} - z_{exp,i}}{z_{exp,i}} \\ |r_{rel,z}| &= \left| \frac{z_{calc,i} - z_{exp,i}}{z_{exp,i}} \right| \end{aligned} \tag{2.11}$$

$$\begin{aligned} r_{abs,z} &= z_{calc,i} - z_{exp,i} \\ |r_{abs,z}| &= |z_{calc,i} - z_{exp,i}| \end{aligned} \tag{2.12}$$

If the residual is small, the metric in Eq. 2.11 is similar to (and preferred over) the difference between logarithms.

For our calibrated model, the arithmetic mean μ over n (the number of tests) of the relative residuals (i.e. $\mu(r_{rel,z})$) is expected close to zero by definition [43] and estimates the accuracy of the correlation. The standard deviation σ of the same residuals batch gives the precision of the estimation. The mean of the values with the modulus (i.e. $\mu(|r_{rel,z}|)$) is also proposed since it indicates the average error over the prediction.

Sometimes, it makes more sense from an engineering point of view to analyse the absolute residuals. When appropppriate, the same statistics (i.e. μ and σ) can also be computed for the absolute residuals in Eq. 2.12.

2.4 . Statistical validation

The normality assumptions of the model uncertainty $\ln(\Lambda)$ needs a statistical validation. Since the experiments are limited and the thermal-hydraulic databases are often small, the same tests can be used both for model calibration and normality validation. Thus, a cross validation technique named Leave One Out (LOO) [44] is employed. It is composed of two steps:

1. The assessment database is reduced to $n-1$ experimental data removing the test ν. The new database is referred as $\ln(\mathbf{z}_{exp}^{-\nu}(\mathbf{x}^{-\nu}))$;
2. The predictive *posterior* distribution of the unused experiment $\tau(\ln(z^{\nu}(x^{\nu}))|\ln(\mathbf{z}_{exp}^{-\nu}(\mathbf{x}^{-\nu})))$ is compared to the removed experimental value $\ln(z_{exp}^{\nu}(x^{\nu}))$.

The predictive distribution of step 2 reads:

$$\tau(\ln(z^{\nu}(x^{\nu}))|\ln(\mathbf{z}_{exp}^{-\nu}(\mathbf{x}^{-\nu}))) = \int_{\mathbb{R}^{\Theta}} \int_{0}^{+\infty} \overbrace{\tau(\ln(z^{\nu}(x^{\nu}))|\ln(\mathbf{z}_{exp}^{-\nu}(\mathbf{x}^{-\nu})), \boldsymbol{\theta}, \sigma^2)}^{\mathscr{N}} \overbrace{\tau(\boldsymbol{\theta}, \sigma^2|\ln(\mathbf{z}_{exp}^{-\nu}(\mathbf{x}^{-\nu})))}^{\mathscr{NIG}} d\sigma^2 d\theta \tag{2.13}$$

If n is adequately high, the analytical solution of the integral (i.e. a Student law [41]) can be approximated by a Gaussian distribution.

The two steps are repeated n times, interchanging each time the suppressed test ν. Finally, the n standardised residuals between the suppressed values and the associated predictions (Eq. 2.4) can be plotted. The resulting distribution is compared with a standard Gaussian distribution through the Kolmogorov-Smirnov test [45] and the Quantile-Quantile (QQ) plot [46] (i.e. experimental quantiles plotted as a function of the theoretical ones). If these tests are not rejected at 5% threshold, the normality assumption is not put into question.

2.5 . Uncertainty quantification

The model and parameter uncertainties can be evaluated after the calibration and statistical validation phases.

2.5.1 . Propagation of the parameter uncertainties

The marginal *posterior* distribution $\tau(\boldsymbol{\theta}|\ln(z_{exp}(\mathbf{x})), \sigma^2)$ in Eq. 2.9 can be used to propagate the parameter uncertainties to the model output. The probability density of the calculated value i is a normal distribution with expected value $\mathbb{E}(\mathbf{z}_{calc}(\mathbf{x}, \boldsymbol{\theta})|\ln(\mathbf{z}_{exp}(\mathbf{x})))$ and variance $\mathbb{V}(\mathbf{z}_{calc}(\mathbf{x}, \boldsymbol{\theta})|\ln(\mathbf{z}_{exp}(\mathbf{x})))$. It reads:

$$\tau(\ln(\mathbf{z}_{calc,i}(\mathbf{x}_i, \boldsymbol{\theta}))|\ln(\mathbf{z}_{exp}(\mathbf{x}))) \sim \mathcal{N}(\mathbb{E}(\ln(\mathbf{z}_{calc}(\mathbf{x}, \boldsymbol{\theta}))|\ln(\mathbf{z}_{exp}(\mathbf{x}))), \mathbb{V}(\ln(\mathbf{z}_{calc}(\mathbf{x}, \boldsymbol{\theta}))|\ln(\mathbf{z}_{exp}(\mathbf{x})))) \quad (2.14)$$

In Eq. 2.14, the model variance σ^2 is not taken into account, which results in propagating only the parameter uncertainty.

2.5.2 . Derivation of the model uncertainty

If the features of the model are sufficiently influential on the modelled physical phenomenon, the parameters θ have low uncertainty, which may be neglected. The parameters can then be fixed at their MAP values and the model uncertainty Λ stems from the *posterior* distribution of σ^2. The *predicted* value for a test i has the following distribution:

$$\tau(\ln(\mathbf{z}_{pred,i}(\mathbf{x}_i))|\ln(\mathbf{z}_{calc,i}(\mathbf{x}_i, \boldsymbol{\theta}^{MAP}))) = \int_{\mathbb{R}^\Sigma} \overbrace{\tau(\ln(\mathbf{z}_{pred,i}(\mathbf{x}_i))|\ln(\mathbf{z}_{calc,i}(\mathbf{x}_i, \boldsymbol{\theta}^{MAP})), \sigma^2)}^{\mathcal{N}} \overbrace{\tau(\sigma^2|\ln(\mathbf{z}_{exp}(\mathbf{x})))}^{\mathcal{IG}} d\sigma^2 \quad (2.15)$$

For practical applications, the MAP value of σ^2 can be used to compute the distribution of the *predicted* output:

$$\ln(z_{pred,i}(\mathbf{x}_i)) = \ln(z_{calc,i}(\mathbf{x}_i, \boldsymbol{\theta}^{MAP})) + \ln(\lambda_i) \quad \text{with} \quad \ln(\lambda_i) \sim \Lambda = \mathcal{N}(0, {\sigma^2}^{MAP}) \quad (2.16)$$

In Eq. 2.16, the *predicted* QoI is the sum of the *calculated* value plus the model uncertainty. Neglecting the uncertainty on σ^2 and fixing its value to ${\sigma^2}^{MAP}$, the fluctuation interval at 95% ($IF_{95\%}$) can be computed from the model uncertainty log-normal distribution:

$$IF_{95\%}(\Lambda) = \left[exp(-1.96 \cdot \sqrt{\sigma^{2MAP}}), exp(1.96 \cdot \sqrt{\sigma^{2MAP}})\right] \tag{2.17}$$

3 - The extension of the CIRCE methodology for the inverse uncertainty quantification of several coupled thermal-hydraulic models

This chapter is related to the second part of Paper III, where the CIRCE methodology is summarised and improved for CETs under the name of CIRCE 2-Steps. Moreover, the methodologies are applied to some analytical exercises.

The CIRCE (French acronym for *Calculation of the Uncertainties Related to the Elementary Correlations*) methodology was developed at CEA [20] and its comprehensive description can be found in [47] and [48]. It aims at quantifying the model uncertainty of p correlations $z_{calc}(\mathbf{x})$ (with their θ already calibrated) used as closure laws in computer codes. CIRCE represents this model uncertainty, similarly to Eq. 2.4, through a multiplicative factor λ applied to the reference model. If the experimental database is composed by n experimental realisations, we can write for $1 \leq j \leq p$ and $1 \leq i \leq n$:

$$z_{pred,j}(\mathbf{x}_i) = \lambda_{i,j} \cdot z_{calc,j}(\mathbf{x}_i) \tag{3.1}$$

where $\lambda_{i,j}$ is the realisation i of the uncertainty distribution j, Λ_j.

As already explained in Section 2.1, the use of a multiplicative factor has the advantage to define a model uncertainty that can adapt to the different scales of the experiments in a database.

3.1 . Brief introduction to the CIRCE methodology

In this section, the CIRCE methodology and its hypotheses are briefly recalled. The vector of (log)-normal distributions $\mathbf{\Lambda} = (\mathscr{L})\mathscr{N}(\mathbf{m}_\lambda, \mathbf{\Sigma}_\lambda)$ models the multiplicative realisations in Eq. 3.1. The distributions are described by a p-sized mean vector $\mathbf{m}_\lambda$ and a diagonal variance-covariance matrix $\mathbf{\Sigma}_\lambda = diag(\sigma^2_{\lambda_1}, ..., \sigma^2_{\lambda_j}, ..., \sigma^2_{\lambda_p})$ of size $p \times p$. The matrix is diagonal since the correlations are assumed to be independent.

The mean $\mathbf{m}_\lambda$ and the variance-covariance matrix $\mathbf{\Sigma}_\lambda$ can be estimated through the resolution of the following probabilistic equation, for $1 \leq i \leq n$:

$$z_{exp}(\mathbf{x}_i) = z_{code}(\mathbf{x}_i, \mathbf{z}_{pred}(\mathbf{x}_i)) \; + \; \epsilon_i \tag{3.2}$$

where $z_{code}(\mathbf{x}_i, \mathbf{z}_{pred}(\mathbf{x}_i))$ is the code output (function of the input parameters and the reference models) that takes into account the model uncertainties and ϵ_i is the realisation of the experimental uncertainty $\sim \mathscr{N}(0, \sigma^2_{\epsilon_i})$ (where $\sigma^2_{\epsilon_i}$ is the experimental variance of the test i).

In Fig. 3.1, the function of the code output in Eq. 3.2 $z_{code}(\mathbf{x}_i, \mathbf{z}_{pred}(\mathbf{x}_i))$ (in green) is unknown and time-consuming to compute. It is therefore approximated with a first-order Taylor expansion (in red). As explained in Paper III, two linearization strategies can be adopted: w.r.t. $\boldsymbol{\lambda}_j$ or $log(\boldsymbol{\lambda})_j$. In this chapter, the linearization w.r.t. $\boldsymbol{\lambda}_j$ is briefly recalled. In the figure, the code output function at the reference value is $z_{code}(\mathbf{x}_i, \mathbf{z}_{calc}(\mathbf{x}_i))$. This reference code output is the result of the simulation where no models have been modified (i.e. the best-estimate value $\lambda_{i,j}^{ref} = 1$).

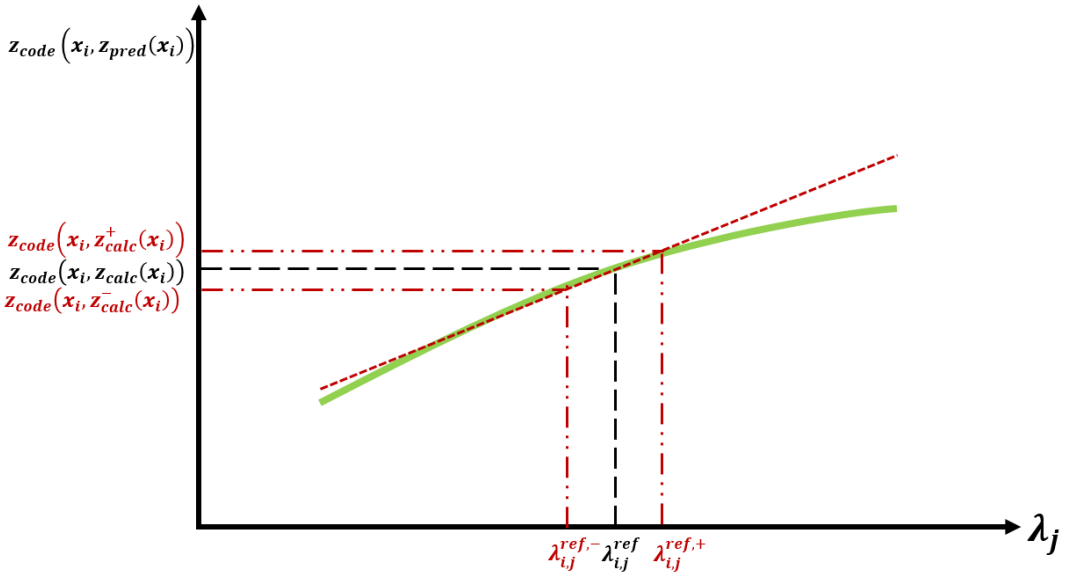

Figure 3.1: Code output i (in green) and its first-order Taylor approximation (in red) as function of the model uncertainty j λ_j.

In order to approximate the green function, its partial derivatives i w.r.t. the model uncertainties j are computed in the neighborhood of the reference calculation through the finite difference method. For each uncertain model j, the following derivative can be computed: $\frac{\partial z_{code}(\mathbf{x}_i)}{\partial \lambda_j} = \frac{z_{code}(\mathbf{x}_i, \mathbf{z}^{+}_{calc}(\mathbf{x}_i)) - z_{code}(\mathbf{x}_i, \mathbf{z}^{-}_{calc}(\mathbf{x}_i))}{\lambda^{ref,+}_{i,j} - \lambda^{ref,-}_{i,j}}$.

Thus, Eq. 3.2 can be rewritten as:

$$z_{exp}(\mathbf{x}_i) \approx z_{code}(\mathbf{x}_i, \mathbf{z}_{calc}(\mathbf{x}_i)) + \mathbf{J}(\mathbf{x}_i) \cdot \mathbf{b}_i^T + \epsilon_i \tag{3.3}$$

where $\mathbf{J}(\mathbf{x}_i) = (\frac{\partial z_{code}(\mathbf{x}_i)}{\partial \lambda_1}, ..., \frac{\partial z_{code}(\mathbf{x}_i)}{\partial \lambda_p})\Big|_{\boldsymbol{\lambda}=\boldsymbol{\lambda}^{ref}}$ is the row i of the Jacobian matrix (i.e. the vector of the partial derivatives i w.r.t. the model j) computed at the value of reference and $\mathbf{b}_i \in \mathbb{R}^{1\times p}$ is the bias vector corresponding to the shift w.r.t. the reference value.

The realisations of the bias vector are the only unknowns of Eq. 3.3 and they are supposed to follow a vector of normal distributions, $\mathbf{b}_i \sim \mathcal{N}(\mathbf{m}_b, \boldsymbol{\Sigma}_b)$ with $\mathbf{m}_b = (\lambda_1 - \lambda_1^{ref}, ..., \lambda_p - \lambda_p^{ref})$ and $\boldsymbol{\Sigma}_b = diag(\sigma^2_{\lambda_1}, ..., \sigma^2_{\lambda_p})$.

The CIRCE methodology then operates the following steps:

1. The algorithm ECME [49] is applied to estimate $m_{b_j}^{MLE}$ and $\sigma^{2\ MLE}_{b_j}$ for each model j;
2. The realisations $\mathbf{b}_i$ are verified to be normally distributed;

3. The code output near the reference value (in this work assumed $\lambda_j^{ref} = 1$) is verified to be linear. If the model j is linear w.r.t. λ_j, then $\Lambda_j = \mathcal{N}(m_{b_j}^{MLE} + 1, \sigma_{b_j}^{2\ MLE})$. If the model j is linear w.r.t. $log(\lambda)_j$, then $\Lambda_j = \mathcal{LN}(m_{b_j}^{MLE}, \sigma_{b_j}^{2\ MLE})$.

Finally, a statistical validation similar to the one described in Section 2.4 is applied to the estimated uncertainty. CIRCE is applied to $n-1$ experimental data (removing data ν from the IUQ database) and the resulting uncertainty $\mathbf{\Lambda}^{-\nu}$ is propagated to find the output distribution $z_{code}(\mathbf{x}_\nu, \mathbf{z}_{pred}(\mathbf{x}_\nu) \,|\, \boldsymbol{\lambda}^{-\nu}) \sim \mathcal{N}(\mathbb{E}(z_{code}(\mathbf{x}_\nu, \mathbf{z}_{pred}(\mathbf{x}_\nu) \,|\, \boldsymbol{\lambda}^{-\nu})), \mathbb{V}(z_{code}(\mathbf{x}_\nu, \mathbf{z}_{pred}(\mathbf{x}_\nu) \,|\, \boldsymbol{\lambda}^{-\nu})))$. The uncertainty is statistically validated if at least 95% of the experimental QoIs $z_{exp}(\mathbf{x}_\nu)$ lay in the 95% level quantile of the associated distribution $z_{code}(\mathbf{x}_\nu, \mathbf{z}_{pred}(\mathbf{x}_\nu) \,|\, \boldsymbol{\lambda}^{-\nu})$.

3.2 . The identifiability problem

When CETs are employed for the joint estimation of more than one model uncertainty ($p > 1$), the statistical resolution of the inverse problem in Eq. 3.3 may be affected by unidentifiability [47]. This means that the mean and variance of the bias distribution of a model j $\mathcal{N}(m_{b_j}^{MLE}, \sigma_{b_j}^{2\ MLE})$ may be difficult to statistically estimate. Several combinations of means and variances of the estimated uncertainties may explain the discrepancy between the experimental and computed values, leading to unidentifiability [22].

In [49], the identifiability of a parameter is assessed through the computation of the Normalised Error Coefficients (NECs). They are defined as the ratio of the epistemic uncertainty of a parameter over the intrinsic variability of the distribution. For a bias j, they read:

$$\begin{aligned} NEC(m_{b_j}^{MLE}) &= \frac{\sigma(m_{b_j}^{MLE})}{\sqrt{\sigma_{b_j}^{2\ MLE}}} \\ NEC\left(\sqrt{\sigma_{b_j}^{2\ MLE}}\right) &= \frac{\sigma\left(\sqrt{\sigma_{b_j}^{2\ MLE}}\right)}{\sqrt{\sigma_{b_j}^{2\ MLE}}} \end{aligned} \tag{3.4}$$

When the NEC is close to zero the problem is well identifiable and, consequentially, the CIRCE estimations are robust.

In [21, 50], the low sensitivity of the calculated QoI $z_{code}(\mathbf{x}_i, \mathbf{z}_{calc}(\mathbf{x}_i))$ to the model j is identified as one of the causes that might lead to non-identifiability. In order to quantify the sensitivity, the first-order Sobol index [51] must be computed. However, its computation is dependent on the model uncertainty variance (which is unknown as we want to estimate it) and some hypotheses must be made *a priori* [52].

Another way to investigate the identifiability of the inverse problem is to use the model derivatives as sensitivity indicators (as shown in Paper III). Thus, a scale parameter k between two models can be computed as the increment of the derivative mean of the first model with respect to one of the second model:

$$k = \frac{\mu\left(\mathbf{J}_1(\mathbf{x})\right)}{\mu\left(\mathbf{J}_2(\mathbf{x})\right)} - 1 \tag{3.5}$$

The parameter k is indipendent on the uncertainties variance and it is computed without *a priori* hypotheses.

3.3 . Assessement of CIRCE on an analytical case

In order to visualise and quantify the identifiability problem an analytical case was performed. The full description can be found in Paper III, while the main results are summarized here.

In the analytical exercise, CIRCE is applied to the joint estimation of the uncertainties of two different models $z_{calc,1}(\mathbf{x})$ and $z_{calc,2}(\mathbf{x})$. The parameter k links the arithmetic means of the two model derivatives ($\mathbf{J}_1(\mathbf{x})$ and $\mathbf{J}_2(\mathbf{x})$ respectively) in the following way:

$$\mu\left(\mathbf{J}_1(\mathbf{x})\right) = (1+k)\cdot\mu\left(\mathbf{J}_2(\mathbf{x})\right) \tag{3.6}$$

The data is generated from known distributions, especially the bias distributions from centered reduced normal distributions:

$$\begin{aligned} b_{1,i} &\sim \mathcal{N}(m_{b_1},\, \sigma^2_{b_1}) = \mathcal{N}(0,\, 1) \\ b_{2,i} &\sim \mathcal{N}(m_{b_2},\, \sigma^2_{b_2}) = \mathcal{N}(0,\, 1) \end{aligned} \tag{3.7}$$

Then, CIRCE is run 1000 times (each run with different sampled data) and the resulting estimations (1000 values for $m_{b_1}^{MLE}$, $\sigma_{b_1}^{2\ MLE}$, $m_{b_2}^{MLE}$ and $\sigma_{b_2}^{2\ MLE}$) are compared to the associated actual values.

In Fig. 3.2, the arithmetic mean μ and the standard deviation σ of the 1000 realisations are plotted.

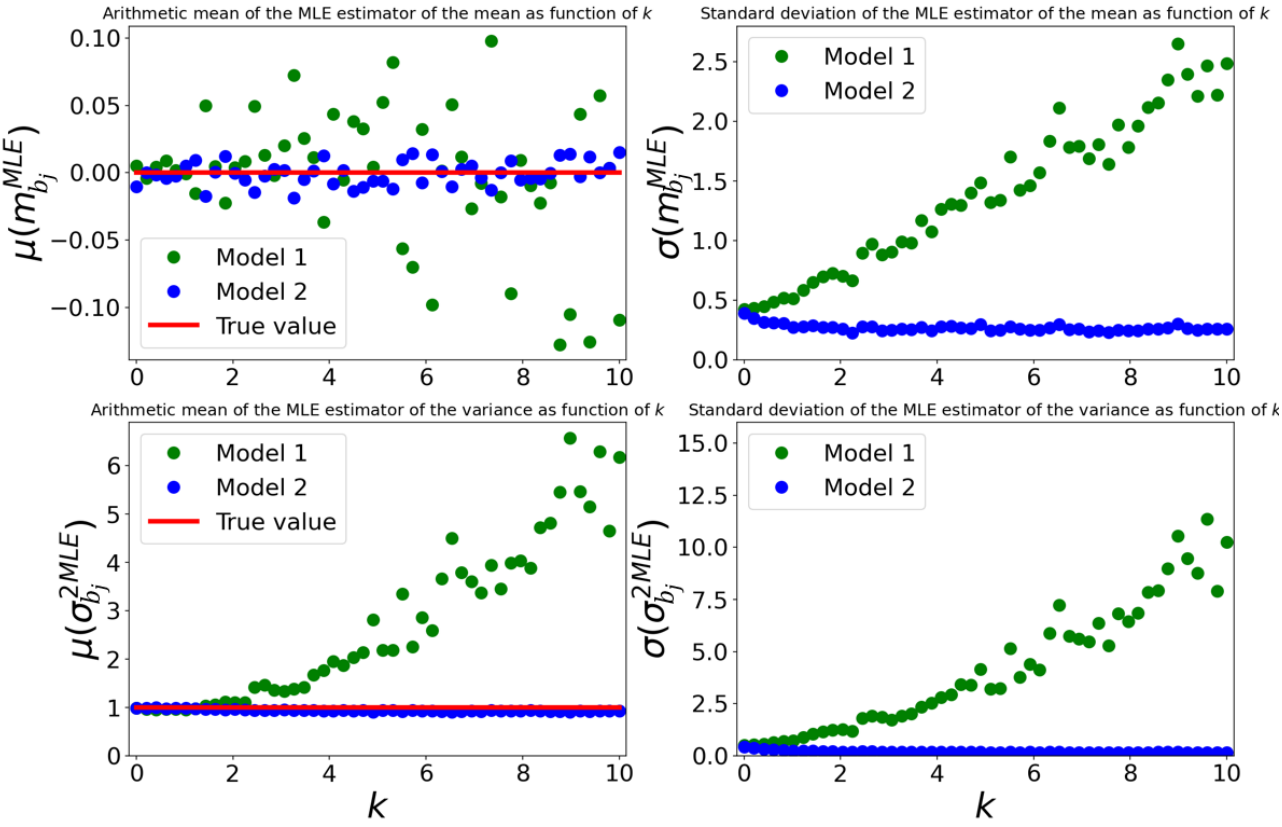

Figure 3.2: Statistical indicators of the MLE estimators for the two models as a function of the scaling parameter k.

The more the estimated mean departs from the actual value (i.e. low accuracy) and its standard deviation is high (i.e. low precision), the less the problem is statistically well-identified.

In the top left subgraph, the bias mean of the least influential model (Model 1) has low accuracy and high dispersion as opposed to Model 2 (i.e. the most influential one). For the other subgraphs, the accuracy and precision of Model 1 degrade as k increases. A degradation of the accuracy and precision of the model with the largest derivatives (i.e. $z_{calc,2}(\mathbf{x})$ for $k \gtrsim 3$) was also observed.

In order to improve the estimation of the most influential bias distribution, a new extension of the CIRCE methodology called CIRCE 2-Steps is developed.

3.4 . CIRCE 2-Steps methodology

The new methodology CIRCE 2-Steps is established for a CETs database characterised by p combined phenomena. Each phenomenon is modelled by a physical correlation. In particular, p^+ models are more influential than the others (i.e. $p - p^+$) over the output QoI. In order to minimize the identifiability problem, CIRCE 2-Steps reduces the number of uncertainties to be jointly estimated when using CETs.

In the first step, the uncertainties of the $p - p^+$ least influential models (marked with an asterisk in Eqs. 3.8, 3.10 and 3.11) are separately assessed using the CIRCE methodology against the available SETs. In the second step, the p^+ most influential model uncertainties (marked with a plus in the following equations) are estimated from the CETs database taking into account the previously quantified uncertainties. In this step, Eq. 3.3 is modified in:

$$z_{exp}(\mathbf{x}_i) \approx z_{code}(\mathbf{x}_i, \mathbf{z}_{calc}(\mathbf{x}_i)) \; + \; \mathbf{J}_p^+(\mathbf{x}_i) \cdot \mathbf{b}_i^+ \; + \; \mathbf{J}^*(\mathbf{x}_i) \cdot \mathbf{b}_i^* \; + \; \epsilon_i \tag{3.8}$$

where $\mathbf{b}_i^* \in \mathbb{R}^{1 \times p - p^+}$ has already been estimated from the first step. Each bias j follows a known normal distribution $\mathcal{N}(m_{b_j}, \sigma_{b_j}^2)$.

The $p - p^+$ means and variances of the distributions are added respectively to the code output and the experimental uncertainty distribution. Hence, Eq. 3.8 can be rewritten as:

$$z_{exp}(\mathbf{x}_i) \approx z'_{code}(\mathbf{x}_i, \mathbf{z}_{calc}(\mathbf{x}_i)) \; + \; \mathbf{J}^+(\mathbf{x}_i) \cdot \mathbf{b}_i^+ \; + \; \epsilon'_i \tag{3.9}$$

where:

$$z'_{code}(\mathbf{x}_i, \mathbf{z}_{calc}(\mathbf{x}_i)) = z_{code}(\mathbf{x}_i, \mathbf{z}_{calc}(\mathbf{x}_i)) + \sum_{j=1}^{p-p^+} (J_j^*(\mathbf{x}_i) \cdot m_{b_j}) \tag{3.10}$$

$$\epsilon'_i \sim \mathcal{N}(0, \, \sigma_{\epsilon_i}^2 + \sum_{j=1}^{p-p^+} (J_j^{*2}(\mathbf{x}_i) \cdot \sigma_{b_j}^2)) \tag{3.11}$$

The CIRCE methodology is then applied to Eq. 3.9 as described in Section 3.1.

3.5 . Evaluation of the performances of CIRCE 2-Steps

CIRCE 2-Steps is applied to the same analytical case of Section 3.3 for the IUQ of the most influential model uncertainty (Model 2). In Fig. 3.3, the arithmetic mean μ and the standard

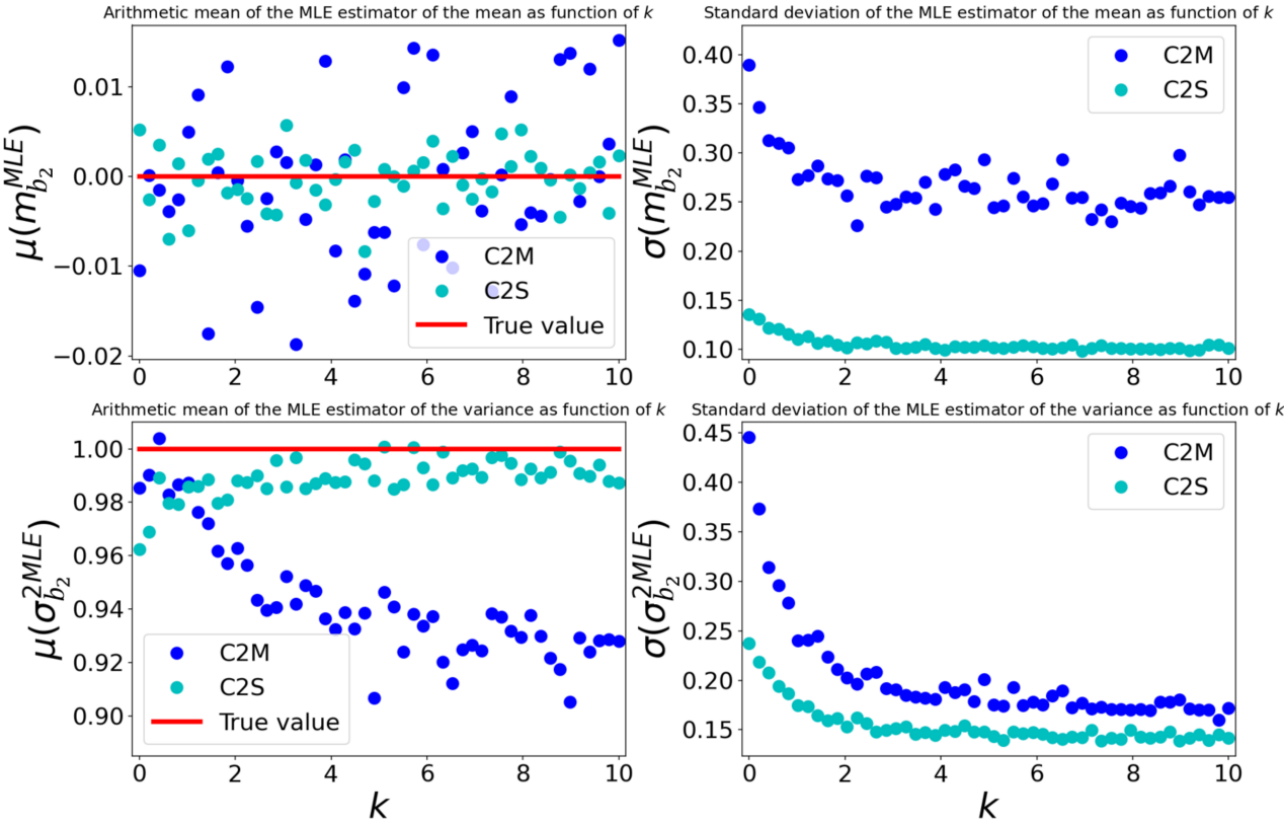

Figure 3.3: Statistical indicators of the MLE estimators for $z_{calc,2}(\mathbf{x})$ computed by C2M and C2S as a function of the scaling parameter k.

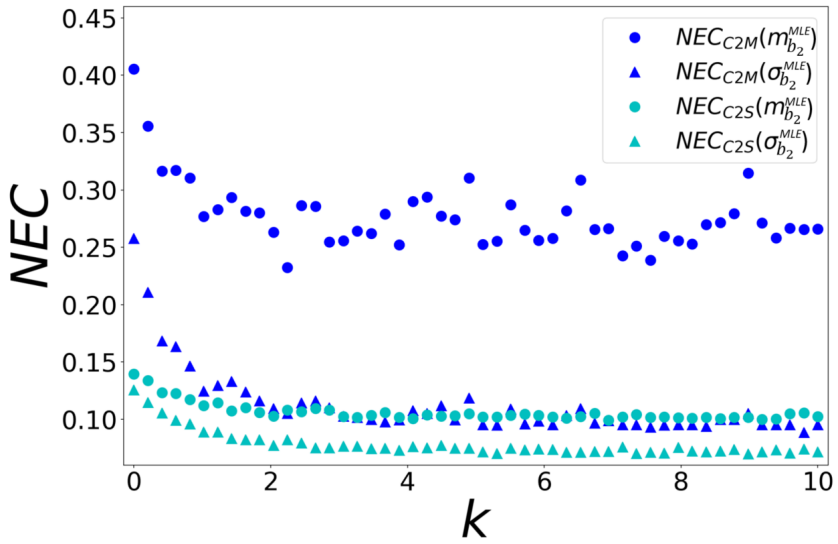

Figure 3.4: NECs of the MLE estimators for $z_{calc,2}(\mathbf{x})$ computed by C2M and C2S as a function of the scaling parameter k.

deviation σ respectively corresponding to CIRCE applied jointly to two models (C2M) and CIRCE 2-Steps (C2S) are shown as functions of k. The accuracy and precision of the estimations obtained by C2S are improved for both the mean and variance of the uncertainty distribution.

The NECs in Eq. 3.4 are computed and shown in Fig. 3.4. For both the mean and standard deviation, C2S gives more identifiable results than C2M. The most relevant improvement is related to the identiafibility of the mean.

4 - Thermal-hydraulic analysis of the experimental database

This chapter is related to the first part of Paper II, where the thermal-hydraulic analysis of the experimental tests is carried out.

In this chapter, the experimental database used for the assessment of the condensation modelling at the ECC injection is presented. Then, a thermal-hydraulic analysis is carried out.

4.1 . Experimental databases

The data were obtained from three experimental facilities: COSI, TOPFLOW-PTS and UPTF.

4.1.1 . The COSI experiments

The COSI (*COndensation at Safety Injection*) experiments have been carried out using two test sections, simulating the cold leg of a French (Framatome or Fra) and American (Westinghouse or West) PWR.

In Fig. 4.1, the two configurations are composed by:

- A cold leg of 0.118 m in diameter and long 1.4 m for Fra and 3.77 m for West;
- An inlet pipe for the steam produced in the boiler;
- An outlet pipe to evacuate the steam to the condenser;
- A vertical pipe representing the downcomer (DC);
- Different ECC pipes, welded to the cold leg.

The orange arrows show the direction of the steam. In Fig. 4.1, the steam is in co-current with the liquid as highlighted by the orange arrows. Nevertheless, in the experimental database

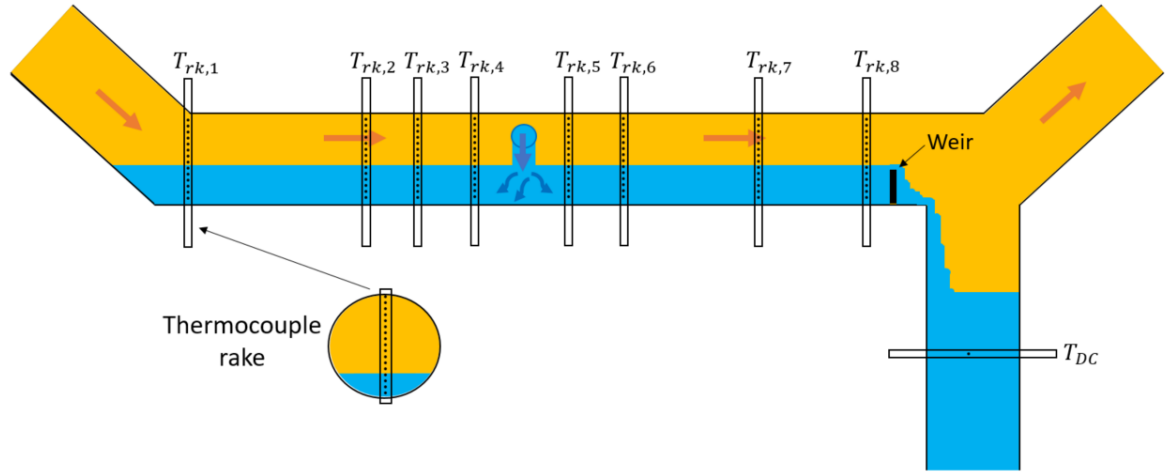

(a) Framatome test section in the COSI experiment.

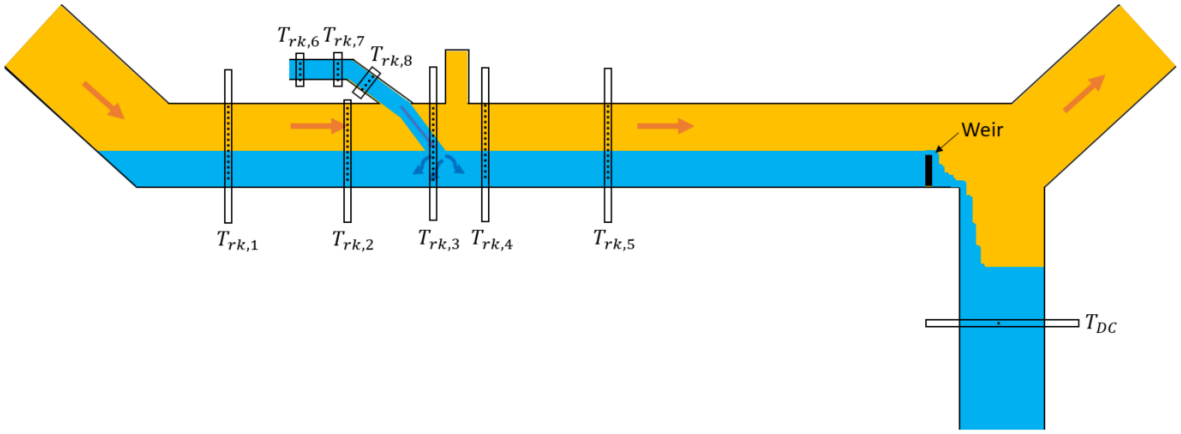

(b) Westinghouse test section in the COSI experiment.

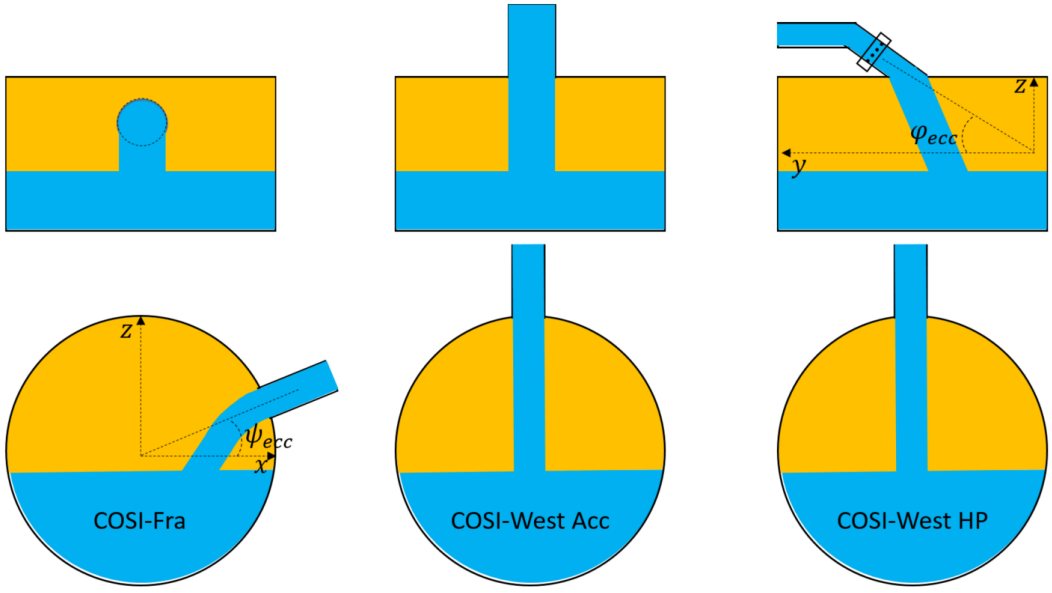

(c) Geometrical configurations of the COSI ECC pipe.

Figure 4.1: Test sections features of the COSI experiment.

there are tests with steam also in counter-current flow.

The Fra cold leg is equipped with 8 thermocouple rakes (whose geometry is illustrated in 4.1a), the West one with 5 rakes. Each rake has 16 thermocouples. One injection pipe in the West test section is equipped with 3 rakes. One thermocouple is also present in the DC.

A weir of adjustable height is placed at the end of the cold leg, just before the DC. It keeps the water level constant in the experimental section.

In Fig. 4.1c, the different ECC pipe configurations are shown. The Fra configuration has an injection pipe with an angle $\psi_{ecc} = 30°$ in the vertical plane and a diameter $d_{ecc} = 22$ mm. The West configuration presents two different types of ECC: the Accumulator (shortened Acc) and the High Pressure (shortened HP) injections. Both pipes have $\psi_{ecc} = 90°$ but the HP pipe is also inclined in the horizontal plane $\varphi_{ecc} = 45°$. The accumulator has two configurations, one with $d_{ecc} = 5.6$ mm and the other with $d_{ecc} = 23$ mm. The HP pipe has a diameter of 38 mm.

A total of 219 Fra and 96 West tests compose the COSI database.

In Fig. 4.2, the phenomena occurring in the COSI experiment during the ECC injection are schematised.

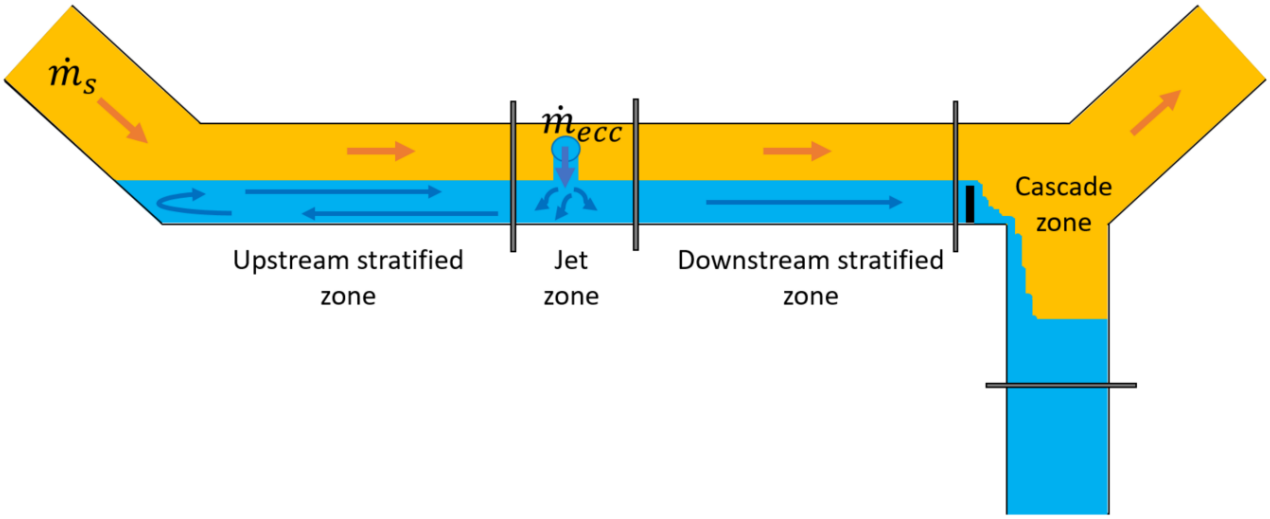

Figure 4.2: Phenomenology in the COSI cold leg.

Four different zones are identified [53]:

- The ECC jet zone, where the jet impacts the liquid entraining the steam in the liquid phase;
- The upstream zone, which is a recirculation zone originated by large temperature gradients;
- The downstream zone, where thermal stratification occurs. Moreover, a recirculation zone may be created by the presence of the weir;
- The zone after the weir, where a cascade is generated by the water falling in the DC.

4.1.2 . The TOPFLOW-PTS experiments

The goal of the TOPFLOW-PTS (Pressurised Thermal Shock) experiment was to study and improve the knowledge of the phenomena behind the PTS.

In Fig. 4.3a, the test section is composed by:

- A pump simulator (PS) where water can be injected and/or extracted. The PS is defined enabled if water is injected and disabled otherwise;
- An horizontal pipe 2.95 m long to simulate the cold leg, with a diameter of 0.2792 m;
- An annular space to simulate the DC;
- An ECC pipe welded at 30° in the vertical plane (see Fig. 4.3b) with a diameter of 0.0531 m.

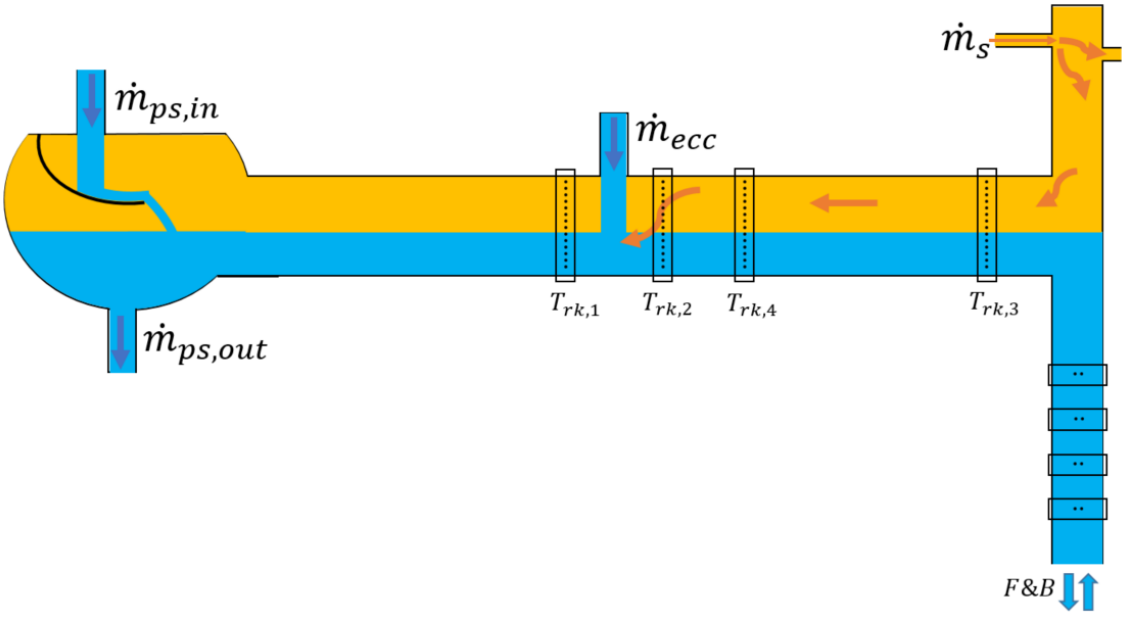

(a) Test section in the TOPFLOW-PTS experiment.

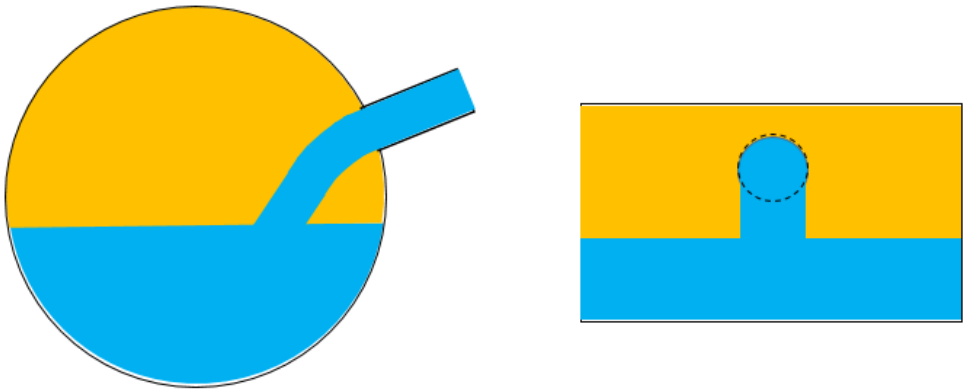

(b) Geometrical configuration of the TOPFLOW-PTS ECC pipe.

Figure 4.3: Test section features of the TOPFLOW-PTS experiment.

Four thermocouple rakes of 25 thermocouples each equip the test section, while in the DC there are several other rakes.

The TOPFLOW-PTS database consists of 28 sssw tests with PS enabled, 9 sssw tests with PS disabled and 3 tsw tests defined below.

Excluding the cascade zone, the same phenomena occurring in COSI are also present in TOPFLOW-PTS. That is because the liquid free level is kept constant by a Feed & Bleed (F&B) system, which keeps the liquid level constant in the DC.

Two different typologies of tests have been realised:

1. Steady-state steam water (called sssw): the condensation at the ECC is evaluated after a stabilisation phase, when the steady-state conditions are reached (i.e. the last 60 seconds of the test). The PS can be either enabled or disabled.

2. Transient state steam water (called tsw): the whole transient is registered, from the start of the ECC injection until the steady-state conditions are obtained. The last 100 seconds of each transient are time-averaged and used to evaluate the condensation in this work. In that period, all the thermal-hydraulic parameters are approximately constant and can be considered steady-state. The PS is always disabled.

4.1.3 . The UPTF experiments

The UPTF (*Upper Plenum Test Facility*) facility [54] is an IET since it is composed of all the thermal-hydraulic components of a PWR. Hence, all the main phenomena taking place in a nuclear reactor interact with each other. The primary system is shown in Fig. 4.4.

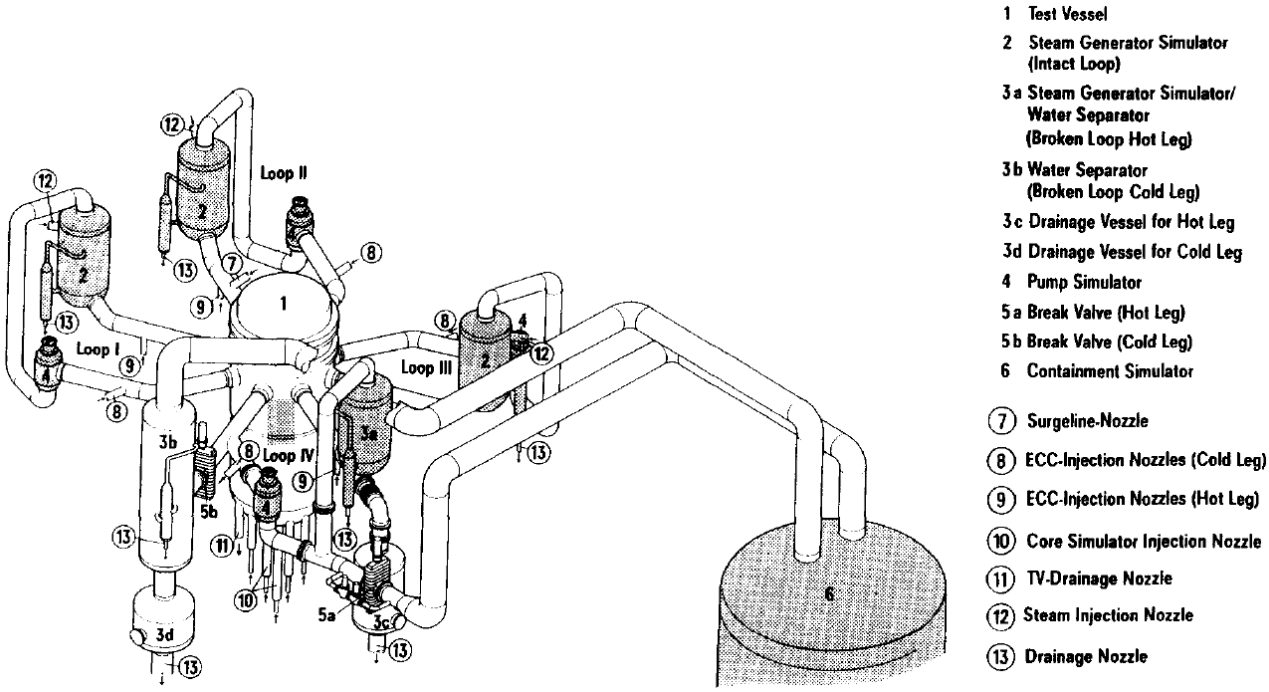

Figure 4.4: UPTF primary system [55].

The cold leg in loop II is well instrumented and can be used to investigate the condensation at the ECC injection.

The test section in Fig. 4.5a is equipped with:

- A PS, always disabled;
- A horizontal pipe 9.48 m long with a diameter of 0.75 m;

- An annular space as a DC;
- An injection pipe welded at 60° in the horizontal plane (see Fig. 4.5b) of 0.2225 m in diameter.

The cold leg is equipped with 4 thermocouple rakes of 6 thermocouples each (8 in TRAM configuration). In UPTF, the liquid flow is oriented towards the DC through the ECC pipe angle. Since the liquid level is not constant, there is no recirculation zone. Thus, the phenomena occurring during the ECC injection are different compared to COSI's.

The UPTF database consists of 24 tests, of which UPTF 8, 25 and 27 with steam coming from the PS and UPTF TRAM C2 6a with steam coming from the DC (since the PS is full of water and blocks the steam flow).

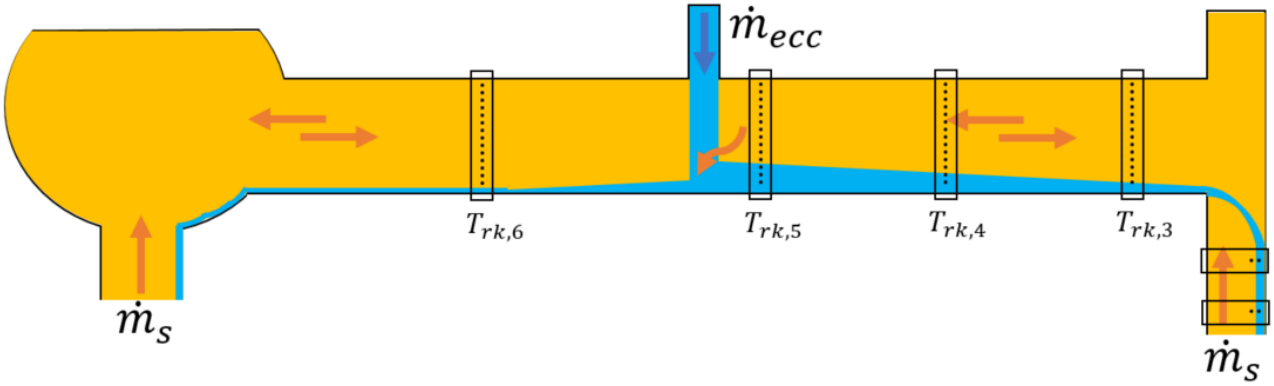

(a) Cold leg in loop II.

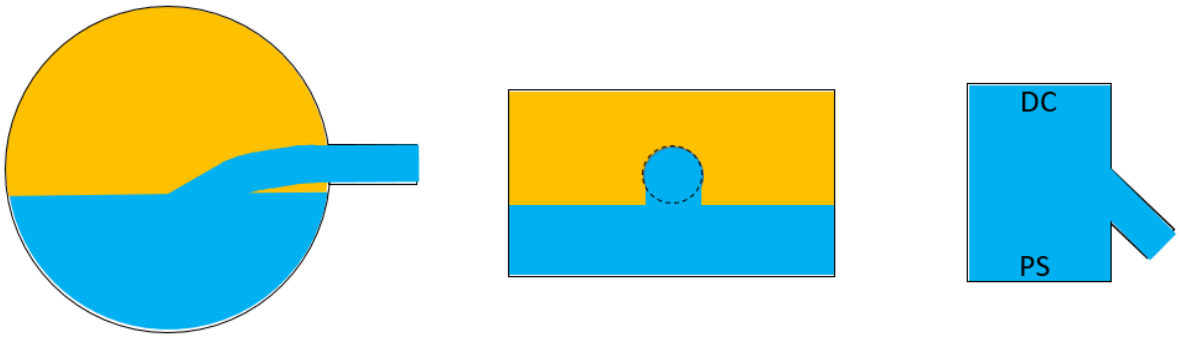

(b) Geometrical configuration of the ECC pipe.

Figure 4.5: Main features of the UPTF experimental setup.

4.1.4 . Summary and experimental uncertainties

The main physical characteristics are briefly summarised in Table 4.1.

	COSI	TOPFLOW-PTS	UPTF
Number of tests	315	42	24
Pressure [MPa]	[2; 7]	[3; 5]	[0.3; 1.5]
Injection temperature [°C]	20, 80	[45; 210]	[30; 40]
Injection mass flowrate [kg/s]	[0.1; 0.6]	[0.7; 2.5]	[10; 160]

Table 4.1: Main characteristics of the experiments.

The several types of ECC configurations of the experimental database are summarised in Table 4.2. The test section diameter and the volumetric scale of the experiments are also reported. The volumetric scale is the scale in volume (of the primary circuit) of the experiments with respect to the actual PWR.

	COSI Fra	COSI West Acc	COSI West HP	TOPFLOW-PTS	UPTF	UPTF TRAM
Diameter [mm]	22	5.6, 23	38	53.1	222.5	222.5
Inclination in the vertical plane ψ_{ecc} [°]	30	90	90	30	0	0
Inclination in the horizontal plane φ_{ecc} [°]	0	0	45	0	60	60
Test section diameter [mm]	118	118	118	279.2	750	750
Volumetric scale [%]	1*	1*	1*	40*	100**	100**

Table 4.2: ECC pipe configurations and volumetric scales for the experimental database. The scale is w.r.t. a 900* (1300**) MWe French PWR.

In Table 4.3, the measurement errors (also called experimental uncertainties) are shown. These uncertainties are associated to pressure, temperature, mass flowrate and geometries (e.g. cold leg and ECC pipes).

	COSI	TOPFLOW-PTS	UPTF
Diameter	±0.5 mm	±0.5 mm	±0.5 mm
ECC temperature	±0.5 °C	±1 °C	±2.9 °C
ECC flowrate	±0.005 kg/s	±0.5 %	±1.5 %
Pressure	±0.5 %	±0.5 %	±0.0146 MPa

Table 4.3: Experimental uncertainties.

4.2 . Thermal-hydraulic analysis

A thermal-hydraulic analysis is required to make the experimental data reliable and coherent with the phenomenon of interest to be modelled (i.e. the condensation at the ECC).

Several tests are immediately suppressed because of different problems: no available data, defective instrumentations, incoherent measurements, no ECC injections, no stabilised tests, presence of overheated steam, repeated tests, tests without condensation and calibration tests. For these reasons, from 382 experimental tests, 198 are the object of the thermal-hydraulic analysis.

In the following subsections, some not-trivial physical phenomena affecting the condensation and present in the experimental database are discussed. The goal is to point out the phenomenologies not yet highlighted and justify the final experimental database. Among these, some physical phenomena affecting the condensation are the flow stratification inside the ECC pipe, the ECC injection in the liquid and the hot ECC injections in TOPFLOW-PTS.

4.2.1 . Stratified flow in the ECC pipe

At low ECC mass flowrates, a stratification in the ECC pipe was sometimes observed as shown in Fig. 4.6. This phenomenon has been observed in all three experiments (COSI, TOPFLOW-PTS and UPTF).

In TOPFLOW-PTS [56], experimenters discovered (thanks to a camera pointed over the jet) the presence of a stratified flow in the ECC pipe. They identified a threshold ECC mass flowrates of 1.7 kg/s. Hence, 2 sssw and 1 tsw tests are suppressed from our database.

In the COSI experiment, despite the absence of a camera, a stratification is observed in the HP injection of the West configuration. Indeed, the thermocouple rake 8 shows a stratified flow at every injection mass flowrate (probably bacause of the injection diameter d_{ecc} being the biggest one for COSI).

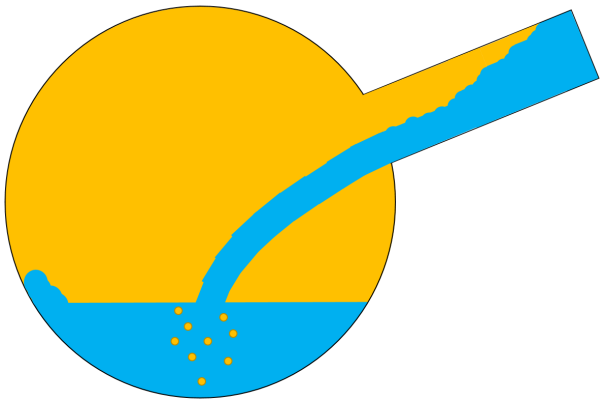

Figure 4.6: Representation of a stratified flow in the ECC pipe.

The UPTF experimenters observed the same phenomenon [57], as shown in Fig. 4.7.

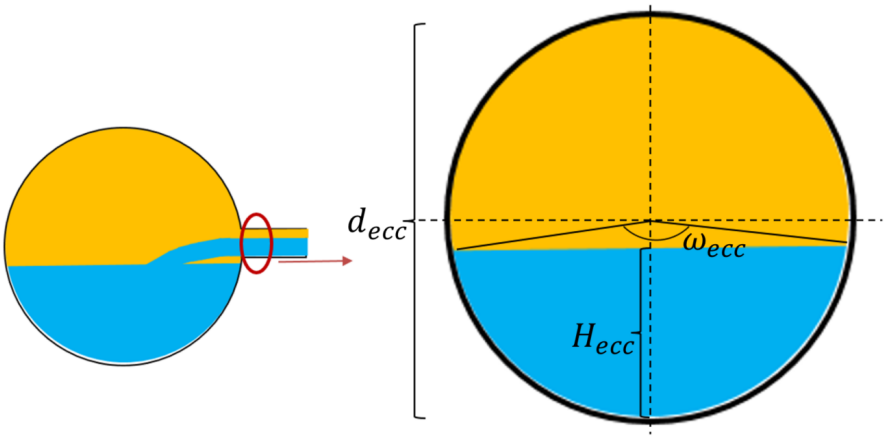

Figure 4.7: Stratified flow in the UPTF ECC pipe.

In Fig. 4.7, ω_{ecc} is the angle at the center of the ECC pipe.

In the UPTF tests, no camera nor thermocouples in the ECC pipe are present. Nevertheless, the experimenters evaluated the stratification through the Schröder formula [58]. It calculates the liquid height inside a two-phase low inclined pipe:

$$\frac{(\omega_{ecc} - sin(\omega_{ecc}))^3}{sin(\omega_{ecc}/2)} = \frac{512 \cdot \dot{Q}_{ecc}^2 \cdot \rho_{ecc}}{g \cdot d_{ecc}^5 \cdot (\rho_{ecc} - \rho_v)} \tag{4.1}$$

The formula is solved iteratively for ω_{ecc}. Then, the liquid height can be calculated as:

$$H_{ecc} = d_{ecc} \cdot sin^2(\omega_{ecc}/4) \tag{4.2}$$

The Schröder formula is applied to COSI and TOPFLOW-PTS experiments, well predicting the occurrence of stratification in the tests where it was experimentally observed. In 2 TOPFLOW-PTS tests (1 sssw and 1 tsw), the stratification in the ECC pipe can be estimated through the experimental images. As reported in Table 4.4, the actual surface S_{ecc} (the surface associated to H_{ecc} in Fig. 4.7) is approximately 50% of the injection surface (i.e. $S_{inj} = \pi \cdot {}^{d^2_{ecc}}/_4$). The Schröder formula in Eq. 4.1 is applied and it gives overestimated results.

TOPFLOW-PTS	T_{ecc} [°C]	$S_{ecc,exp}$	S_{ecc} by Schröder
sssw	143.7	~50 % S_{inj}	87 % S_{inj}
tsw	42.6	~50 % S_{inj}	78 % S_{inj}

Table 4.4: ECC stratification quantification in some TOPFLOW-PTS tests.

This formula predicts in a reliable way the occurrence of stratification in the ECC pipe, but unfortunately it does not provide a good quantification of the liquid height. Eq. 4.1 was thus used as a criterion for the ECC stratification.

The criterion is applied to the whole database, highlighting 13 UPTF tests and 46 COSI tests where stratification occurs. Since the condensation is highly affected by the stratification phenomenon, which influences the calculation of the ECC jet velocity u_{ecc} and the heat exchange area A_{ex}, a high uncertainty is expected. Hence, the tests with a stratified ECC pipe are excluded from both the assessment and validation databases.

4.2.2 . Injection in the liquid

When the liquid level in the cold leg is too high, the ECC injection occurs directly into the liquid. In TOPFLOW-PTS, the phenomenon is shown by the camera pointing towards the jet.

The COSI tests with the highest weir ($0.6 \cdot D$) may show the same behaviour, as shown in Fig. 4.8.

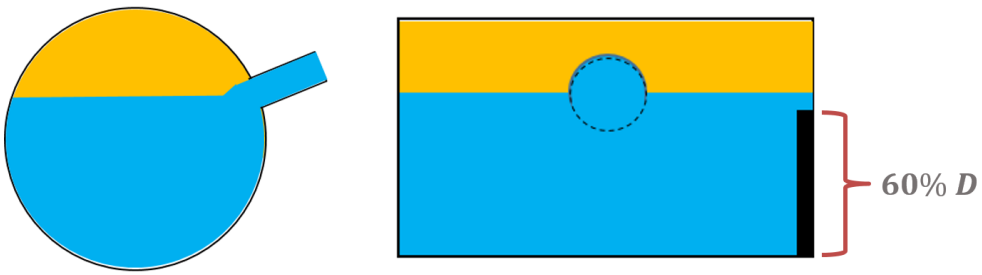

Figure 4.8: Assumed behaviour of COSI tests with a 0.6 weir.

Due to the small condensation flowrates and the short jet length, the estimation of the condensation may be unreliable. Two TOPFLOW-PTS and 6 COSI tests are thus eliminated from the assessment database.

4.2.3 . Hot ECC injections in TOPFLOW-PTS

The TOPFLOW-PTS tests with enabled PS are charactherised by a hot water ECC injection (i.e. a sub-cooling ($T_{sat} - T_{ecc}$) between 27 and 80 $°C$). The resulting condensation mass flowrates are very low and their computation is greatly impacted by the experimental uncertainties. Thus, these tests are moved to the validation database in order to prevent any bias in the calibration of the model.

4.2.4 . Reduced database

In Table 4.5, the revised database is shown. The COSI and TOPFLOW experiments are CETs, suitable to calibrate the condensation model. Thus, they are included in the assessment database. The UPTF experiments, as IETs, and TOPFLOW-PTS tests with hot ECC injection are used for the physical validation of the new correlation. The range of the most important variables is different between the assessement and the validation database. Assuming that the condensation phenomena at full scale are similar to the ones assessed on the development database, the new condensation model should behave well even outside the assessment ranges.

Test	P [MPa]	T_{ecc} [°C]	$\dot{m}_{ecc}$ [kg/s]	Tests in the assessment database	Tests in the validation database
COSI-Fra	2, 7	20, 80	[0.2, 0.6]	73	0
COSI-West	4.2, 5.6, 7	20	[0.06, 0.4]	29	0
TOPFLOW-PTS sssw	3, 5	[110, 220]	[1.7, 2.5]	6	11
TOPFLOW-PTS tsw	5	45	1.7, 2	2	0
UPTF	[0.3, 1.5]	[29, 39]	[61, 161]	0	7
Total number of tests				110	18

Table 4.5: Reduced database after the thermal-hydraulic analysis.

At the end of the experimental analysis, 110 tests compose the assessment database and 18 tests the validation database. The experimental conditions range between 0.3 and 7 MPa for the pressure, 0.2-161 kg/s for the ECC flowrate and between 20 and 220 °C for the ECC temperature.

4.3 . Methodology for the quantification of the condensation rate

The next two subsections describe the methodologies for the evaluation of the QoIs required to evaluate the condensation in the cold leg:

1. The mean liquid temperature $\overline{T}_{rk,i}$ from the thermocouple rake. It is based on the weighted mean, where the weight is the surface of every thermocouple immerged in the liquid. The definition of the liquid heigth is necessary to evaluate $\overline{T}_{rk,i}$;

2. The condensation mass flow rate at the ECC $\dot{m}_{cond,ecc}$, obtained by a mass and energy balance in a defined control volume for each experimental device.

4.3.1 . Evaluation of the liquid level height and of the mean liquid temperature

The mean liquid temperature of each rake and the free level height in the cold leg must be computed in order to calculate respectively the condensation mass flowrate and the heat

exchange area A_{ex} between the sub-cooled liquid and the steam.

The waves created at the interface between the steam and the liquid by the jet impact in the cold leg complicate the calculation of the rake mean liquide temperature. As observed in the TOPFLOW-PTS tests (Fig. 4.9), the effect of these waves modifies the thermocouple temperature profiles in time. The temperature is normalised with respect to the saturation temperature plus a random small constant ξ and plotted as function of time. Three thermocouples are plotted: one in the steam (in yellow) at the saturation temperature, one in the liquid (in light blue) and one at the interface (in grey).

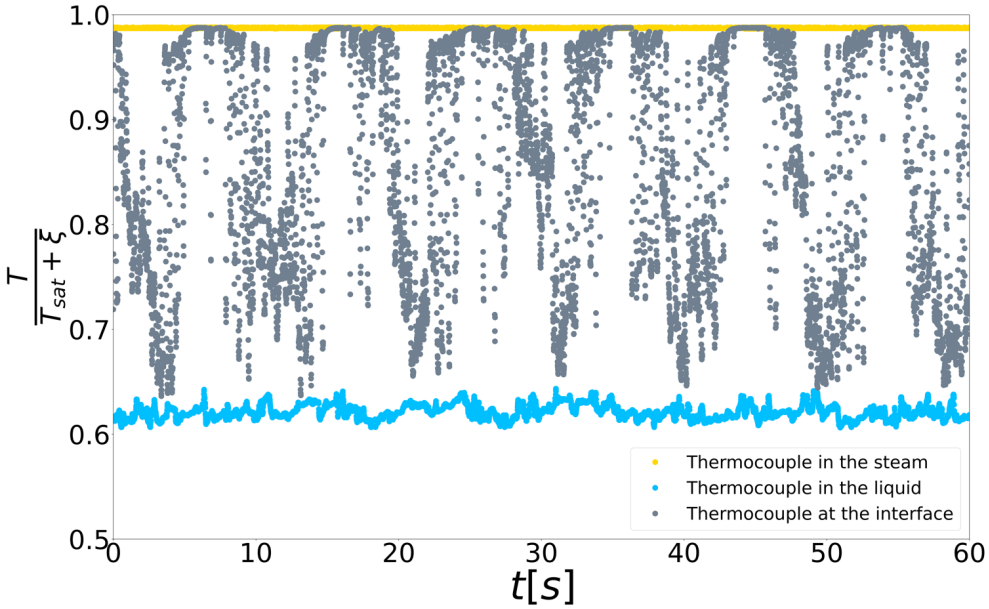

Figure 4.9: Typical temperature profiles in time in a TOPFLOW-PTS test.

The thermocouple at the interface is in the steam and wetted regularly by the waves.

In Fig. 4.10, the normalised temperature is plotted as function of the dimensionless height of the thermocouple in the test section, showing the typical time-averaged temperature profile of a rake. The saturation temperature T_{sat} and $T_{sat} - 5\,°C$ are plotted as a black and red line respectively.

In Fig. 4.10, three regions can be identified. For $z/D < 0.4$, the thermocouples are considered in the liquid. The remaining thermocouples are either in the middle zone at the liquid-steam interface ($0.4 < z/D < 0.5$ and $T < T_{sat} - 5\,°C$) or in the steam ($T > T_{sat} - 5\,°C$). In this test, three thermocouples are characterised by significant temperature fluctuations in the experiment (as seen in Fig. 4.9) and thus are identified at the liquid-steam interface (they are marked by a black cross).

To rigorously identify the thermocouples in the liquid and those at the interface, a criterion has been developed and validated according to the experimental observations on the TOPFLOW-PTS tests. The first thermocouple on the left (i.e. the bottom thermocouple) is always supposed in the liquid. Then, the temperature difference of two successive thermocouples is compared to the sub-cooling of the thermocouple (i.e. $T_{sat} - T_{thermocouple}$). If the temperature difference is above 80 % of the sub-cooling, the thermocouple is supposed to be at the interface. Thus, all the above thermocouples are neglected in the mean liquid temperature calculation since they are considered in the steam.

In the end, the liquid-steam interface is evaluated as the halfway between the last thermocouple in the liquid and the first one selected at the interface by the criterion.

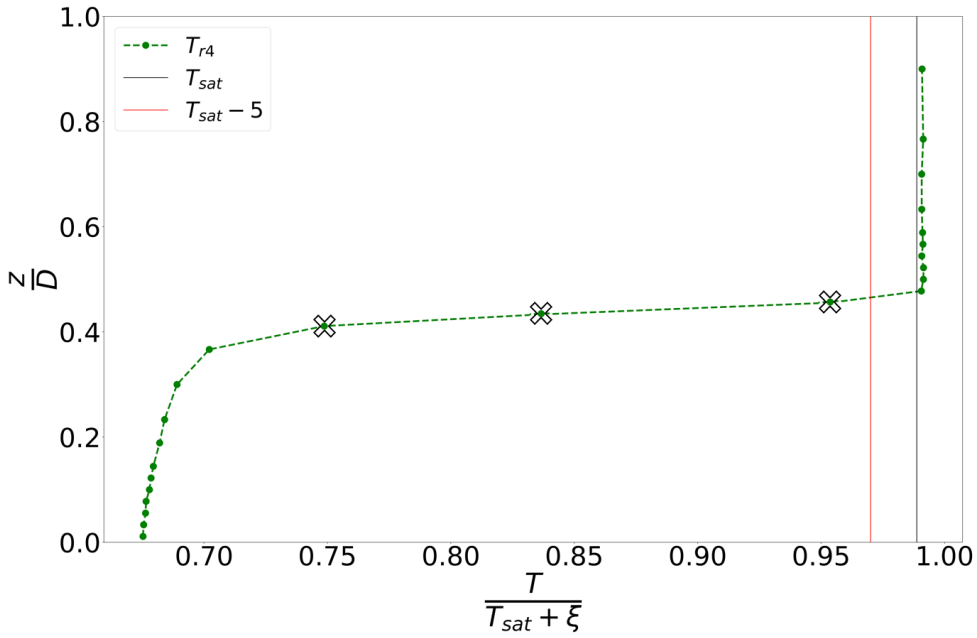

Figure 4.10: Typical time-averaged temperature profile of a rake in a TOPFLOW-PTS test.

Both COSI and UPTF have very similar time-averaged thermocouple profiles to the TOPFLOW-PTS one (Fig. 4.10). Nevertheless, their time evolution is not available. Thus, the new developed criterion is used to identify all the thermocouples in the liquid.

Finally, for all the experiments and assuming a uniform liquid velocity field, the rake mean liquid temperature is calculated as the weighted mean of the liquid temperatures with the associated surfaces as weights [59]:

$$\overline{T}_{rk} = \frac{\sum_{t=1}^{t=last\,TC\,in\,the\,liquid} T_t \cdot S_t}{\sum_{t=1}^{t=last\,TC\,in\,the\,liquid} S_t} \tag{4.3}$$

The experimental uncertainties in Table 4.3 influence the mean liquid temperature computation. Those uncertainties are propagated to compute the uncertainty on the mean liquid temperature. The calculation is made under two main hypotheses: no uncertainty on which thermocouple is the last in the liquid and the uncertainty on the liquid height in the test section H is equal to the half space between the last thermocouple in the liquid and the first in the steam.

The uncertainties on the rake mean liquid temperature are then estimated to be: $\pm 6\,°C$ for COSI, $\pm 4\,°C$ for TOPFLOW-PTS and $\pm 3.5\,°C$ for UPTF experiments.

4.3.2 . Quantification of the condensation mass flowrate

The COSI experiments have always been considered as SETs. This introduced a systematic bias in their model since the condensation due to the cascade and to the stratification were accounted to the jet.

In this work, a new methodology has been developed to separate the effects and rearrange the CETs as SETs. It quantifies the condensation in each region, isolating the one at the

ECC injection. First, a control volume (Fig. 4.11) is defined from the ECC injection and a thermocouple rake (whose mean temperature is known).

Second, the condensation mass flowrate is quantified by applying an entalphy balance to that control volume:

$$\dot{m}_{cond,ecc} = \dot{m}_{ecc} \cdot \frac{\overline{I}_{rk,i} - I_{ecc}}{I_{s,sat} - \overline{I}_{rk,i}} \tag{4.4}$$

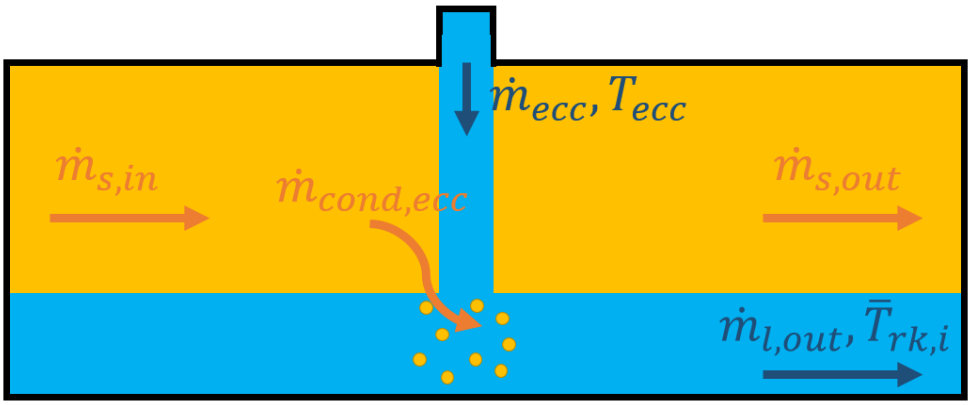

Figure 4.11: Control volume between the ECC and a thermocouple rake.

Due to the reduced test section length after the ECC, the condensation in the stratification zone can be neglected and Eq. 4.4 can be applied between the ECC and rake 8 for COSI-Fra (rake 5 for COSI-West). A similar control volume can be defined from the rake 8 for COSI-Fra (rake 5 for COSI-West) and the thermocouple inside the DC. In that control volume, we estimate the condensation at the cascade. In Fig. 4.12, the condensation at the cascade is compared to the global one as function of the injection flowrate. At low ECC mass flowrates, the condensation in the cascade zone ramps up to 60% of the global condensation. Thus, a coherent control volume is of extreme importance to properly quantify the condensation in the ECC region.

This methodology allows us to have a versatile experimental database (Table 4.5) since, based on which thermocouple rake is considered, the database can be composed by either SETs (where the only effect is the condensation at the ECC) or CETs (where the phenomena are the condensation at both the jet and the stratified interface). The thermocouple to be considered for this division is reported in Table 4.6.

For the COSI-Fra experiments, the rake 8 is always used regardless of SET or CET. That is because the distance between rakes 5 and 8 is so small than the stratified condensation can be neglected. The COSI-West tests cannot be used as CETs, since there is no thermocouple rake at the end of the cold leg.

Regarding the TOPFLOW-PTS experiments, the stratified condensation is not negligible anymore. Hence, the ECC condensation mass flowrate must be calculated between the ECC and rake 4. On the contrary, the TOPFLOW-PTS tests are considered CETs if the condensation is computed between the ECC and rake 3.

For UPTF, the ECC condensation is estimated using rake 5, while the global condensation in the cold leg is computed with rake 3. These estimations may be affected by the behaviour of the thermal-hydraulic loop, since UPTF is an IET. This explains why the UPTF data are used

exclusively for the validation of the model and not in the assessment database, as discussed in Subsection 4.2.4.

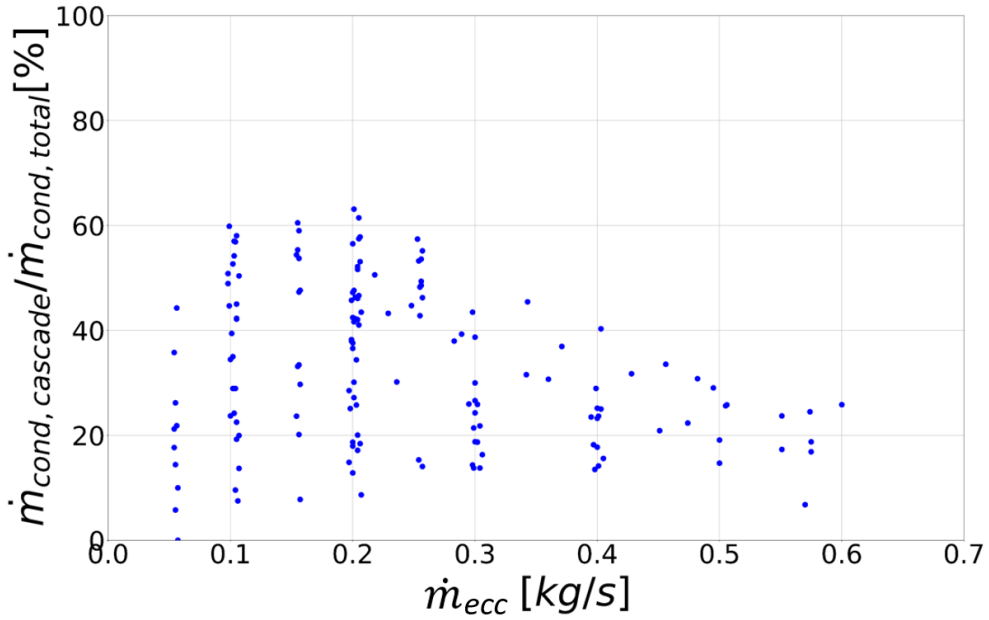

Figure 4.12: Percentage of the condensation due to the cascade over the total condensation for the COSI experiments.

Test	$\overline{T}_{rk,exp}$ SET	$\overline{T}_{rk,exp}$ CET
COSI-Fra	8	8
COSI-West	5	-
TOPFLOW-PTS sssw	4	3
TOPFLOW-PTS tsw	4	3
UPTF	5	3

Table 4.6: Thermocouple rake to be considered for a SET or CET experiment.

5 - Development and validation of a new ECC condensation model

This chapter is related to the second part of Paper II, where a new ECC condensation model is developed and validated.

In this chapter, the condensation models found in the literature are reviewed and assessed in Section 5.1 using the COSI and TOPFLOW-PTS new revised databases (Table 4.5). The classical modelling of the Nusselt number as a function of other dimensionless numbers does not seem to lead to accurate results. Thus, a new modelling strategy is proposed. In Section 5.2, the cold jet is modelled as a concentric heat exchanger with the steam. Sections 5.3 and 5.4 model respectively the heat exchanger area and the condensation potential. The condensation potential R, which describes the ECC capability to condense the steam, is function of a shape term and a functional variable called η. In Section 5.5, the Bayesian framework described in Chapter 2 is applied to calibrate a new correlation for η. Then, in Sections 5.6 and 5.7 the model is statistically and physically validated respectively. The uncertainties of the model are quantified in Section 5.8. Finally, the impact of the ECC stratification on the condensation is analysed in Section 5.9.

5.1 . Assessment of correlations found in the literature

In the introduction, the main condensation phenomena occuring in the cold leg during a LOCA have already been illustrated (Fig. 1.4) and commented. At the ECC, the condensation is mainly generated by the contact between the steam and the cold jet. However, this type of condensation was studied in a limited number of works and the proposed physical models should be assessed as proposed in Paper II.

The condensation phenomenology at the ECC jet was described in [60] by Bestion and Gros d'Aillon. They based the thermal-hydraulic analysis on the experimental results obtained in the COSI facility, finding out that the turbulence generated by the injection into the stratified liquid was responsible for the largest part of condensation in the test section. Hence, they decided to model the steam condensation using the Nusselt, Reynolds and Prandtl dimensionless numbers. The correlation depending only on the Reynolds was then improved by Janicot and Bestion in [53]. They modelled the turbulence as proportional to the liquid height in the test section H

and the exchange area as function of the void fraction and the ECC diameter.

In 2015, Liao et al. [25] proposed a new physical model based on the same features and using some other COSI tests. However, the turbulence length was defined as a function of the liquid height $f(H)$ and the heat exchange area was proportional to $f(H)$. The correlation has also been tested against some UPTF experiments.

Always in 2015, Ren et al. [61] described the Emergency Core Cooling System (ECCS) facility, which is very similar to COSI. The authors proposed some condensation models with the same heat exchange area defined by Liao et al.

Finally, Gaillard and Rodio [62] proposed a thermal stratification criterion for cold legs with ECC enabled. In their article, the condensation at the ECC injection is calculated by a new model but the tests used to calibrate the correlation are unknown. In this new model, the Froude number, the void fraction and the ratio of the ECC diameter over the test section diameter were added to better model the phenomenon. Indeed, their addition takes into account the disruption of the free surface of the jet. Differently from the other thermal-hydraulic correlations, the heat exchange area is defined as the cross section of the jet.

These physical models, as well as their characteristic lengths, reference temperature and temperature difference, are summarised in Table 5.1.

Authors	Correlation	Characteristic lengths, T_{ref} and ΔT
Janicot et al. [53]	$Nu = 0.5 \cdot Re$	$l_{Nu} = l_{Re} = H$ $u_{Re} = u_{ecc}$ $A_{ex} = d_{ecc} \cdot \sqrt{(1-\alpha) \cdot \alpha} \cdot D$ $T_{ref} = unknown$ $\Delta T = T_{sat} - T_{ecc}$
Liao et al. [25]	$Nu = 0.245 \cdot Re^{1.1} \cdot Pr^{0.6}$	$l_{Nu} = f(H) \cdot D$ $l_{Re} = d_{ecc}$ $u_{Re} = u_{ecc}$ $A_{ex} = d_{ecc} \cdot f(H) \cdot D$ $T_{ref} = (T_{sat} + T_{ecc})/2$ $\Delta T = T_{sat} - T_{ecc}$
Ren et al. [61]	$Nu = 3.773 \cdot Re$	$l_{Nu} = unknown$ $l_{Re} = d_{ecc}$ $u_{Re} = u_{ecc}$ $A_{ex} = d_{ecc} \cdot l_{Nu}$ $T_{ref} = unknown$ $\Delta T = T_{sat} - T_{ecc}$
Gaillard et al. [62]	$Nu = Re \cdot Pr \cdot Fr^{0.5} \cdot \alpha \cdot \frac{d_{ecc}}{D}$	$l_{Nu} = l_{Re} = l_{Fr} = H$ $u_{Re} = u_{Fr} = u_{ecc}$ $A_{ex} = d_{ecc}^2$ $T_{ref} = unknown$ $\Delta T = T_{sat} - T_{ecc}$

Table 5.1: ECC condensation correlations found in the literature.

These correlations are mainly calibrated using the COSI experiments (except for Ren et al.

who used the ECCS data) but the modelling features do not seem coherent with each other (i.e. different choices for dimensionless numbers and characteristic lengths). Thus, an assessment of these models against the new defined database is required. The correlation ability to calculate the output physical quantity is assessed through the absolute residuals defined in Eq. 2.12.

The performances of the models in Table 5.1 are tested against the reduced database in Table 4.5. If the reference temperature of the correlation is unknown, it is assumed to be equal to the Liao et al. one. The results are summarised in Table 5.2.

Model	$\mu(\lvert r_{abs,T_{rk}}\rvert)_{COSI}$ [°C]	$\mu(\lvert r_{abs,T_{rk}}\rvert)_{TOPFLOW-PTS}$ [°C]
Janicot et al.	53	87
Liao et al.	48	86
Gaillard et al.	72	20
Ren et al.	71	89

Table 5.2: Model errors against the new revised database.

The correlations do not show good predictive capabilities.

The Janicot et al., Liao et al. and Ren et al. physical models overestimate the mean liquid temperatures $\overline{T}_{rk,calc}$. This might be due to the wrong choice of control volume (e.g. the whole test section) to evaluate the ECC condensation.

The bad results of these correlations with respect to the TOPFLOW-PTS experiments could be explained by the models not scaling well with bigger geometries of ECC.

The Gaillard et al. model underestimates instead the condensation and performs better when applied to the TOPFLOW-PTS database. An explication could be the implementation of a shape factor d_{ecc}/D, which takes into account the jet dimensions.

With these poor results, a new approach for modelling the condensation of a liquid jet in a stratified flow is necessary.

5.2 . Modelling of the ECC jet as a heat exchanger

The jet can be modelled as a concentric heat exchanger, where the primary side is composed by the ECC jet and the secondary side by the steam. A visualisation of the heat exchanger is given in Fig. 5.1. The liquid enters the heat exchanger at T_{ecc} and leaves at $\overline{T}_{rk}$ while the steam is always at T_{sat}.

Along the jet length, the representative temperature differences between liquid and steam driving the heat exchange is chosen as the logarithmic mean temperature difference. It reads:

$$\Delta T_{ln} = \frac{\Delta T_{in} - \Delta T_{out}}{\ln\left(\Delta T_{in}/\Delta T_{out}\right)} = \frac{\overline{T}_{rk} - T_{ecc}}{\ln\left((T_{sat} - T_{ecc})/(T_{sat} - \overline{T}_{rk})\right)} \tag{5.1}$$

where ΔT_{in} and ΔT_{out} are the inlet and outlet temperature difference between the liquid and the steam respectively. From the definition in Eq. 5.1, the condensation heat flux can be rewritten as:

$$\dot{q}_{cond} = \dot{m}_{cond} \cdot I_{ls} = h \cdot A_{ex} \cdot \Delta T_{ln} \tag{5.2}$$

where I_{ls} is the latent heat of condensation, h is the heat transfer coefficient and A_{ex} is the heat transfer area, which should be carefully modelled.

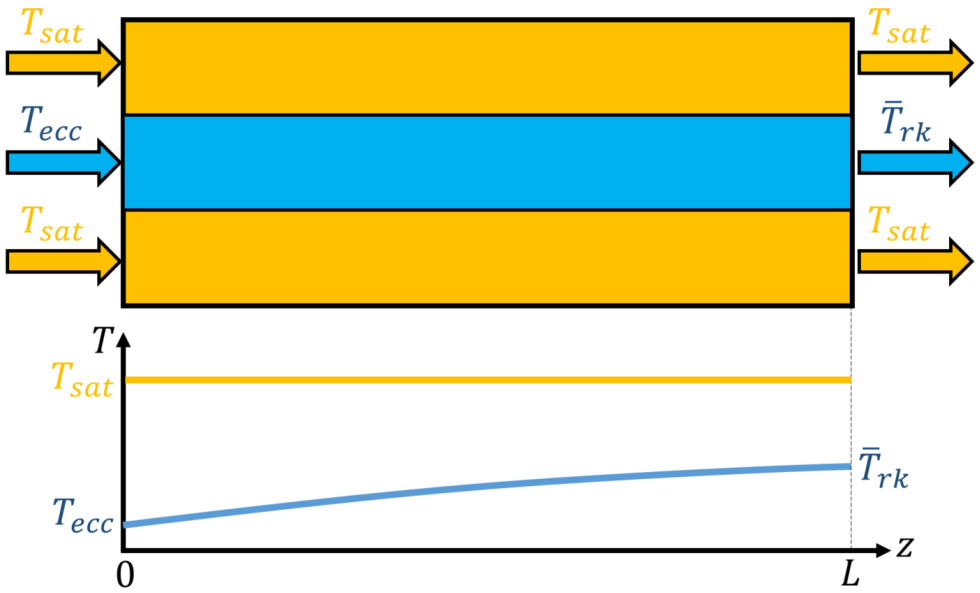

Figure 5.1: Visualisation of the ECC jet as a heat exchanger.

5.3 . Modelling of the heat transfer area A_{ex}

The heat transfer area A_{ex} in Eq. 5.2 has to be modelled. However, the chaotic and turbulent nature of the phenomena leads to different types of exchange areas (as shown schematically in Fig. 5.2 for a vertical injection).

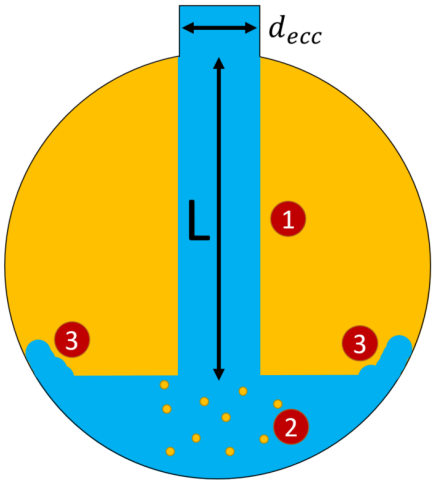

Figure 5.2: Heat exchange areas for a vertical ECC injection.

At least three zones may be identified. The first one is ideally cylindrical, from the outlet of the ECC pipe to the liquid flow. The second one is the entrainment zone, where the jet impacts the liquid. The third zone is called "rebound" zone, as the liquid rebounds on the cold leg sides (i.e. above the liquid free level). The last two areas are difficult to model. As supposed in [63], most of the condensation occurs in the cylindrical zone. For that reason, the heat exchange area in Eq. 5.2 is supposed to be:

$$A_{ex} = \pi \cdot d_{ecc} \cdot L = 4 \cdot A_{ecc} \cdot \frac{L}{d_{ecc}} \tag{5.3}$$

The jet length L can be estimated (for ψ_{ecc} <90° in Fig. 4.1c) by the Clausnitzer & Hager formula [64], which computes the lower trajectory (also called nappe) of a water jet exiting a quasi-horizontal pipe:

$$y' = \frac{1}{3} \cdot x' \cdot Fr^{-0.8} + \frac{1}{4 \cdot d_{ecc}} \cdot x'^2 \cdot Fr^{-1.6} \tag{5.4}$$

where (x', y') is the reference system in Fig. 5.3.

The velocity u_{ecc} and the diameter d_{ecc} of the ECC jet describe the Froude number. Hence, the nappe is dependent on the geometry and kinetic energy of the jet: a faster and thinner jet (high Froude) results in a longer trajectory.

The Clausnitzer & Hager formula has originally been developed for horizontal pipes with stratified flows at 1 bar. Thus, its application to our experimental database must be properly justified. Its application for inclined pipes at high pressure is validated thanks to the TOPFLOW-PTS tests images. In Fig. 5.3, the dimensionless experimental nappes (in light blue) of a TOPFLOW-PTS test are plotted. Eq. 5.4 is applied (using the experimental Froude number of the test) and rotated counter-clockwise of the injection angle ψ_{ecc} (Fig. 4.1c), resulting in a lower nappe (in green) that reproduces accurately the experimental curve. Then, the jet trajectory (in black) is obtained translating the green curve of $d_{ecc}/2$ towards the centre of symmetry of the jet. Finally, the segment between the ECC pipe exit and the parabola first point (the thin black segment) is added to the nappe. The length is finally obtained integrating the black curve.

This process is applied to the available TOPFLOW-PTS test images, leading to very good results. Thus, it is applied to the whole experimental database.

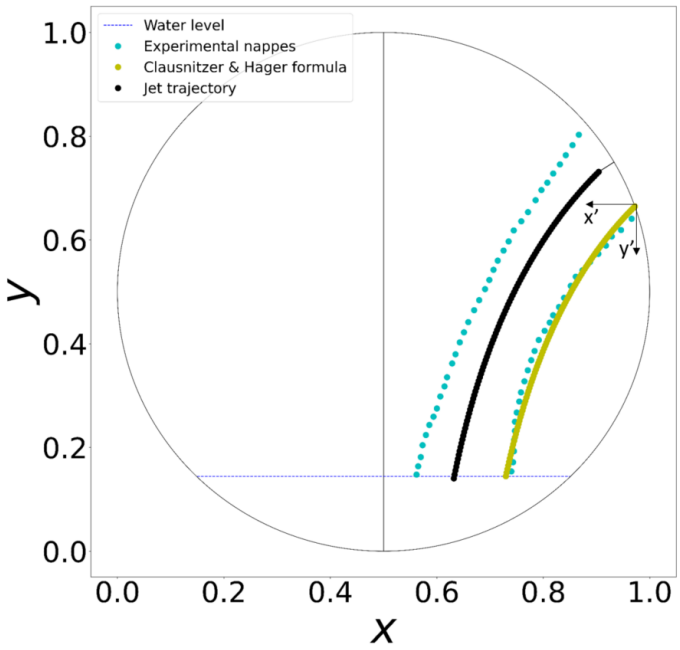

Figure 5.3: Application of the Clausnitzer & Hager formula to compute the lower nappe and the centred trajectory of the ECC jet in a TOPFLOW-PTS test.

5.4 . Modelling of the condensation potential R

As shown in Fig. 5.1, the temperature of the jet increases along its length due to the condensation of steam. The final temperature $\overline{T}_{rk}$ can vary between T_{ecc} (if no condensation occurs) and T_{sat}. We can thus define an ECC condensation potential R as:

$$R = \frac{\overline{T}_{rk} - T_{ecc}}{T_{sat} - T_{ecc}} \tag{5.5}$$

R can range between 0 and 1 and it can be interpreted as a measure of the efficiency of the jet to condense the steam.

In the literature, a condensation potential has already been analytically modelled [65] in analogy with the potential used to describe boiling [66, 67]. Eqs. 4.4 (to compute the ECC condensation mass flowrate), 5.2 and 5.3 can be combined to obtain the temperature difference between the outlet and the inlet of the heat exchanger:

$$\overline{T}_{rk} - T_{ecc} = \frac{q"_{cond}}{\dot{G}_{ecc} \cdot c_{p,ref}} \cdot 4 \cdot \frac{L}{d_{ecc}} \cdot \frac{I_{s,sat} - \overline{I}_{rk}}{I_{ls}} \tag{5.6}$$

Assuming that the Nusselt and Reynolds numbers have the same characteristic lengths, the Stanton number (defined from the heat flux in Eq. 5.2) can be written as:

$$St = \frac{q"_{cond}}{\dot{G}_{ecc} \cdot c_{p,ref}} \cdot \frac{\rho_{ecc}}{\rho_{ref}} \cdot \frac{1}{\Delta T_{ln}} \tag{5.7}$$

Thus, Eq. 5.6 can be combined with Eq. 5.7 giving:

$$\overline{T}_{rk} - T_{ecc} = St \cdot \frac{\rho_{ref}}{\rho_{ecc}} \cdot \Delta T_{ln} \cdot 4 \cdot \frac{L}{d_{ecc}} \cdot \frac{I_{s,sat} - \overline{I}_{rk}}{I_{ls}} \tag{5.8}$$

In the end, Eq. 5.8 can be put in Eq. 5.5:

$$R = 1 - exp\left(-4 \cdot St \cdot \frac{\rho_{ref}}{\rho_{ecc}} \cdot \frac{I_{s,sat} - \overline{I}_{rk}}{I_{ls}} \cdot \frac{L}{d_{ecc}}\right) \tag{5.9}$$

where the argument of the logarithm in Eq. 5.1 has been rewritten as $(1 - R)^{-1}$.

To summarise, the condensation potential can be analytically written as:

$$\begin{cases} R = 1 - exp\left(-4 \cdot \eta \cdot \frac{L}{d_{ecc}}\right) \\ \eta = St \cdot \frac{\rho_{ref}}{\rho_{ecc}} \cdot \frac{I_{s,sat} - \overline{I}_{rk}}{I_{ls}} \end{cases} \tag{5.10}$$

The condensation potential is thus dependent on a jet shape parameter L/d_{ecc} and a variable η.

In Fig. 5.4, R is plotted as function of the shape parameter.

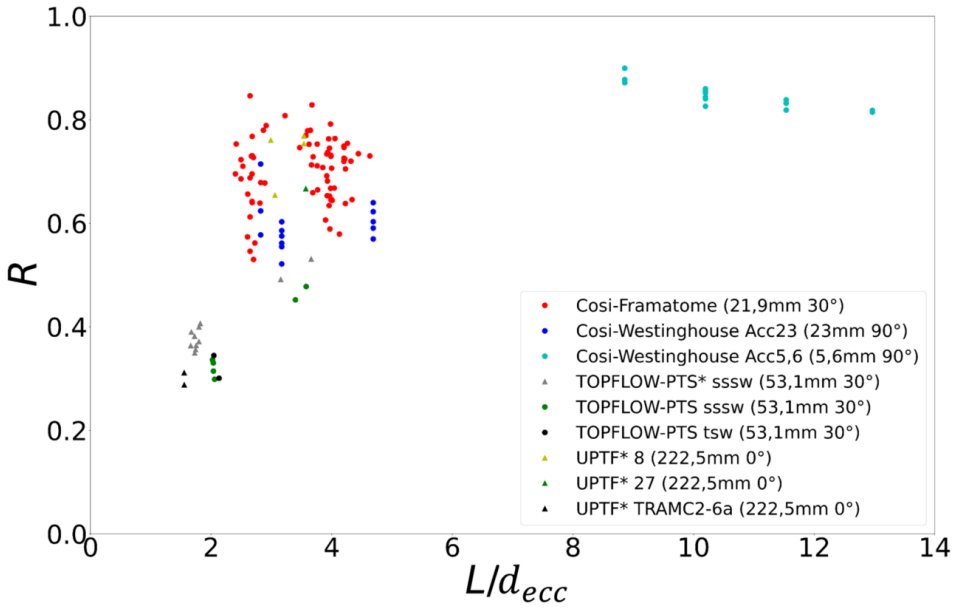

Figure 5.4: Condensation potential R plotted against the jet length over diameter ratio. The triangles are the validation tests (also marked as * in the legend).

The relationship between the two quantities seems to be exponential. The better exploited jet are thus the longer and thinner ones.

The analytical dependence in Eq. 5.9 matches with the exponential behaviour observed experimentally. A correlation for η can then be calibrated in order to fit the experimental data.

5.5 . Development of the correlation for η

During the experiments, the steam flowrate entering the test section (and consequently reaching the jet) varied and was often larger than the measured ECC condensation flowrate. It could be observed experimentally that increasing the steam flowrate (and therefore its velocity) could lead to a higher condensation due to the improved heat exchange between the steam and the jet. This phenomenon is visualised in Fig. 5.5, where the condensation potential of 11 COSI-Fra tests at different pressures are plotted against the steam mass flowrate $\dot{m}_s$ reaching the jet. These tests have the same (or very similar) $\dot{m}_{ecc}$, T_{ecc}, L/d_{ecc} and no weir at the end of the cold leg.

In Fig. 5.5, the condensation potential R is proportional to the steam reaching the jet. This dependency is modelled through the following Nusselt number:

$$Nu_{pot} = \frac{\dot{m}_s \cdot I_{ls} \cdot l_{Nu_{pot}}}{A_{ex} \cdot k_{th,ref} \cdot (T_{sat} - T_{ecc})} \tag{5.11}$$

where the characteristic length $l_{Nu_{pot}}$ is equal to the ECC diameter d_{ecc} and $k_{th,ref}$ is the thermal conductivity calculated at the reference temperature, which is assumed to be $(T_{sat} + T_{ecc})/2$. This Nusselt number is defined *potential* (subscripted *pot*) since it is calculated assuming that all the steam flowrate reaching the jet condenses, with the maximum temperature difference possible (i.e. $T_{sat} - T_{ecc}$).

In Fig. 5.6, the experimental values of η are plotted against Nu_{pot}. The axes are in a logarithmic scale.

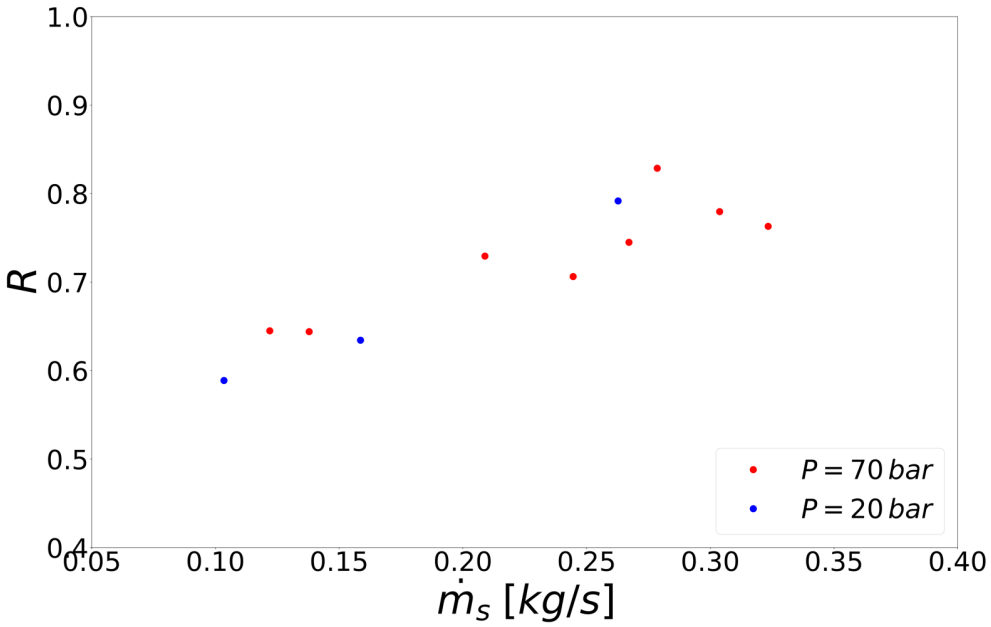

Figure 5.5: Condensation potential R plotted against the steam mass flowrate reaching the jet for some COSI-Fra tests. All the tests have the same $\dot{m}_{ecc}$, T_{ecc}, L/d_{ecc} and no weir at the end of the cold leg.

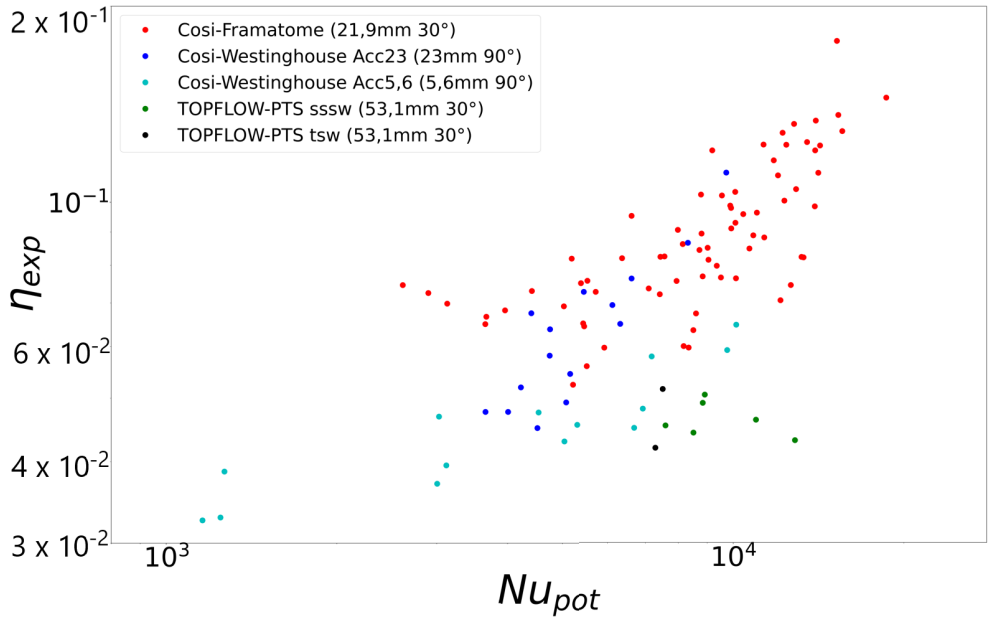

Figure 5.6: Experimental η plotted against the potential Nusselt dimensionless number. The axes are logarithmic.

The variable η is logarithmically proportional to the potential Nusselt number with a slope of about 0.5. Thus, the condensation occurring at the jet is not only dependent on its geometrical features (i.e. L/d_{ecc}), but a high steam mass flowrate reaching the jet enhances the condensation phenomena.

Moreover, η was observed to depend on the ECC injection properties. In order to isolate

the effect of the steam on the condensation, η is divided by $Nu_{pot}^{0.5}$ and it is plotted against the Reynolds number of the ECC injection (where $l_{Re_{ecc}} = d_{ecc}$). The axes are in a logarithmic scale.

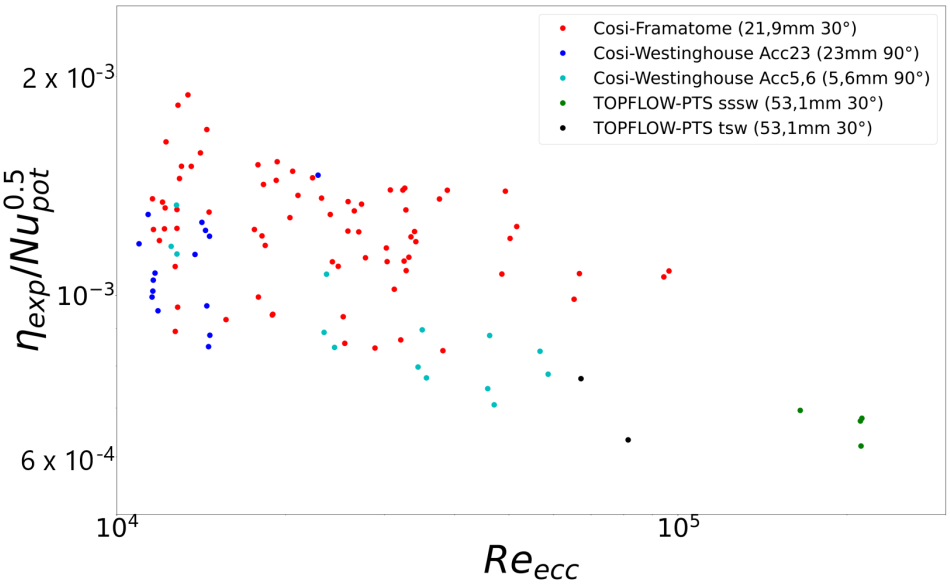

Figure 5.7: Ratio of η_{exp} over $Nu_{pot}^{0.5}$ plotted against the injection Reynolds dimensionless number. The axes are logarithmic.

In Fig. 5.7, the relationship between $\eta/Nu_{pot}^{0.5}$ and Re_{ecc} seems to be logarithmically linear and negative. To parity of steam arriving to the cold jet, an higher Reynolds jet has a lower η than a lower Reynolds jet, resulting in an higher condensation potential R.

Since the dependencies in Figs. 5.6 and 5.7 show high dispersion, the Prandtl number (calculated at the reference temperature $T_{ref} = (T_{sat} + T_{ecc})/2$) is introduced to obtain a better fit of the data. The variable η can thus be modelled as a function of these three dimensionless numbers:

$$\eta_{calc}(\mathbf{x}) = \theta_0 \cdot Nu_{pot}(\mathbf{x})^{\theta_1} \cdot Re_{ecc}(\mathbf{x})^{\theta_2} \cdot Pr_{ref}(\mathbf{x})^{\theta_3} \tag{5.12}$$

The coefficients θ are calibrated applying the Bayesian framework presented in Section 2.2 to the assessment database.

The range of applicability is given in Table 5.3.

	Applicability range
Nu_{pot}	[1159; 18624]
Re_{ecc}	[6216; 312118]
Pr_{ref}	[0.85; 1.47]
Fr_{ecc}	[1.04; 44.52]

Table 5.3: Range of applicability for the new condensation model for the development database.

The physical model in Eq. 5.12 is applied to the statistical model in Eq. 2.6:

$$\ln(\eta_{exp,i}(\mathbf{x}_i)) = \ln(\theta_0) + \theta_1 \cdot \ln(Nu_{pot,i}(\mathbf{x}_i)) + \theta_2 \cdot \ln(Re_{ecc,i}(\mathbf{x}_i)) + \theta_3 \cdot \ln(Pr_{ref,i}(\mathbf{x}_i)) \quad (5.13)$$

Through the Bayes theorem in Eq. 2.5, the joint *posterior* distribution $\tau(\ln(\theta_0), \theta_1, \theta_2, \theta_3, \sigma^2 | \ln(\eta_{exp,i}(\mathbf{x}_i)))$ can be calculated, sampled and the marginal *posterior* distributions plotted. The relative histograms are shown in Fig. 5.8. In these distributions, the MAP values are shown and the associated low standard deviations prove the accuracy of their Bayesian calibration.

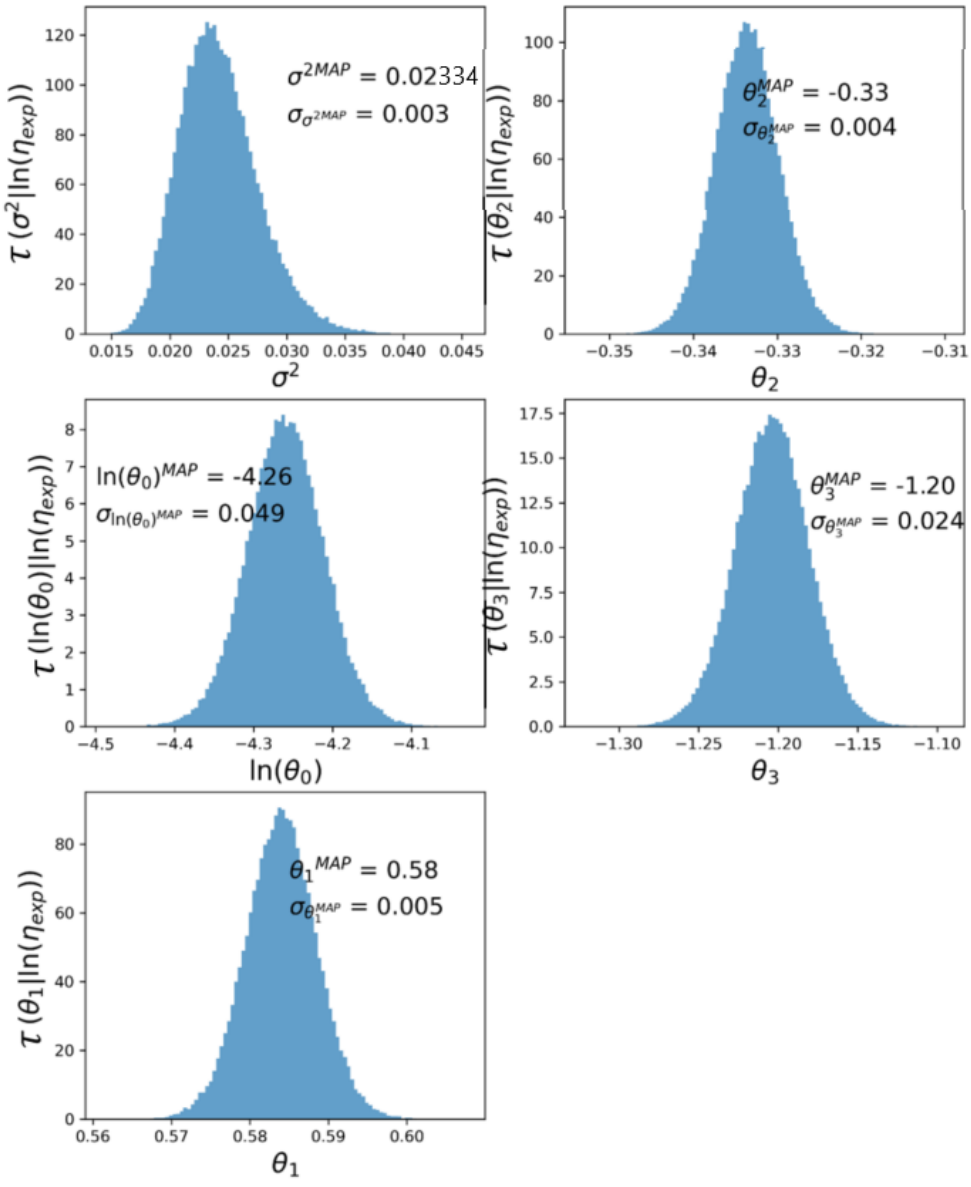

Figure 5.8: Marginal *posterior* distributions for the new condensation model.

In each distribution, the MAP value and the associated standard deviation are shown. The standard deviation are 2 orders of magnitude smaller than the MAP values, proving the accuracy of the Bayesian inference. Then, the MAP values are put in Eq. 5.13 and the assessed correlation for Eq. 5.12 is written through the application of the exponential function:

$$\eta_{calc}(\mathbf{x}, \boldsymbol{\theta}^{MAP}) = 0.014 \cdot Nu_{pot}(\mathbf{x})^{0.58} \cdot Re_{ecc}(\mathbf{x})^{-0.33} \cdot Pr_{ref}(\mathbf{x})^{-1.2} \tag{5.14}$$

with the associated model uncertainty:

$$\Lambda = \mathscr{L}\mathscr{N}(0,\, 0.02334) \tag{5.15}$$

The correlation capability to reproduce the experimental data is good since the coefficient R^2 (referred to the log-log model) is equal to 0.82.

Eq. 5.14 is applied to the assessment database and the results are plotted in Fig. 5.9. In Table 5.4, the errors are quantified.

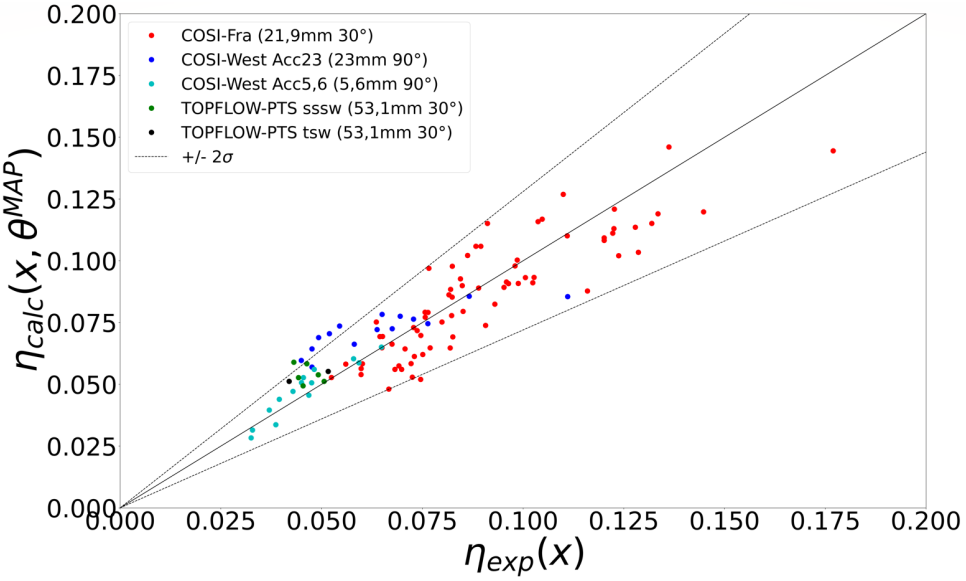

Figure 5.9: The η variable issued by the new condensation model (Eq. 5.14) against experimental over the assessment database.

Statistical indicator	Mean μ [%]	Standard deviation σ [%]	Min [%]	Max [%]
$r_{rel,\eta}$	1.2	15.4	-30.3	40
$\lvert r_{rel,\eta}\rvert$	12.3	-	-	-
$\lvert r_{rel,\eta}\rvert_{COSI}$	12	-	-	-
$\lvert r_{rel,\eta}\rvert_{TOPFLOW-PTS}$	16.3	-	-	-

Table 5.4: Relative prediction error on η for the new condensation model (Eq. 5.14).

The statistical indicators in Table 5.4 prove the good accuracy and precision of the model, with $2\sigma = 30.8\%$ and 12.3% average relative error.

Eq. 5.10 is then coupled with the new model and the mean liquide temperature $\overline{T}_{rk}$ is shown (as experimental versus calculated) for the assessment database. In Fig. 5.10, the red error bands quantify an error of ±30°C.

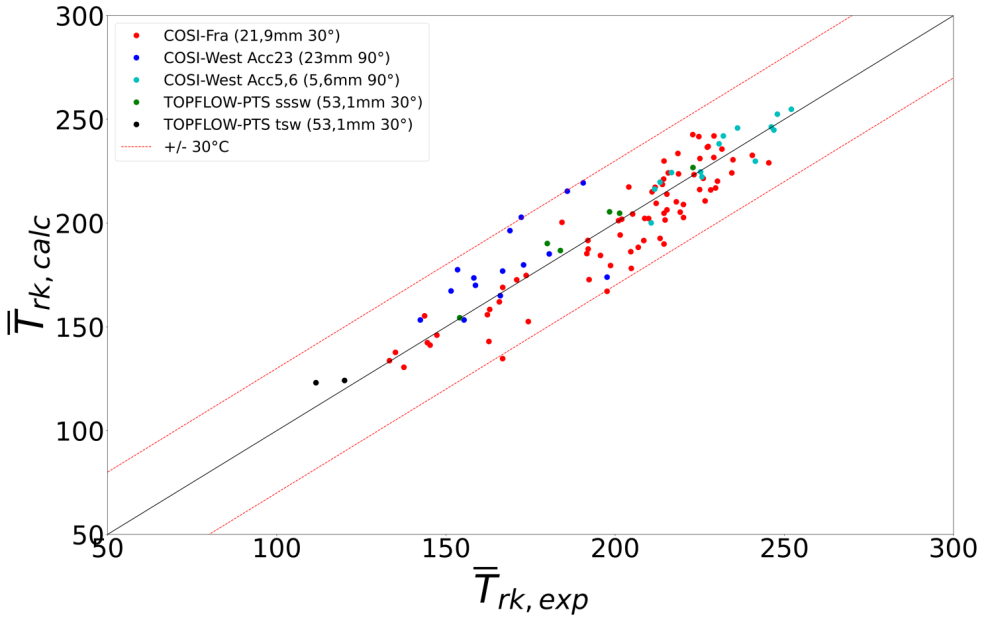

Figure 5.10: Prediction of the mean liquid temperature issued by the new condensation model against the assessment database.

In Table 5.5, the errors on the temperature are quantified:

Statistical indicator	Mean μ [°C]	Standard deviation σ [°C]	Min [°C]	Max [°C]
$r_{abs,\overline{T}_{rk}}$	-1	13	-32	31
$\lvert r_{abs,\overline{T}_{rk}} \rvert$	10	-	-	-
$\lvert r_{abs,\overline{T}_{rk}} \rvert_{COSI}$	10	-	-	-
$\lvert r_{abs,\overline{T}_{rk}} \rvert_{TOPFLOW-PTS}$	5	-	-	-

Table 5.5: Absolute errors on the temperature with respect to the assessment database.

The predictions are centred and the dispersion is equal to $2\sigma = 26°C$. Since the min and max are similar, the correlation is not systematically biased (i.e. the model does not have the trend to under- or over-estimate the temperature). Moreover, the model capability to simulate the experimental data is proved by the mean absolute errors being comparable with the experimental errors quantified in Subsection 4.3.1.

5.6 . Statistical validation of the condensation model

The statistical validation by LOO (described in Section 2.4) is applied to the correlation in Eq. 5.14. Figs. 5.11 and 5.12 show respectively the LOO residuals and the QQ plot. They seem confirming the normality assumption. The Kolmogorov-Smirnov normality test yields a p-value = 0.97, which is higher than the significance level (5%). Thus, the normality hypothesis is not contested.

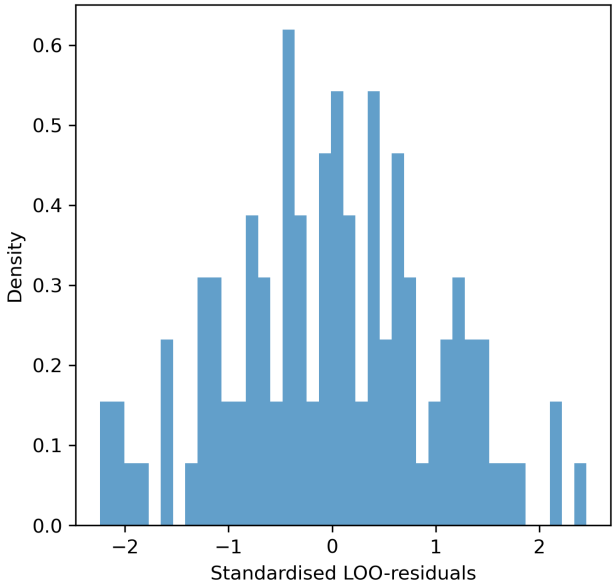

Figure 5.11: Standard residual histogram computed by LOO technique for the new condensation model (Eq. 5.14).

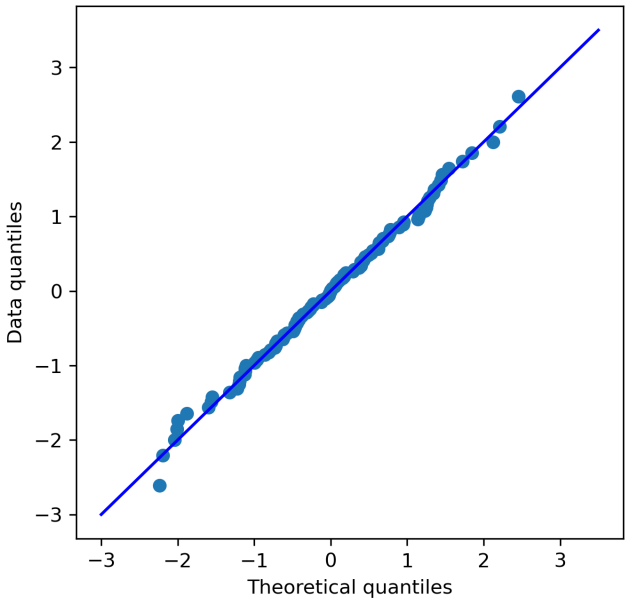

Figure 5.12: Calculated against theoretical quantiles for the new condensation model (Eq. 5.14).

5.7 . Physical validation of the condensation model

Once the correlation for η is statistically validated, the condensation model should be physically validated against the independent validation database (i.e. 7 UPTF tests and 11 TOPFLOW-PTS tests with a hot injection, as shown in Table 4.5). The dimensionless numbers range is shown in Table 5.6.

Applicability range	TOPFLOW-PTS	UPTF
Nu_{pot}	[12 013; 22 210]	[79 023; 439 013]
Re_{ecc}	[262 406; 337 139]	[435 417; 1 309 511]
Pr_{ref}	[0.84; 0.91]	[1.54; 2.16]
Fr_{ecc}	[1.22; 1.35]	[1.07; 2.81]

Table 5.6: Dimensionless numbers range for the validation database.

While the TOPFLOW-PTS ranges are slightly above the range of applicability in Table 5.3, the UPTF tests are far above those limits. However, the UPTF experiments (see Subsection 4.1.3) are representative of a full scale PWR and the prediction of these experiments is essential to establish the good behavior of the model in the reactor case. Assuming that the condensation phenomena at full scale are similar to the ones modelled by the new-developed correlation in Eq. 5.14, the condensation model should behave well even outside the assessment ranges.

In Fig. 5.13, the experimental and calculated temperatures are shown.

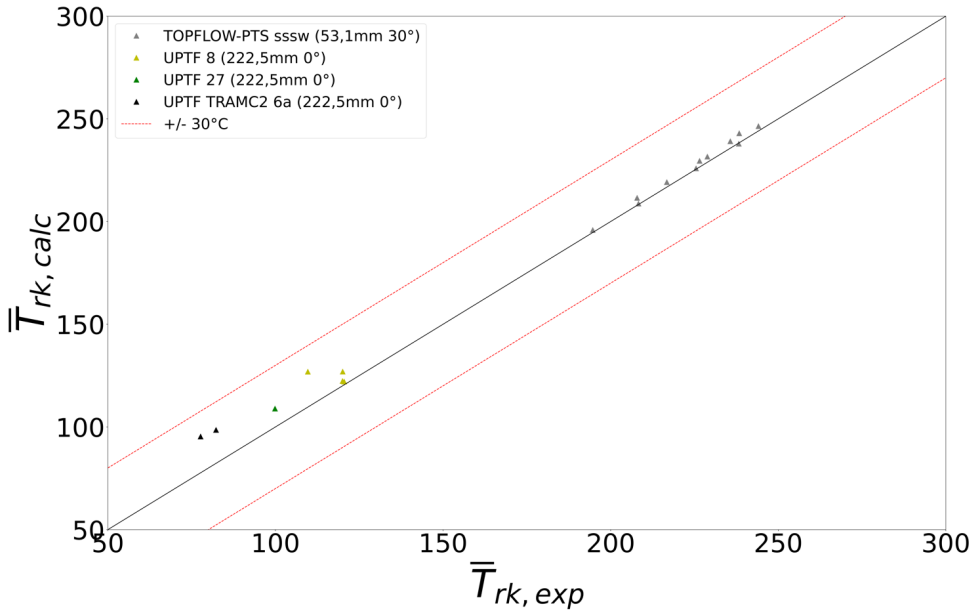

Figure 5.13: Prediction of the mean liquid temperature against the validation database.

In Table 5.7, the absolute errors on the temperature are summarised.

Statistical indicator	Mean μ [°C]
$\lvert r_{abs,\overline{T}_{rk}} \rvert_{UPTF}$	10
$\lvert r_{abs,\overline{T}_{rk}} \rvert_{TOPFLOW-PTS}$	2

Table 5.7: Absolute errors on the temperature with respect to the validation database.

The errors have the same order of magnitude of the ones computed for the assessment database (see Table 5.5), confirming the good capability of the model to predict the condensation at the ECC.

5.8 . Uncertainty quantification

In Fig. 5.14, the model and parameters uncertainties of Eq. 5.14 are computed and compared. For each test in the assessment database, the value calculated by the correlation is plotted as a blue point, the parameter uncertainty is the blue error bar (i.e. the 95% level quantile of the distribution in Eq. 2.14) and the model uncertainty is the red error bar (i.e. the 95% level quantile of the exponential values of Eq. 2.16).

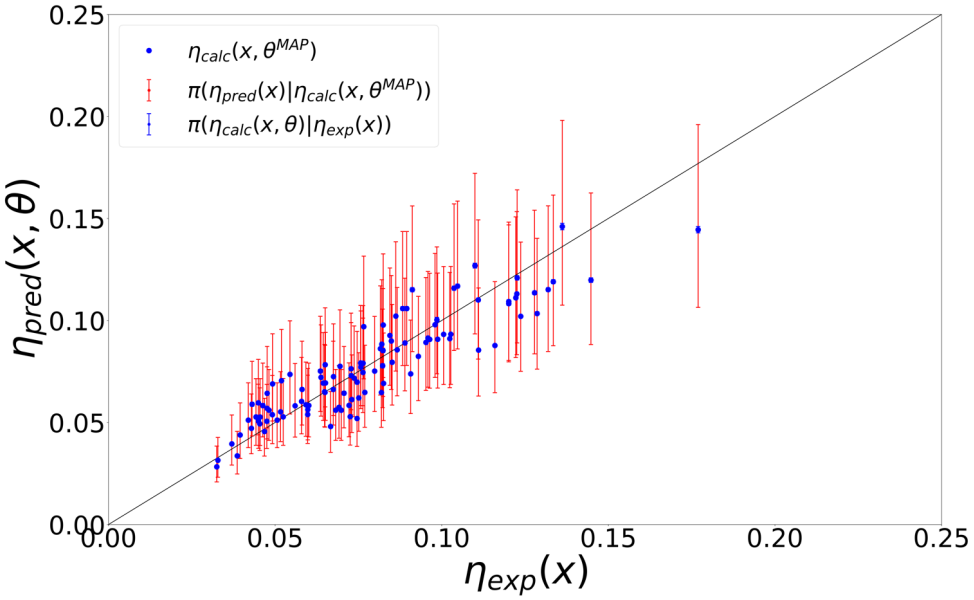

Figure 5.14: Uncertainties quantification for the new condensation model (Eq. 5.14).

As expected from the small standard deviations of the parameters in Fig. 5.8, the blue bars are negligible with respect to the model uncertainty. This can be explained by the relatively high number of tests in the experimental database that reduces the parameter uncertainty, but not the uncertainty intrinsically associated to the model.

Eq. 2.17 is applied to compute the fluctuation interval at 95% of the new correlation:

$$IF_{95\%}(\Lambda) = [0.74, 1.35] \tag{5.16}$$

5.9 . Impact of the ECC stratification on condensation

As shown in Subsection 4.2.1, a stratification can occur in the ECC pipe at low injection mass flowrates. This phenomenon strongly impacts the injection velocity and the heat exchange area, thus the condensation.

To investigate the impact of the stratification on the condensation, the new condensation model is applied to the 2 tests in Table 4.4 doing two different hypotheses: the ECC pipe is either full or half-full. The results are in Table 5.8.

For both tests, taking into account the stratification results in a smaller absolute error between the calculated and experimental mean liquid temperature.

A reliable modelling of the stratification phenomenon is thus necessary for the rigorous simulation of the ECC condensation.

	$\overline{T}_{rk,exp}$	$\overline{T}_{rk,calc}$ with $S_{ecc} = 100\%\, S_{inj}$	$\overline{T}_{rk,calc}$ with $S_{ecc} = 50\%\, S_{inj}$
sssw	195.4	188.6	195
tsw	146.9	130.7	142.9

Table 5.8: Impact of the ECC stratification on the condensation in some TOPFLOW-PTS tests (values in °C).

6 - Application of CIRCE and CIRCE 2-Steps

This chapter is related to the second part of Paper III, where CIRCE and CIRCE 2-Steps are applied to the correlations simulating the condensation in the cold leg.

In Chapter 5, a new ECC condensation model was developed and its uncertainties quantified using an appropriate SETs database. This has been possible since the CETs presented in Chapter 4 have been carefully analysed and finally reduced to SETs. However, the possibility of separating the effects is not always available in practical applications.

In this chapter, we are thus interested in applying the newly developed CIRCE 2-Steps methodology (see Chapter 3) to our CETs database and compare it to the standard CIRCE methodology. Section 6.1 presents the CETs database used for the IUQ and its modelling. In Section 6.2, the standard CIRCE methodology is applied to jointly quantify the two model uncertainties. In Section 6.3, the model uncertainty of the newly developed correlation (Eq. 5.14) is quantified with CIRCE 2-steps and the results are discussed.

6.1 . The CETs experimental database and its modelling

The CETs database for the IUQ is composed by 73 COSI-Fra and 8 TOPFLOW-PTS tests. As explained at the end of Subsection 4.3.2, the COSI-West configuration cannot be used since there are no experimental measurements at the end of the cold leg. As seen in Table 4.6, the chosen experimental QoI for the IUQ is $\overline{T}_{rk8}$ for COSI-Fra and $\overline{T}_{rk3}$ for TOPFLOW-PTS.

The modelling of the experiments is shown in Fig. 6.1.

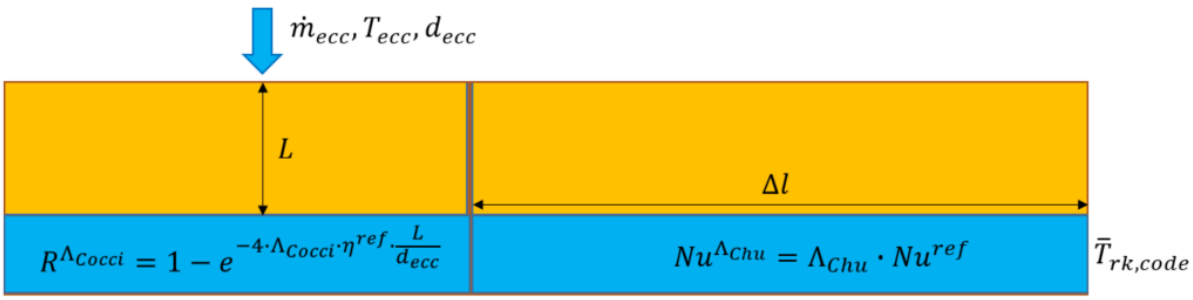

Figure 6.1: Control volumes to model the two condensation phenomena.

The test section is modelled with two cells where L is the jet length and Δl is the liquid-steam interface length. In the cell on the left, the newly developed model (Eq. 5.14) is used to calculate the ECC condensation. For simplicity, this model will be indicated as Cocci in the rest of the chapter. In the other cell, the Chu model [68] quantifies the condensation due to the contact of the two phases at the stratified interface:

$$Nu = 2.21 \cdot 10^{-8} \cdot Re_s^{0.31} \cdot Re_l^{1.32} \cdot Ja_l^{1.36} \tag{6.1}$$

This model has been calibrated against experiments simulating a two-phase flow (at different values of liquid and steam mass flowrates) inside an horizontal circular pipe without sub-cooled injection.

In Eq. 6.1, the input dimensionless numbers are computed from the QoIs calculated by the first model.

The associated model uncertainty has already been estimated at CEA [69] and it is equal to:

$$\Lambda_{Chu} = \mathscr{N}(0.98,\, 0.101) \tag{6.2}$$

The system in Fig. 6.1 is solved in Python 3 where the models are coupled with the conservation equations for energy and mass. The final $\overline{T}_{rk,code}$ is used in the CIRCE statistical equation (Eq. 3.3) as the code output:

$$\overline{T}_{rk,exp}(\mathbf{x}_i) \approx \overline{T}_{rk,code}(\mathbf{x}_i, R^{\Lambda_{Cocci,ref}}(\mathbf{x}_i), Nu^{\Lambda_{Chu,ref}}(\mathbf{x}_i)) \,+\, \mathbf{J}(\mathbf{x}_i) \cdot \mathbf{b}_i^T \,+\, \epsilon_i \tag{6.3}$$

6.2 . CIRCE joint estimation of the model uncertainties

The CIRCE methodology is applied to the CETs to jointly calculate the uncertainties of both the models where, for the model j and the test i, the derivative is calculated through the finite difference method:

$$\left.\frac{\partial \overline{T}_{rk,code}(\mathbf{x}_i)}{\partial \lambda_j}\right|_{\lambda_{j,ref}=1} = \frac{\overline{T}^{\lambda_j=1.1}_{rk,code}(\mathbf{x}_i) - \overline{T}^{\lambda_j=0.9}_{rk,code}(\mathbf{x}_i)}{1.1 - 0.9} \tag{6.4}$$

where $\overline{T}^{\lambda_j=\lambda^*}_{rk,code}(\mathbf{x}_i)$ is the code output computed modifying Λ_j in Fig. 6.1. The calculated derivatives are shown in Fig. 6.2. The arithmetic mean of the Cocci derivatives is equal to 78.3 °C, while the Chu one is equal to 0.9 °C. The scaling parameter k is thus ~ 86. Hence, the estimation of the Chu model uncertainty is expected to be affected by great uncertainty and poor identifiability.

CIRCE is applied to jointly estimate the two model uncertainties. As discussed in Section 2.1, the safety authorities agree to consider only the model uncertainty, neglecting the experimental one.

In Table 6.1, the bias distribution estimated through the ECME algorithm are reported. In Table 6.2, the associated NECs are available.

	Distribution
b_{Cocci}	$\mathscr{N}(0.05253,\, 0.01837)$
b_{Chu}	$\mathscr{N}(-1.12071,\, 0.00334)$

Table 6.1: Bias probability distribution estimated by the CIRCE methodology.

	$NEC(m^{MLE})$	$NEC\left(\sqrt{\sigma^{2MLE}}\right)$
b_{Cocci}	0.17	0.02
b_{Chu}	21.48	85.89

Table 6.2: NECs associated to the parameters in Table 6.1.

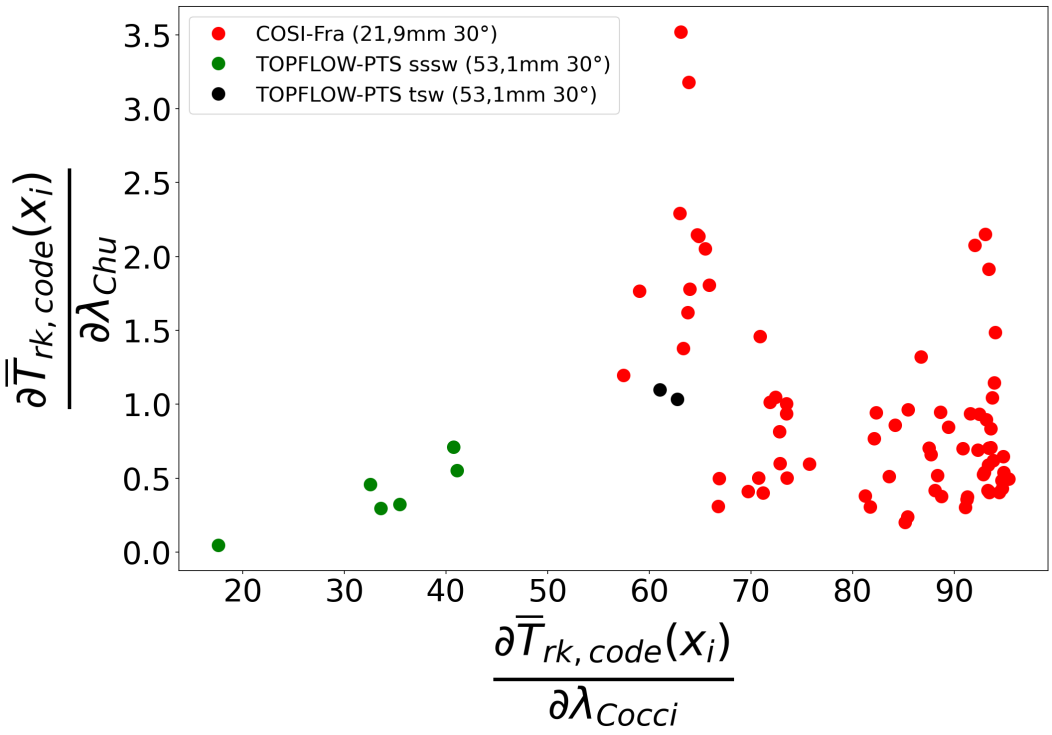

Figure 6.2: Derivatives of the two models obtained with the finite difference method.

While the NECs of the Cocci model are small, the indicators of the Chu correlation are dramatically above 1. This proves that the Chu bias distribution is not identifiable and the values obtained by CIRCE are affected by low accuracy and precision.

After an analysis about the linearisation of the code output near the reference value, the Cocci model uncertainty is assumed to follow a log-normal probability density while Chu a normal one. From Table 6.1, the model uncertainties read:

$$\begin{aligned} \Lambda_{Cocci} &= \mathscr{LN}(0.05253,\, 0.01837) \\ \Lambda_{Chu} &= \mathscr{N}(-0.12071,\, 0.00334) \end{aligned} \tag{6.5}$$

In Eq. 6.5, the Cocci uncertainty is similar to Eq. 5.15 but the CIRCE methodology penalises the mean estimation trading a part of the variance for an increased mean. However, the difference between the two approaches may be due to the different assumptions made during the IUQs. The Bayesian IUQ neglected the contribution of the stratified condensation on $\overline{T}_{rk,8}$ in the COSI-Fra experiments. It used a different thermocouple rake than CIRCE for the TOPFLOW-PTS tests ($\overline{T}_{rk,4}$ replaces $\overline{T}_{rk,3}$), since the stratified condensation is not negligible. Finally, the COSI-West tests were not considered in the estimation with CIRCE.

Taking those in account, it is not surprising that the two estimations sligthly differ.

The Chu model uncertainty distribution is however very different from Eq. 6.2 and has a negative mean. This results in a negative Nusselt number (on average) and thus a negative condensation mass flowrate (i.e. the cold water evaporates in the hot steam). Hence, the CIRCE estimation is physically inconsistent.

The high value of the scaling parameter led to a degradated joint estimation of the model uncertainties. The CETs database is thus not appropriate to quantify the uncertainty of the Chu model (too small derivatives) but can be used to estimate the Cocci model uncertainty through the CIRCE 2-Steps methodology.

6.3 . Application of CIRCE 2-Steps

As discussed in Section 6.1, the model uncertainty of the Chu model was already quantified on an appropriate SETs database (Step 1 of CIRCE 2-Steps). We can then apply the second step of the methodology (see Section 3.4) to evaluate the model uncertainty of the Cocci model, which is the most influent model on the QoI. The bias distribution reads:

$$b_{Cocci} = \mathscr{N}(0.03670,\, 0.01857) \tag{6.6}$$

The mean is significantly lower than the value in Table 6.1 while the variance is nearly unchanged.

The associated NECs read:

$$NEC(m^{MLE}_{b_{Cocci}}) = 0.11,\; NEC\left(\sqrt{{\sigma^2}^{MLE}_{b_{Cocci}}}\right) = 0.02 \tag{6.7}$$

While the NEC of the standard deviation is unchanged, the mean one is reduced. This results in a better inverse problem identificability, as well as a more accurate and precise estimation of the bias mean (i.e. closer to the zero-mean).

The Cocci model uncertainty is written as:

$$\Lambda_{Cocci} = \mathscr{LN}(0.03670,\, 0.01857) \tag{6.8}$$

and its interval of fluctuation at 95% (Eq. 2.17) reads:

$$IF_{95\%}(\Lambda_{Cocci}) = [0.79,\, 1.35] \tag{6.9}$$

The uncertainties calculated in Eqs. 6.1 and 6.8 should be validated through the LOO cross validation described at the end of Section 3.1.

The experimental QoIs are enveloped by the computed distributions 76 times out of 81. The associated envelope rate is 93.8%. It can be accepted for two main reasons: the size of the IUQ database is quite small (less than 100 tests) and the 5 tests which fail the cross validation are not enveloped by less than the experimental error (quantified in Subsection 4.3). The uncertainties are thus considered validated.

In Table 6.3, the results of the three IUQ methodologies are summarised.

	Bayesian IUQ	CIRCE	CIRCE 2-Steps
Λ_{Cocci}	$\mathscr{LN}(0,\ 0.02334)$	$\mathscr{LN}(0.05253,\ 0.01837)$	$\mathscr{LN}(0.03670,\ 0.01857)$
$IF_{95\%}(\Lambda_{Cocci})$	[0.74, 1.35]	[0.81, 1.37]	[0.79, 1.35]
NEC($m_{b_{Cocci}}^{MLE}$)	-	0.17	0.11
NEC $\left(\sqrt{{\sigma^2}_{b_{Cocci}}^{MLE}}\right)$	-	0.02	0.02

Table 6.3: Summary of the IUQ of the Cocci model with different IUQ methodologies.

CIRCE 2-Steps improves the estimation of the fluctuation interval: the higher bound is equal to the one computed by Bayesian IUQ in Eq. 5.16. However, the lower bound is higher resulting in a more narrow fluctuation interval. The identifiability of the mean is also improved (i.e. lower NEC).

It would be interesting to apply CIRCE 2-Steps using the derivatives and the calculated quantities issued by a thermal-hydraulic system code. In this case, the estimated model uncertainties may interact with other uncertainties linked to the simulation (e.g. the code uncertainty), resulting in a more uncertain estimations.

7 - Conclusions and perspectives for future work

In this doctoral work, advanced statistical methodologies for the calibration and the inverse uncertainty quantification of thermal-hydraulic correlations have been developed and applied to the condensation model at the Emergency Core Cooling (ECC) system of a nuclear Pressurised Water Reactor. These contributions have the goal to improve the thermal-hydraulic system simulations and uncertainty quantification for nuclear safety analyses and licensing processes.

7.1 . Summary and conclusions

The summary and conclusions are divided according to the main contribution of this Ph.D. thesis:

- Proposal of a new Bayesian framework for the calibration and inverse uncertainty quantification of thermal-hydraulic correlations using a multiplicative model uncertainty (Paper I and Chapter 2);
- Development of a new ECC condensation model based on a detailed thermal-hydraulic and physical analysis of available experimental data (Paper II and Chapters 4 and 5);
- Extension of the CIRCE methodology to better predict the model uncertainties in the presence of Combined Effect Tests (CETs) (Paper III and Chapters 3 and 6).

7.1.1 . Bayesian framework for the calibration and inverse uncertainty quantification of thermal-hydraulic models

In nuclear thermal-hydraulic, the experiments are expensive and difficult to perform, resulting in a limited number of available data. However, they are necessary to assess physical models (or correlations) for thermal-hydraulic codes through the calibration of parameters. Since the dimension of the experimental database can be small, the calibrated parameters may have high uncertainty.

In this thesis, a new framework for the calibration and inverse uncertainty quantification of thermal-hydraulic correlations is proposed. The physical models are calibrated through Bayesian inference, which allows modelling the uncertain parameters as random variables. In order to take into account the scaling of the model, the model uncertainty is represented as a multiplicative distribution between the calculated and experimental data.

After the calibration, a set of statistical indicators are proposed to assess the linearity, accuracy and precision of the physical model. Moreover, the normality assumption of the model uncertainty is statistically checked through a Leave-One-Out cross validation technique. In the end, the probability densities of the model uncertainty and the parameters are used to quantify the global uncertainty of the thermal-hydraulic correlation.

7.1.2 . Development of a new ECC condensation model

The condensation phenomena at the ECC injection have been studied in different experiments called COSI, TOPFLOW-PTS and UPTF. The first two experiments are classified as CETs, since at least two macroscopic condensation phenomena take place in the cold leg. The UPTF experiment is an Integral Effect Test (IET), since it has all the main components of a PWR.

A detailed physical analysis is performed over the experimental database and two methodologies are proposed to improve the computation of some experimental quantities:

1. The mean liquid temperature of a thermocouple rake: the methodology selects the last thermocouple in the liquid and, assuming a uniform velocity field, averages the temperatures;

2. The ECC condensation mass flowrate: following local heat balances between different thermocouple rakes, it allows establishing the distribution of the condensation in the different zones of the cold leg.

The second methodology allows us to reduce the CETs/IETs in Separate Effect Tests (SETs). The condensation mass flowrate in the ECC region can be isolated and thus be modelled by a correlation.

The reduced database is composed by 110 tests for the assessment of the model and 18 tests for its physical validation. The assessment database is used to assess the correlations found in the literature, which are all characterised by a heat transfer coefficient modelled through the Nusselt number (i.e. as a function of other dimensionless numbers). The results show a large discrepancy between the calculated and experimental values. Thus, a new modelling approach is proposed. The jet is modelled as a concentric heat exchanger through a condensation potential, which quantifies the efficiency of the ECC to condense the steam. The equation of the potential is analytically derived. It follows an exponential function of a variable η and a shape factor $^{L}/_{d_{ecc}}$ (i.e. proportional to the ratio between the heat exchange and jet cross section areas). An empirical model for η is calibrated as a function of the steam potential Nusselt, the ECC Reynolds and the Prandtl numbers. The steam potential Nusselt takes into account the quantity of steam reaching the jet and the maximum temperature difference driving the heat exchange. The condensation model is assessed on the assessment database and validated independently on the validation one, showing a good agreement between the calculated and experimental results. The mean error on the liquid temperature in the cold leg is around 10°C for both database.

7.1.3 . Extension of the CIRCE methodology to CETs

The CIRCE methodology is usually devoted to the inverse uncertainty quantification of physical models. The model uncertainty is modelled through a multiplicative (log-)normal distribution, which is applied to the reference model. The goal of CIRCE is the empirical estimation of the mean and variance of the probability distribution. However, when the uncertainties of several models are jointly estimated using CETs (where two or more models interact

with each other and impact the code output), the estimation of the least influential model uncertainty may suffer of unidentifiability (i.e. the mean and variance are affected by large statistical uncertainty). The problem is investigated thanks to analytical examples through a scaling parameter between two correlations, which is proportional to the ratio of the derivatives mean. We have shown that the unidentifiability of the problem gets worse as the scaling parameter grows.

The new methodology CIRCE 2-Steps is proposed in order to reduce the identifiability problem. In the first step, the least influential model uncertainties are estimated using the available SETs (where the model whose uncertainty has to be assessed is the only one that impacts the code output). In the second step, the most influential model uncertainty is calculated through CETs, taking into account the uncertainties already quantified in the first step. CIRCE 2-Step is then applied to some analytical exercises, leading to better accuracy and precision.

Finally, CIRCE 2-Steps is applied to two condensation models simulating the condensation in the cold leg. The new methodology is used to estimate the uncertainty of the new condensation model at the ECC, leading to coherent results with the Bayesian IUQ.

7.2 . Perspectives for future work

This research has identified some points that would require further investigations. The recommendations for future works can be divided in two: from a physical and a statistical point of view.

7.2.1 . Future work to improve the physical modelling

- The flow stratification inside the ECC pipe can impact significantly the condensation occurring during a safety injection. Thus, this phenomenon should be further investigated, both from the experimental and the modelling point of view to obtain the stratification height in the ECC pipe. In particular, new experiments are necessary for the stratification in inclined pipes. The development of an experimental database may begin from the study of the flow in an inclined pipe with air-water at atmospheric pressure. Then, more complex experiments with steam-water stratification at high pressure would be needed;

- Once a physical model for the stratified height in inclined pipes is assessed, it should be coupled with the newly developed condensation model which is valid only for fully filled ECC pipes. In this way, the applicability and validity of the ECC modelling could be extended;

- The new condensation model should be implemented in a thermal-hydraulic system code. Its performance and potential interaction with other physical models in the code should be analysed. The Clausnitzer & Hager formula should be implement as well to compute the ECC jet length.

7.2.2 . Future works to improve the Inverse Uncertainty Quantification

- The experimental uncertainty ϵ (if it is available) should be integrated in the model updating equation of the Bayesian framework and CIRCE 2-Steps to study its potential impact. The CIRCE algorithm implemented in the URANIE platform [70, 71] is already developed to take into account ϵ and just need the values as input data. Currently, the quantified uncertainty is fully associated to the model, resulting in a more conservative fluctuation interval;

- The proposed Bayesian framework with a multiplicative model uncertainty should be compared to the approach with additive uncertainty function of the experimental conditions. This additive uncertainty could be modelled by a Gaussian process;
- The proposed methodologies should be compared to other IUQ techniques, e.g. the improved Modular Bayesian Approach [37] or IPREM [72];
- CIRCE 2-Steps has been applied to compute Maximum Likelihood Estimation of factors' mean and variance. However, the parameter uncertainty should also be quantified. The recently developed Bayesian CIRCE [73] should thus be tested. It computes posterior probability of factor's mean and variance, which can then be propagated to the calculation of fluctuation intervals;
- CIRCE 2-Steps should be applied to three or more coupled models. For example, it would be interesting to study the case with three models of which two are more influential than the third one over the code output. The less influential model uncertainty could then be estimated with appropriate SETs and the other two uncertainties could be jointly estimated against CETs;
- CIRCE 2-Steps should be tested to estimate the uncertainties of two models with similar influence over the code output. The results should be compared with the ones obtained with the standard CIRCE methodology;
- The application of CIRCE 2-Steps should be studied in combination with thermal-hydraulic system codes to identify possible interactions/compensations with other uncertainties linked to the simulation (e.g. the code uncertainty). Basically, CIRCE 2-Steps should use input data (i.e. code outputs and derivatives) calculated by the system code;
- The non-linear approach of CIRCE [73] based on Gaussian process [74] could be used if the linearity assumption is not well respected.

Bibliography

[1] Nuclear Power in France. https://world-nuclear.org/information-library/country-profiles/countries-a-f/france.aspx?

[2] F. S. D'Auria et al. *Deterministic Safety Analysis for Nuclear Power Plants. IAEA Specific Safety Guide*. IAEA, 2009.

[3] J. Mahaffy et al. Best practice guidelines for the use of CFD in nuclear reactor safety applications-revision. *NEA/CSNI/R(2014)11*, 2015.

[4] V.H. Ransom. RELAP5/MOD2: for PWR transient analysis. In *Proceedings of the International Conference of Nucmerical Methods in Nuclear Engineering, Montreal, Canada*, 1983.

[5] NRC-US. TRACE V5. 0 Assessment Manual Main Report. *Division of Risk Assessment and Special Projects, Office of Nuclear Regulatory Research, Washington, DC*, 58, 2008.

[6] G. Geffraye et al. CATHARE 2 v2.5_2: A single version for various applications. *Nuclear Engineering and Design*, 241(11):4456–4463, 2011.

[7] C. Demazière. Multi-physics modelling of nuclear reactors: current practices in a nutshell. *International Journal of Nuclear Energy Science and Technology*, 7(4):288–318, 2013.

[8] N. E. Todreas and M. S. Kazimi. *Nuclear systems volume I: Thermal hydraulic fundamentals*. CRC press, 2021.

[9] R.H.S. Winterton. Where did the Dittus and Boelter equation come from? *International journal of heat and mass transfer*, 41(4-5):809–810, 1998.

[10] P. R. Bevington, D. K. Robinson, J. M. Blair, A. J. Mallinckrodt, and S. McKay. Data reduction and error analysis for the physical sciences. *Computers in Physics*, 7(4):415–416, 1993.

[11] U.S. Nuclear Regulatory Commission. Acceptance criteria for emergency core cooling systems for light-water nuclear power reactors. *Code of Federal Regulations: 10 CFR 50.46*, 2007.

[12] T.K.S. Liang et al. Development of LOCA licensing calculation capability with RELAP5-3D in accordance with Appendix K of 10 CFR 50.46. *Nuclear Engineering and Design*, 211(1):69–84, 2002.

[13] *Best Estimate Safety Analysis for Nuclear Power Plants: Uncertainty Evaluation*. Number 52 in Safety Reports Series. International Atomic Energy Agency, Vienna, 2008.

[14] Autorité de Sûreté Nucléaire. Qualification des outils de calcul scientifique utilisés dans la démonstration de sûreté nucléaire. *Guide 28*, 2017.

[15] B.E. Boyack et al. Quantifying reactor safety margins part 1: an overview of the code scaling, applicability, and uncertainty evaluation methodology. *Nuclear Engineering and Design*, 119(1):1–15, 1990.

[16] H. Glaeser. GRS method for uncertainty and sensitivity evaluation of code results and applications. *Science and Technology of Nuclear Installations*, 2008, 2008.

[17] F. D'Auria and W. Giannotti. Development of a code with the capability of internal assessment of uncertainty. *Nuclear technology*, 131(2):159–196, 2000.

[18] A. Petruzzi and F. D'Auria. Approaches, relevant topics, and internal method for uncertainty evaluation in predictions of thermal-hydraulic system codes. *Science and Technology of Nuclear Installations*, 2008, 2008.

[19] U. S. Rohatgi and J. S. Kaizer. Historical perspectives of BEPU research in US. *Nuclear Engineering and Design*, 358:110430, 2020.

[20] A. De Crécy. Determination of the uncertainties of the constitutive relationships of the CATHARE 2 code. In *M & C conference*, Salt Lake City, Utah, USA, 2001.

[21] X. Wu, Z. Xie, F. Alsafadi, and T. Kozlowski. A comprehensive survey of inverse uncertainty quantification of physical model parameters in nuclear system thermal–hydraulics codes. *Nuclear Engineering and Design*, 384:111460, 2021.

[22] J. Freixa, E. De Alfonso, and F. Reventós. Testing methodologies for quantifying physical models uncertainties. A comparative exercise using CIRCE and IPREM (FFTBM). *Nuclear Engineering and Design*, 305:653–665, 2016.

[23] D. Lucas et al. An overview of the pressurized thermal shock issue in the context of the NURESIM project. *Science and Technology of Nuclear Installations*, 2009, 2008.

[24] T.-P. Luu. Analyse des essais COSI pour les modeles de condensation lors d'un choc thermique pressurise. *Master's thesis, Université Paris-Saclay, CEA, Service de Thermohydraulique et de Mécanique des Fluides*, 2019.

[25] J. Liao, C. Frepoli, and K. Ohkawa. Cold leg condensation model for analyzing loss-of-coolant accident in PWR. *Nuclear Engineering and Design*, 285:171–187, 04 2015.

[26] T. Skorek et al. Quantification of the uncertainty of the physical models in the system thermal-hydraulic codes – PREMIUM benchmark. *NEA/CSNI/R(2016)9*, page 62, 2016.

[27] E.F. Adiutori. A Critical Examination of Correlation Methodology Widely Used in Heat Transfer and Fluid Flow. volume 1 of *Heat Transfer Summer Conference*, pages 929–934, 07 2004.

[28] M. C. Kennedy and A. O'Hagan. Bayesian calibration of computer models. *Journal of the Royal Statistical Society: Series B (Statistical Methodology)*, 63(3):425–464, 2001.

[29] U. von Toussaint. Bayesian inference in physics. *Reviews of Modern Physics*, 83:943–999, 2011.

[30] N. W. Porter and V. A. Mousseau. Bayesian calibration of empirical models common in melcor and other nuclear safety codes. *NURETH 18 - 18th International Topical Meeting on Nuclear Reactor Thermal Hydraulics*, pages 5816–5826, March 2019.

[31] N. W. Porter, V. A. Mousseau, and M. N. Avramova. Quantified validation with uncertainty analysis for turbulent single-phase friction models. *Nuclear Technology*, 205(12):1607–1617, 2019.

[32] X. Wu, T. Kozlowski, H. Meidani, and K. Shirvan. Inverse uncertainty quantification using the modular bayesian approach based on gaussian process, part 2: Application to TRACE. *Nuclear Engineering and Design*, 335:417–431, 2018.

[33] C. Soize. *Stochastic Models of Uncertainties in Computational Mechanics*. American Society of Civil Engineers, 2013.

[34] M. Pourgol-Mohamad, A. Mosleh, and M. Modarres. Structured treatment of model uncertainty in complex thermal-hydraulics codes: Technical challenges, prospective and characterization. *Nuclear Engineering and Design*, 241(1):285–295, 2011.

[35] P. D. Arendt, D. W. Apley, and W. Chen. Quantification of Model Uncertainty: Calibration, Model Discrepancy, and Identifiability. *Journal of Mechanical Design*, 134(10), 09 2012.

[36] T. Skorek et al. Quantification of the uncertainty of the physical models in the system thermal-hydraulic codes – PREMIUM benchmark. *Nuclear Engineering and Design*, 354:110199, 2019.

[37] X. Wu, T. Kozlowski, H. Meidani, and K. Shirvan. Inverse uncertainty quantification using the modular Bayesian approach based on Gaussian process, Part 1: Theory. *Nuclear Engineering and Design*, 335:339–355, 2018.

[38] E. Zio and N. Pedroni. How to effectively compute the reliability of a thermal–hydraulic nuclear passive system. *Nuclear Engineering and Design*, 241(1):310–327, 2011.

[39] P. Congdon. Bayesian statistical modelling. *Measurement Science and Technology*, 13:643–643, 2002.

[40] H. Jeffreys. *The Theory of Probability*. Oxford Classic Texts in the Physical Sciences. OUP Oxford, 1998.

[41] S. Banerjee. Bayesian Linear Model : Gory Details. `https://ams206-winter19-01.courses.soe.ucsc.edu/system/files/attachments/banerjee-bayesian-linear-model-details.pdf`, 2008.

[42] T. O. Kvålseth. Note on the R2 measure of goodness of fit for nonlinear models. *Bulletin of the psychonomic society*, 21:79–80, 1983.

[43] C. Tofallis. A better measure of relative prediction accuracy for model selection and model estimation. *Journal of the Operational Research Society*, 66, 2015.

[44] C.R. Rao and Y. Wu. Linear model selection by cross-validation. *Journal of Statistical Planning and Inference*, 128(1):231–240, 2005.

[45] F. J. Massey Jr. The Kolmogorov-Smirnov test for goodness of fit. *Journal of the American Statistical Association*, 46(253):68–78, 1951.

[46] J. A. Rice. *Mathematical statistics and data analysis*. Cengage Learning, 2006.

[47] F. Reventós et al. PREMIUM, a benchmark on the quantification of the uncertainty of the physical models in the system thermal-hydraulic codes: methodologies and data review. *NEA/CSNI/R(2016)9*, 2016.

[48] R. Cocci, G. Damblin, A. Ghione, L. Sargentini, and D. Lucor. Extension of the CIRCE methodology to improve the inverse uncertainty quantification of several combined thermal-hydraulic models, submitted to Nuclear Engineering and Design, available at SSRN:. `https://ssrn.com/abstract=4153287`, 2022.

[49] G. Celeux, A. Grimaud, Y. Lefèbvre, and E. de Rocquigny. Identifying intrinsic variability in multivariate systems through linearized inverse methods. *Inverse Problems in Science and Engineering*, 18(3):401–415, 2010.

[50] X. Wu, K. Shirvan, and T. Kozlowski. Demonstration of the relationship between sensitivity and identifiability for inverse uncertainty quantification. *Journal of Computational Physics*, 396:12–30, 2019.

[51] I.M Sobol. Global sensitivity indices for nonlinear mathematical models and their Monte Carlo estimates. *Mathematics and Computers in Simulation*, 55(1):271–280, 2001. The Second IMACS Seminar on Monte Carlo Methods.

[52] L. Sargentini and G. Damblin. Sensitivity analysis on the critical mass flowrate based on Sobol' indices through replicated LHS. In *18th International Topical Meeting on Nuclear Reactor Thermal Hydraulics (NURETH-18)*, August 2019.

[53] A. Janicot and D. Bestion. Condensation modelling for ECC injection. *Nuclear Engineering and Design*, 145(1):37–45, 1993.

[54] P. Weiss. UPTF experiment: Principal full-scale test results for enhanced knowledge of large break LOCA scenarios in PWR's. In *Fourth international topical meeting on nuclear reactor thermal-hydraulics (NURETH-4). Proceedings. Vol. 1*, 1989.

[55] F. Mayinger, P. Weiss, and K. Wolfert. Two-phase flow phenomena in full-scale reactor geometry. *Nuclear Engineering and Design*, 145(1):47–61, 1993.

[56] T. Seidel, M. Beyer, U. Hampel, and D. Lucas. TOPFLOW-PTS air-water experiments on the stratification in the ECC nozzle and the ECC water mixing during PTS scenarios. In *The 14th International Topical Meeting on Nuclear Reactor Thermal Hydraulics (NURETH-14), Toronto, Ontario, Canada*, 2011.

[57] Siemens AG Division Production d'Energie. Essai C1/C2 Refroidissement par panache et par lame de la paroi de la cuve. *NT31/96/17*, 1996.

[58] H. Press and R. Schröder. *Hydrodynamik im Wasserbau (Hydrodynamic in hydraulic structures)*. Ernst & Sohn, Berlin, 1966.

[59] R. Cocci, A. Ghione, L. Sargentini, G. Damblin, and D. Lucor. Model Assessment for Direct Contact Condensation Induced by a Sub-cooled Water Jet in a Circular Pipe. *accepted in International Journal of Heat and Mass Transfer*, 2022.

[60] D. Bestion and L. Gros D'Aillon. Condensation tests analysis and correlation for the CATHARE code. In *NURETH 4 - 4th International Topical Meeting on Nuclear Reactor Thermal Hydraulics*, Karlsruhe (Germany, F.R.), October 1989.

[61] W.Y. Ren, G.J. Yu, B. JW, W.X. Tian, G.H. Su, S.Z. Qiu, and X.L. Fu. Experiment of Condensation in T-junction: Steam-water Flow in Water-injected Condition. In *16th international topical meeting on nuclear reactor thermal-hydraulics (NURETH-16), Chicago, IL*, 2015.

[62] P. Gaillard and M. G. Rodio. A general thermal stratification criterion for single and two-phase flows in a pipe after subcooled injection. *International Journal of Multiphase Flow*, 101:1–10, 2018.

[63] J. Iciek. The hydrodynamics of a free, liquid jet and their influence on direct contact heat transfer—III. Direct contact heating of a cylindrical, free falling liquid jet. *International Journal of Multiphase Flow*, 9(2):167–179, 1983.

[64] B. Clausnitzer and W. H. Hager. Outflow characteristics from circular pipe. *Journal of Hydraulic Engineering*, 123(10):914–917, 1997.

[65] F. X. Buschman and D. L. Aumiller. Use of fundamental condensation heat transfer experiments for the development of a sub-grid liquid jet condensation model. *Nuclear Engineering and Design*, 312:147–160, 2017.

[66] R. H. Whittle and R. Forgan. A correlation for the minima in the pressure drop versus flow-rate curves for sub-cooled water flowing in narrow heated channels. *Nuclear Engineering and Design*, 6(1):89–99, 1967.

[67] R. Stelling, E. V. McAssey Jr, T. Dougherty, and B. W. Yang. The onset of flow instability for downward flow in vertical channels. *Journal of Heat Transfer*, 118(3):709–714, 1996.

[68] I.-C. Chu, K.-Y. Lee, S. O. Yu, and H. J. Chung. Direct contact condensation in steam-water stratified flow. In *International Heat Transfer Conference 13*. Begel House Inc., 2006.

[69] A. Du Cluzeau. Quantification d'incertitude du nouveau modèle de condensation en surface libre sur les essais PARK. *NT DES/ISAS/DM2S/STMF/LMES/NT/2022-69675/A*, 2022.

[70] F. Gaudier. URANIE: The CEA/DEN Uncertainty and Sensitivity platform. *Procedia - Social and Behavioral Sciences*, 2(6):7660–7661, 2010.

[71] J.-B. Blanchard, G. Damblin, J.-M. Martinez, G. Arnaud, and F. Gaudier. The uranie platform: an open-source software for optimisation, meta-modelling and uncertainty analysis. *arXiv preprint arXiv:1803.10656*, 2018.

[72] A. Kovtonyuk, S. Lutsanych, F. Moretti, and F. D'Auria. Development and assessment of a method for evaluating uncertainty of input parameters. *Nuclear Engineering and Design*, 321:219–229, 2017.

[73] G. Damblin and P. Gaillard. Bayesian inference and non-linear extensions of the CIRCE method for quantifying the uncertainty of closure relationships integrated into thermal-hydraulic system codes. *Nuclear Engineering and Design*, 359:110391, 2020.

[74] P. Barbillon, G. Celeux, A. Grimaud, Y. Lefebvre, and É. De Rocquigny. Nonlinear methods for inverse statistical problems. *Computational statistics & data analysis*, 55(1):132–142, 2011.

Abstract in French (Résumé substantiel)

Titre : Apprentissage statistique et quantification inverse des incertitudes en simulation thermohydraulique nucléaire : application à la modélisation de la condensation à l'injection de sécurité

Résumé : La méthodologie appelée BEPU (en anglais *Best Estimate Plus Uncertainty*) suscite de plus en plus d'intérêt dans le domaine de la thermohydraulique nucléaire. Elle se compose de deux étapes : la simulation des phénomènes physiques au travers de la meilleure connaissance disponible (e.g. en utilisant des modèles physiques, également appelés corrélations) et l'estimation des incertitudes qui affectent les prédictions. Avant l'application de la méthodologie BEPU aux études de sûreté, les modèles thermohydrauliques utilisés dans les codes nucléaires doivent être correctement developpés, validés et leur incertitudes quantifiées. Ces corrélations sont développées en calibrant leurs paramètres à l'aide des bases de données expérimentales disponibles. Idéalement, la base de données est composée de tests à effets séparés (en anglais Separate Effect Tests – SETs, i.e. des essais où le phénomène à modéliser a un effet sur la quantité d'intérêt mesurable qui peut être séparée et quantifiée). Néanmoins, des SETs ne sont pas toujours disponibles. Le plus souvent, des tests à effets combinés (en anglais Combined Effect Tests – CETs) sont accessibles. Si la base de données est composée par des CETs, la corrélation modélisant le phénomène physique d'intérêt interagit avec, au moins, une autre (qui est également incertaine).

Cette recherche doctorale vise à développer des méthodologies statistiques avancées pour la quantification inverse de l'incertitude (en anglais Inverse Uncertainty Quantification - IUQ, i.e. estimer l'incertitude de paramètres d'entrée incertains à partir de l'incertitude d'une quantité prédite en réponse pour laquelle on dispose de réalisations expérimentales) des modèles thermohydrauliques en présence de CETs et à les appliquer au cas pratique du modèle de condensation à l'Injection de Sécurité (IS) d'un réacteur nucléaire. Elle se compose du développement, la validation et la quantification de l'incertitude d'une nouvelle corrélation physique en présence de SETs et l'IUQ d'un modèle existant par rapport à une base de données CETs. La thèse de doctorat est organisée en trois parties principales. Dans la première partie, l'élaboration, la validation et la quantification de l'incertitude des modèles thermohydrauliques est abordée par inférence bayésienne à l'aide de SETs. Dans cette approche, une variable aléatoire multiplicative (représentant l'incertitude du modèle) relie la valeur expérimentale à la prédiction du modèle. Cette variable multiplicative convient aux modèles qui mesurent de nombreux ordres de grandeur, comme dans le cas des essais thermohydrauliques. Un ensemble d'indicateurs statistiques est défini pour évaluer le rendement prédictif du meilleur modèle. De plus, comme les bases de données thermohydrauliques disponibles sont souvent composées d'un nombre limité d'essais, le modèle physique est validé par le biais d'une technique de validation croisée appelée Leave One Out (LOO), qui permet d'utiliser la même base de données pour les étapes de calibration et de validation.

La deuxième partie est centrée sur l'une des méthodes IUQ les plus largement appliquées en thermohydraulique nucléaire : la méthodologie CIRCE (*Calcul des Incertitudes Relatives aux Corrélations Elementaires*) et son extension aux essais CETs. CIRCE estime la distribution de probabilité (log-)normale représentant l'incertitude du modèle de référence dans le code de calcul. Cependant, lorsqu'elle est appliquée à l'estimation jointe des incertitudes de plusieurs

modèles utilisant des CETs, cette méthodologie peut souffrir de non-identifiabilité (i.e. une combinaison différente d'incertitudes explique l'erreur entre la valeur calculée par le code et les données expérimentales), ce qui entraîne des incertitudes statistiquement peu fiables. La non-identifiabilité peut aboutir à une estimation de l'incertitude du modèle le moins influent (moins influent sur la sortie du code) caractérisée par une faible précision (dans l'estimation des paramètres de la loi (log-)normale) et aussi à la dégradation de l'estimation de l'incertitude du modèle le plus influent. Ainsi, une extension de la méthode (nommée CIRCE 2-Steps) est proposée pour améliorer l'estimation de l'incertitude du modèle le plus influent. La méthodologie est composée par deux étapes successives. Dans la première étape, les incertitudes pour lesquelles des SETs sont disponibles sont évaluées. Ces incertitudes sont ensuite prises en compte lors de la quantification des incertitudes restantes en utilisant des CETs. Il est prouvé que cette nouvelle approche donne des résultats plus précis.

Dans la troisième partie, les deux méthodologies sont appliquées à un cas pratique : les modèles physiques utilisés pour la prédiction de la condensation dans la branche froide d'un Réacteur nucléaire à Eau Pressurisée (REP) lors d'un Accident de Perte de Refrigerant Primaire (APRP). Dans un tel scénario, deux phénomènes de condensation sont influents sur la variable d'intérêt, i.e. la température du liquide à l'entrée du downcomer. Le premier est la condensation de la vapeur sur le jet froid de l'IS et ensuite son impact dans l'écoulement liquide. Le dernier est la condensation de la vapeur à l'interface liquide de l'écoulement stratifié entre la région du jet et le downcomer. Les installations expérimentales COSI, TOPFLOW-PTS et UPTF composent la base de données expérimentale. La configuration et l'échelle sont différentes pour chacune d'entre elles, ce qui donne une large gamme de température d'injection, de débit massique et de pression. Ces expériences sont classées comme CETs. Cependant, comme la condensation à l'IS peut être isolée, elles peuvent également être réarrangées comme SETs. Cette base de données est donc appropriée pour tester les deux méthodologies. Après avoir testé les corrélations de la littérature sur la nouvelle base de données expérimentale avec des résultats non satisfaisants, une nouvelle approche est présentée. La condensation est quantifiée par un potentiel de l'échangeur de chaleur qui modélise le jet froid. De cette façon, la condensation est une fonction de la forme du jet et d'une variable η. Le cadre bayésien présenté dans la première partie est appliqué aux SETs COSI et TOPFLOW-PTS afin de calibrer une corrélation pour la variable η. Le nouveau modèle réduit considérablement l'écart-type entre les prédictions et les valeurs expérimentales correspondantes. La nouvelle corrélation est ensuite validée statistiquement et appliquée à la base de données UPTF pour validation physique. La corrélation montre une bonne capacité à prédire avec précision la condensation à l'IS dans toutes les configurations étudiées. La nouvelle méthodologie CIRCE 2-Steps est ensuite appliquée, montrant des améliorations significatives sur l'estimation de l'incertitude du modèle de condensation è l'IS (i.e. le plus influent). L'incertitude résultante du modèle est comparée à celle calculée par le cadre bayésien, montrant un bon accord entre les deux résultats.

Mots clés : Calage bayésien, Quantification inverse des incertitudes, CIRCE, Tests à effets combinés, Condensation, Injection de Sécurité (IS)

université PARIS-SACLAY

ÉCOLE DOCTORALE
Sciences mécaniques et énergétiques, matériaux et géosciences (SMEMAG)

Titre : Apprentissage statistique et quantification inverse des incertitudes en simulation thermohydraulique nucléaire : application à la modélisation de la condensation à l'injection de sécurité

Mots clés : Calage bayésien, Quantification inverse des incertitudes, CIRCE, Tests à effets combinés, Condensation, Injection de Sécurité (IS)

Résumé : La méthodologie BEPU (Best Estimate Plus Uncertainty) repose sur la validation et la quantification des incertitudes des modèles physiques utilisés dans les codes de calcul nucléaires. Disposer d'une méthodologie robuste permettant de caler un modèle physique, de le valider et d'en quantifier les incertitudes est un enjeu majeur. Cette thèse a donc comme objectif de développer des méthodologies pour la validation et la quantification d'incertitudes appliquées au cas pratique du modèle de condensation à l'Injection de Sécurité (IS). La première étape a été le développement d'un nouveau cadre bayésien pour la calibration et la quantification inverse de l'incertitude des modèles physiques en utilisant une incertitude de modèle multiplicative. La deuxième étape a été une analyse thermohydraulique détaillée des données expérimentales afin d'améliorer la compréhension physique de la condensation à l'IS dans la branche froide d'un reacteur à eau pressurisée lors d'un Accident de Perte de Réfrigérant Primaire (APRP). Pendant cet accident, deux types de condensation surviennent dans la branche froide : la condensation à l'IS et la condensation en aval du jet. La température en sortie de la branche froide, et donc à l'entrée du cœur du réacteur, dépend de ces deux modèles. Le cadre bayésien est appliqué afin de calibrer un nouveau modèle de condensation à l'IS. Ce modèle a été validé et ses incertitudes ont été quantifiées. Dans la dernière étape, une extension de la méthodologie CIRCE (appelée CIRCE 2-Steps) a été développée. CIRCE est une méthodologie pour déterminer l'incertitude du modèle basée sur la différence entre la valeur expérimentale et la valeur calculée d'une quantité d'intérêt. L'extension proposée améliore l'estimation des incertitudes de plusieurs modèles combinés entre eux et qui interagissent sur la même variable de sortie, comme la température en sortie de la branche froide.

Title: Statistical learning and inverse uncertainty quantification in nuclear thermal-hydraulic simulation: application to the condensation modelling at the safety injection

Keywords: Bayesian calibration, Inverse Uncertainty Quantification, CIRCE, Combined Effect Tests, Condensation, ECC

Abstract: The BEPU (Best Estimate Plus Uncertainty) methodology is based on the validation and the uncertainty quantification of the physical models used in the nuclear computer codes. Having a robust methodology to calibrate a physical model, validate it and quantify its uncertainty is a major challenge. Therefore, the objective of this thesis is to develop methodologies for the validation and uncertainties quantification and apply them to the practical case of the condensation model at the Emergency Core Cooling (ECC) system. The first step was the development of a new Bayesian framework for the calibration and inverse uncertainty quantification of physical models using a multiplicative model uncertainty. The second step was a detailed thermohydraulic analysis of the experimental data in order to improve the physical understanding of the ECC condensation in the cold leg of a pressurised water reactor during a Loss Of Coolant Accident (LOCA). Two types of condensations occur in the cold leg: the condensation at the ECC and the condensation downstream the jet. The temperature at the outlet of the cold leg, and therefore at the entrance of the reactor's core, depends on these two models. The Bayesian framework is applied to calibrate a new condensation model at the ECC. This model has been validated and the uncertainties have been quantified. In the last step, an extension of the CIRCE methodology (called CIRCE 2-Steps) was developed. CIRCE is a methodology to determine the model uncertainty based on the difference between the experimental and calculated value of a quantity of interest. The proposed extension improves the estimation of the uncertainties of several models combined together and interacting on the same output variable, such as the temperature at the end of the cold leg.